Progress in Materials Science 77 (2016) 1–79

Contents lists available at ScienceDirect

Progress in Materials Science

journal homepage: www.elsevier.com/locate/pmatsci

Sol–gel based materials for biomedical applications

Gareth J. Owens [a,1], Rajendra K. Singh [b,c,1], Farzad Foroutan [a], Mustafa Alqaysi [a], Cheol-Min Han [b,c], Chinmaya Mahapatra [b,c], Hae-Won Kim [b,c,d,*], Jonathan C. Knowles [a,b,*]

[a] Department of Biomaterials and Tissue Engineering, UCL Eastman Dental Institute, University College London, 256 Gray's Inn Road, London WC1X 8LD, UK
[b] Department of Nanobiomedical Science & BK21 Plus NBM Global Research Center for Regenerative Medicine, Dankook University, Cheonan 330-715, Republic of Korea
[c] Institute of Tissue Regenerative Engineering (ITREN), Dankook University, Cheonan 330-715, Republic of Korea
[d] Department of Biomaterials Science, College of Dentistry, Dankook University, Cheonan 330-715, Republic of Korea

Abbreviations: AAM, anodic alumina membrane; AP, 3-aminopropyl; ASO, antisense oligonucleotides; BCP, biphasic calcium phosphate; BG, bioactive glass; BMSC, bone marrow mesenchymal stem cell; cAMP, cyclic adenosine monophosphate; CaP, calcium phosphate; CHO, Chinese hamster ovary cells; CNT, carbon nanotubes; CTAB, cetyl trimethylammonium bromide; CT, computer tomography; DDS, drug delivery system; DMHA, N,N-dimethylhexadecylamine; DNA, deoxyribonucleic acid; DOX, doxorubicin; ECM, extracellular matrix; EDC, 1-ethyl-3-(3-dimethyl-aminopropyl) carbodiimide; F127, Pluronic® F-127; FAP, N-folate-3-aminopropyl; FITC, fluorescein isothiocyanate; GP, guanidinopropyl; GEGP, 3-[N-(2-guanidinoethyl)guanidine] propyl; GFP, green fluorescent protein; HA, hydroxyapatite; HCA, carbonated hydroxyapatite; INDO, intermediate neglect of differential overlap; MCM, mobile composition of matter; MBG, mesoporous bioactive glass; MNP, magnetic nanoparticle; MRI, magnetic resonance imaging; MSC, mesenchymal stem cell; MSN, mesoporous silica nanoparticle; MTES, methyltriethoxysilane; MTMS, trimethoxymethylsilane; NC, network connectivity; NHS, N-hydroxysuccinimide; NIR, near infrared; NLR, long rod nanoparticles; NMR, nuclear magnetic resonance; NP, nanoparticle; NSR, short rod nanoparticles; P123, Pluronic® P-123; PAMAM, polyamidoamine; PAA, polyacrylic acid; PCL, poly(ε-caprolactone); PDMAAm, poly-(N,N′-dimethyl acrylamide); PDMS, poyldimethylsiloxane; PEG, polyethylene glycol; PEI, polyethyleneimine; PET, position emission tomography; PLL, poly (L-lysine); PLLA, poly-L-lactic acid; PMMA, poly(methyl methacrylate); PS, polystyrene; PVA, polyvinyl alcohol; PVP, polyvinylpyrrolidone; QD, quantum dots; RBC, red blood cells; RNA, ribonucleic acid; ROS, reactive oxygen species; SBF, simulated body fluid; siRNA, small interfering RNA; SPECT, photon emission computed tomography; SPION, superparamagnetic iron oxide nanoparticles; TEA, triethanolamine; TEM, transmission electron microscopy; TEOS, tetraethoxy orthosilicate; TMB, trimethylbenzene; TMES, trimethylethoxysilane; TMOS, tetramethyl orthosilicate; TTCP, tetracalcium phosphate; TTIP, titanium tetraisopropoxide; β-TCP, β-tricalcium phosphate; 3D, three-dimensional.

* Corresponding authors at: Institute of Tissue Regeneration Engineering, Dankook University, Cheonan 330-714, Republic of Korea (H.-W. Kim). Division of Biomaterials and Tissue Engineering, UCL Eastman Dental Institute, University College London, 256 Gray's Inn Road, London WC1X 8LD, UK (J.C. Knowles).

E-mail addresses: kimhw@dku.edu (H.-W. Kim), j.knowles@ucl.ac.uk (J.C. Knowles).

[1] Both authors contributed equally.

http://dx.doi.org/10.1016/j.pmatsci.2015.12.001

ARTICLE INFO

Article history:
Received 19 May 2015
Received in revised form 8 December 2015
Accepted 9 December 2015
Available online 13 January 2016

Keywords:
Sol–gel
Biomaterials
Biomedical
Tissue engineering
Drug delivery
Nanomedicine

ABSTRACT

Sol–gel chemistry offers a flexible approach to obtaining a diverse range of materials. It allows differing chemistries to be achieved as well as offering the ability to produce a wide range of nano-/micro-structures. The paper commences with a generalized description of the various sol–gel methods available and how these chemistries control the bulk properties of the end products. Following this, a more detailed description of the biomedical areas where sol–gel materials have been explored and found to hold significant potential. One of the interesting fields that has been developed recently relates to hybrid materials that utilize sol–gel chemistry to achieve unusual composite properties. Another intriguing feature of sol–gels is the unusual morphologies that are achievable at the micro- and nano-scale. Subsequently the ability to control pore chemistry at a number of different length scales and geometries has proven to be a fruitful area of exploitation, that provides excellent bioactivity and attracts cellular responses as well as enables the entrapment of biologically active molecules and their controllable release for therapeutic action. The approaches of fine-tuning surface chemistry and the combination with other nanomaterials have also enabled targeting of specific cell and tissue types for drug delivery with imaging capacity.

Contents

1. Introduction

In recent years, biomaterials have gained increasing interest within biomedical sciences and across various scientific disciplines. One reason for this is based on an ever increasing demand for regenerative or replacement tissues. Degenerative diseases and injuries have driven the need for more successful and cost effective treatments and this has, in turn, spurred the development of versatile methods to produce bioactive matrices and interfaces with improved functionality. It is therefore not surprising that research into biomaterials has contributed to the development of materials science as a highly interdisciplinary subject utilizing new approaches to previously exhausted synthesis routes. One key development that serves best to exemplify this fact is the use of sol–gel science for biomedical applications. This review therefore focuses on developments and the potential applications of research within this field.

Since its inception, sol–gel methods have typically involved the use of tetraethyl orthosilicate (TEOS) as a principal network forming agent. The first reason for using TEOS is that the formation of robust networks with moderate reactivity and a high degree of control are afforded through simple variations in the synthesis conditions such as pH, temperature, and additives [1–3]. For example, silica-based glass networks possess these properties and have thus provided a basis for some of the most successful bioactive substrates [4–6]. Other reasons can be found in the ease of incorporation of organic molecules or moieties, polymers, and biomolecules or cells, and this ability is due to the liquid-phase reactions that can subsequently be processed at low temperatures [2,3]. Silica and doped silica materials obtained *via* the solution–gelation (“sol–gel”) inorganic polymerization process are also highly functional materials with an impressive range of applications, and utilize two of the pillars of chemistry: synthesis and analysis. However, a wide range of other areas also make use of this same route. The synthesis processes can also occur under very mild conditions, so it can be used to obtain products of various sizes, shapes, formats, and, ultimately, applications.

From a purely physical perspective, sol–gel methods are particularly useful because they permit direct fabrication of multicomponent materials in different configurations (monoliths, coatings, foams, and fibers) without powder intermediates [2,3,7] or the use of expensive processing technologies, such as vacuum methods. The diversity of materials which can be obtained, has made the sol–gel method an important synthesis route in several domains of research, including optics, electronics, semi-/super-conductors, and biomaterials. In this instance, methods have no bearing on the final chemical composition of the material, rather the way that the material is obtain provides the benefit.

Sol–gel science dates back over 150 years. The term “sol–gel” was first coined by Graham in 1864 during his work on silica sols [8]. Although in 1640 van Helmont had discovered “water glass” by dissolving silicate materials in alkali and then precipitating silica gel upon acidification [9]. It was in 1846 when Ebelmen observed the formation of a transparent glass following exposure to the atmosphere of a silane obtained from $SiCl_4$ and ethanol [10,11] when true sol–gel experiments first began. Patrick, during his doctoral studies at the University of Goettingen in 1912–1915, to devise an economically viable and rapid sol–gel method to make silica gel from sodium silicate (Na_2SiO_3) in large quantities [12] and Kistler [13] described the first synthesis of a highly porous silica (SiO_2) form, which he dubbed “aerogel”, by supercritically drying the gel obtained by hydrolytic polycondensation of silicic acid [$Si(OH)_4$]. Each of these efforts can be credited as the starting point for the modern sol–gel approach and serve to demonstrate a long history which is now coming to fruition for biomedical applications.

Sol–gel methods also enable powderless processing of glasses, ceramics and thin films or fibers, directly from solution. Precursors are mixed at the molecular level and variously shaped materials may be formed at much lower temperatures than is possible by traditional preparation methods. One of the major advantages of sol–gel processing is also the possibility to synthesize hybrid organic–inorganic materials. Combinations of inorganic and organic networks facilitate the design of new engineering materials with diverse properties for a wide range of applications. Biomedical applications invariably require the design of new biomaterials, and this can be achieved by merging sol–gel chemistry and biochemistry. The gel derived materials are excellent model systems for studying and controlling biochemical interactions within constrained matrices with enhanced bioactivity because of their surface chemistry, micro-/nano-pores and large specific surface area [5]. In biomedical applications, the coating of medical devices is an important issue. Materials used in medical devices should have appropriate structural and mechanical properties and ideally promote a healing response without causing adverse immune reactions. Medical device designers currently use various surface treatments such as coating that enhance or modify properties such as lubricity, the degree of hydrophobicity, functionalisation and biocompatibility. Sol–gel technology offers an alternative technique for producing bioactive surfaces for these applications.

Sol–gel thin film processing offers a number of advantages including low-temperature processing, ease of fabrication, and precise microstructural and chemical control. The sol–gel derived film or layer not only provides a good degree of biocompatibility, but also a high specific surface area (which can be used as a carrier of adsorbed drugs) and an external surface whose rich chemistry allows ease of functionalization by suitable biomolecules. For example, several research groups [14–17] have described the synthesis of thin, resorbable sol–gel films with controlled release of bactericidal properties on a Ti-alloy substrate, and determined the effect of processing parameters on the degradation and drug release with a close correlation between the two, suggesting the sol–gel processing can be used to control drug release.

The development of multifunctional nanoparticles that can be used as drug delivery vectors remains a significant challenge for material science. For example, superparamagnetic nanoparticles are invaluable to biomedical applications such as in magnetic resonance imaging (MRI), targeted drug delivery and magnetic separation [18,19]. These applications require intimate control of the particle size, and discrete, superparamagnetic iron oxide nanoparticles that can be prepared by the sol–gel method to lower the annealing temperatures required. Silica-based magnetic nanocomposites, formed by magnetic nanoparticles (MNPs, either Fe_3O_4 or γ-Fe_2O_3) dispersed in a silica matrix, are of relevant technological and scientific interest. Here, encapsulation in silica prevents interactions between the MNPs, and consequently assures a uniform dispersion. The latter is essential for efficient performance in most applications, including diagnostic and therapeutic, where particles must display high magnetization, be stable against oxidation, and, most importantly, remain non-aggregated [20,21].

Engineering new bone tissue with cells and a synthetic extracellular matrix (ECM) represents a promising approach for the regeneration of mineralized tissues. Bone regeneration requires a scaffold material upon which cells can attach, proliferate and differentiate into functionally and structurally appropriate tissues for the body location into which they are placed. Bone is a highly mineralized tissue consisting of an apatitic mineral phase most similar to a form of carbonated hydroxyapatite (HCA), although a significant contribution is made by extraneous ions such as sodium, chloride, zinc and, to a lesser extent, fluorides. In general, HCA can be considered a model mineral for natural bone and is widely accepted as a bioactive material with excellent biocompatibility, high osteoconductivity, and reasonable mechanical strength [22–25]. For these reasons it has widely been used in tissue engineering applications, especially for bone and cartilage regeneration. However, *in vivo* data suggest that degradation or ion release from labile sources such as bioactive glasses (BGs) promotes new bone formation, as opposed to the relatively lower ion release that occurs as a result of HCA minerals reaching equilibrium with their surrounding medium. It appears that sol–gel methods hold the potential to apply an ever-increasing range of glass-based bioactive coating to materials, which have previously remained incompatible with alternative coating techniques. Furthermore, the versatility of the sol–gel approach is opening new doors to previously unattainable compositions [26], again increasing the potential applications of sol–gel materials as fillers to replace tissue within necrotic or defect sites.

The sol–gel microencapsulation technology and its broad application potential are now well-known [27]. Relevant here is the use of silica for encapsulation and controlled release of both hydrophilic and hydrophobic molecules, ensuring considerable chemical and physical protection of the valued entrapped dopants. Given the above, it can be seen that sol–gel derived bioactive materials hold great potential value. However, there are still significant hurdles to overcome, particularly with respect to the economic viability of up-scaling sol–gel production. Due to the price of precursors, the production of glass *via* the sol–gel process will cost approximately 100 times that of glass obtained by conventional melting and casting. As a consequence, the production of glass *via* the sol–gel process only makes sense economically when addressing high value-added products.

This review highlights the usefulness of the sol–gel route for preparing bioactive NPs, powders, coatings, foams, bulks and the hybrids for biomedical applications as well as for designing more biocompatible and biofunctional materials to heal and regenerate diseased and damaged tissues. The goal is that the materials covered herein will provide a critical review of the progress, stimulate further research in the field, and inspire for yet further applications for a method that has yet to reach its full potential.

2. Sol–gel methods and chemistry

One group of biomedical materials are those that can be classified into arising from a non-biological source but that are ultimately applied *in vivo* [28]. There are currently a wide range of synthesis routes that are able to produce such materials, and sol–gel is one such synthesis route. In their simplest terms, all sol–gel methods involve two distinct phases: solution and gelation. As the name implies, a sol is a colloidal suspension of solid particles, whereas a gel is an interconnected network of solid phase particles that form a continuous entity throughout a secondary, usually liquid, phase. Throughout sol–gel technology, these phases are conserved though the chemical reactions that take place during the gel evolutions, and can be manipulated in a variety of ways; for instance, altering the initial precursors, time allowed for gelation, catalysts, degree of solvation, gelation conditions or physical processing of the gel itself. Sol–gel processes allow formation of solid materials through gelation of solutions and can be used to produce a large number of useful morphologies (Fig. 2.1).

The processes illustrated in Fig. 2.1 are by no means limiting or exhaustive. Depending on the specific application, these stages can be extended, altered, or with the exception of solvation and gelation, removed entirely. What remains constant for the production of sol–gel derived bioactive materials are the stages that allow for hydrolysis and condensation reactions to occur. Successful

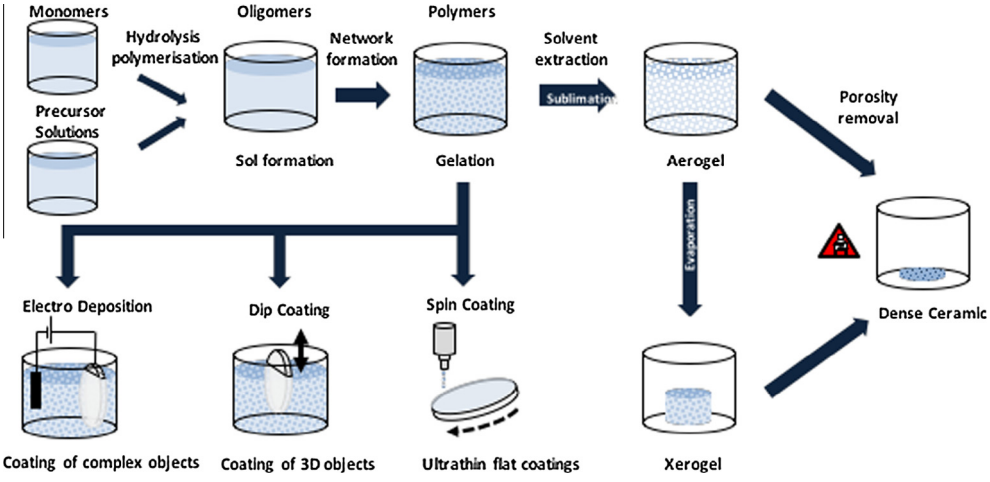

Fig. 2.1. Sol gel synthesis routes. Processes are defined as sol–gel by the transition of colloidal solution to an interconnected gel network (gelation). The further processing stages illustrated are non-redundant and may be combined depending on the specific needs of the application.

manipulation of these reactions was first achieved by Stöber et al. [29] who, by applying alkoxy precursors (both TEOS and TMOS) in the presence of an ammonium hydroxide catalyst, successfully produced colloidal suspensions of nanoscale silica particles. This work was based on earlier observations that TEOS will react to form silica and that the reaction is further favored under basic conditions [30]. Secondary to the purpose of this work, gelation was also observed [29] although this was, at the time, considered an undesirable hazard of a process that aimed to form discrete silica microspheres (i.e. for the purposes of developing compression® technology, a sol–gel derived fiber binder for thermal insulation) [31]. Simple silica microspheres have since seen a plethora of applications, and today, the benefits that are provided by the gelation are well recognized. In addition, advanced processing routes have also been developed that are able to account for or exploit the "undesirable" aspects of the gelation process.

This section aims to describe the sol–gel synthesis routes that are most commonly used to produce ceramic and glass networks for biomedical applications. In addition to providing an overview of the polymerization processes, the use of classical inorganic synthesis routes and colloidal aggregation will be discussed along with adaptations to the synthesis procedures that have allowed for yet further applications. Common links between methodologies are emphasized and techniques themselves are exemplified through some of their most recent uses.

2.1. Organic precursors in sol–gel methods

Silicon alkoxides represent the main network forming agents used in sol–gel preparation methods [5,32,33]. While the sol–gel process provides key benefits, such as the low synthesis temperatures and the vast array of alkoxide precursors available, the cost associated with alkoxide precursors presents some limitations [5,34]. Nevertheless, the efficiency provided by low temperature synthesis and the accuracy with which specific compositions can be achieved have the potential to outweigh any such negative aspects of the process. Low temperature synthesis is achieved through solution-mediated formation of strong covalent bonds between elements that would otherwise require excessively high temperatures to create. For alkoxides, this requires initial hydrolysis of the alkoxy group followed by a condensation between network forming substrates. Fig. 2.2 illustrates the hydrolysis and steps involved in the formation of a basic silica glass network from an alkoxy precursor, TEOS. For the purposes of clarity, the reaction of TEOS with water is used as an example although it is important to note that several functionalised leaving groups are applicable to this process [5].

As is evident from Fig. 2.2, water is essential to the process. In order control polymerization, the medium used to produce the gel must therefore remain largely anhydrous. However, some water must also be present in order to allow the hydrolysis reaction to propagate. Once hydrolysis of the ester linkages starts, subsequent condensation reactions (Fig. 2.3) are able to generate enough water to allow the process to continue without replenishing the water lost during hydrolysis [31]. Hydrolysis and condensation therefore form a chain reaction, which is of critical importance to enabling initial

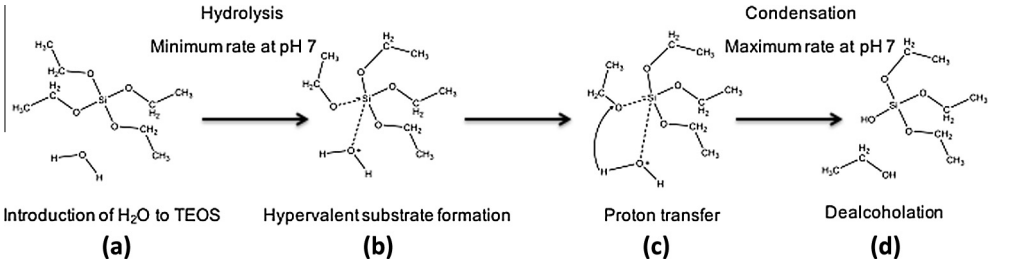

Fig. 2.2. Initial hydrolysis and condensation stages of TEOS in the production of silica oligomers. Initial hydrolysis and condensation stages of TEOS in the production of silica oligomers. (a) Introduction of water to TEOS, (b) H_2O forms a hypervalent substrate with silicon, (c) transfer of the proton from the water to the adjacent alkoxy group, (d) cleavage of the ester bond and dealcoholation.

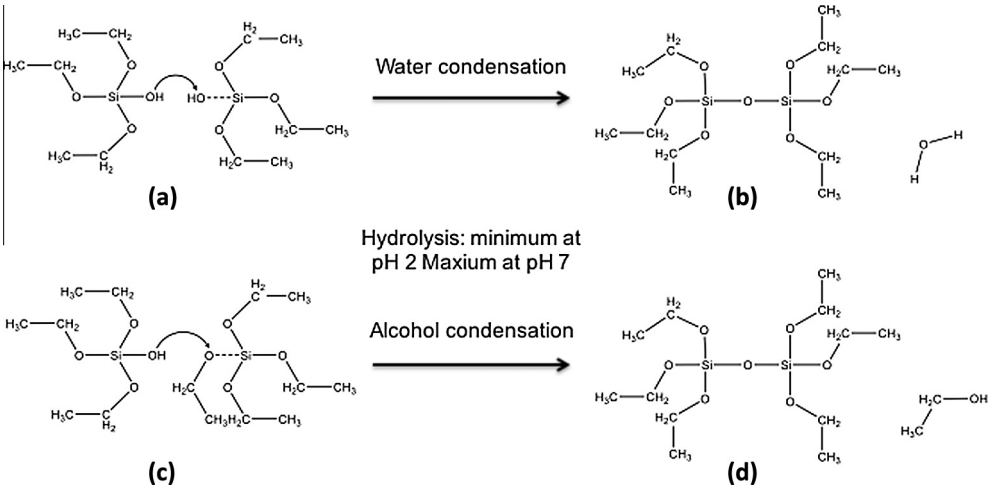

Fig. 2.3. Subsequent condensation stages of TEOS in the production of silica oligomers. Condensation between silanol groups on two hydrolyzed TEOS molecules (a and b) and between a silanol group and an adjacent alkoxy group (c and d) result in the production of free H_2O and ethanol respectively.

control over the process and network structural evolution, as an ability to delay polymerization allows for the specific composition of the solution to be tailored ensuring both homogeneity and unlimited functionality of the end product.

Referring to Fig. 2.2 again, hydrolysis itself occurs as typical S_N2 reaction, whereby the addition of H_2O results in a hypervalent substrate. The central atom of the substrate (e.g., silicon in the case of TEOS) takes on a partial negative charge, whereas the oxygen in H_2O becomes partially positive. This nucleophilic addition has important implications when considering the role of catalysts in the sol–gel process [35]. The variation in charge causes instability in the hypervalent substrate molecule that is immediately rectified by the transfer of a proton from the nucleophile (H_2O) to the ester bond of an opposing alkoxy group. Cleavage of the single σ-bond between the opposing alkoxy (i.e., the leaving group) and the substrate then occurs by the addition of the proton from the nucleophile itself. This results in the formation of an available HO^- group on the substrate and an alcohol from the alkoxy leaving group. The fact that both reactions occur simultaneously defines hydrolysis of alkoxides as S_N2 reactions. Conversely, condensation does not proceed by this same mechanism.

As Fig. 2.3 shows, only one reaction occurs during condensation: the loss of an HO– group from the substrate. This mechanism is therefore an S_N1 reaction and can occur as either dehydration or dealcoholation [36]. For the former to occur, two HO– groups must take part in the formation of an Si–O–Si bond, whereas the latter results from the direct transfer of proton to the leaving group on a neighboring substrate. Evident from these reactions, a decrease in pH can promote hydrolysis through protonation of the leaving groups (therefore reducing the stability of the ligand in question). Alternatively, higher pH will induce the deprotonation of –OH groups and therefore favors condensation [35]. However, OH^- is a highly efficient nucleophilic species and electron transfer from –OH groups can be facilitated by H^+ in the immediate environment. This relationship means that higher and lower pH is also able to promote condensation and hydrolysis, respectively. In silica based systems the reactions proceed by acidic catalysis at pH < 2.5 and basic catalysis when pH > 2.5, which can be explained by the isoelectric point of silica (pH = 2.5) [37]. In the sol–gel route synthesis, a stepwise reaction scheme has been undertaken to control the ratio of hydrolysis to condensation rates [38]. In general, the rate of hydrolysis is fast compared to that of condensation in strong acidic conditions. Therefore, a well-ordered hexagonal arrangement of mesopores (a pore structure that is commonly formed in sol–gel silica materials) is formed at low pH in acidic conditions. Meanwhile, in neutral or basic conditions ranging from pH 7 to pH 9, the rate of condensation is faster than that of hydrolysis, and eventually

Table 2.1
Example alkoxy precursors amenable to the sol–gel process.

Precursor	Leaving group (R–)	Structure	Reference
Tetraethyoxysilane (TEOS)	CH_2–H_3–OH	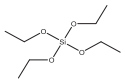	Nandy et al. [43], Stöber et al. [29], Choi et al. [38]
Tetramethoxysilane (TMOS)	–CH_3	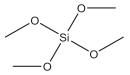	Stöber et al. [29], Choi et al. [38]
di-Butylphosphate	–CH_2–CH_2–CH_2–CH_3	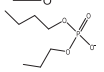	Pickup et al. [46], Foroutan et al. [26]
Titanium tetraisopropoxide	–CH–$(CH_3)_2$	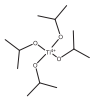	Nabavi et al. [44], Foroutan et al. [26], Han et al. [54]
Vanadium O(Am^t)$_3$	–C(CH_3)(CH_2–CH_3)CH_3–OH	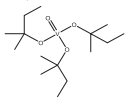	Livage [51], Nabavi et al. [44]

the materials prepared by a single-step reaction at high pH display gel-like structure often without mesopores. It is hence an interesting attempt to synthesize ordered mesoporous materials by a two-step sol–gel route at a lower acidic pH followed by a higher pH. Up to now, however, a two-step sol–gel reaction has not been applied for the fabrication of ordered mesoporous structure, because the reaction mechanism is not yet fully understood with most well-ordered silica structures that have been achieved under strong acidic conditions. Expectedly, reaction kinetics reaches a minimum at the isoelectric point [39]. Thus the promotion or inhibition of alkoxy polymerization can be tailored to the substrate of interest by choosing a pH that provides the optimal set of reaction kinetics.

Several other silane oligomers apart from TEOS can be used to produce a similar result [5,40–45] with the prerequisite being a set of functionalised groups capable of taking part in the hydrolysis and condensation reactions. In addition to silicate, phosphate-based materials may be used for the same purpose [26,46], as can various transition metal elements [5,40,43,46–48] (as shown in Table 2.1). Network modifiers (such as magnesium and calcium) can be introduced to the network in salt form [40] or as alkoxides. However, the higher electronegativity of transition metal species in comparison to silicone and phosphorous can cause issues where condensation reactions proceed with an unfavorable bias away from the desired network composition or the end particulate structure [44,49]. Fortunately, the versatility of the sol–gel process has allowed for phenomena such as steric hindrance, chelation and selective catalysis to be exploited and enable viable production of a far greater range of materials than is possible with traditional synthesis methods alone. These benefits have led to the development of a series of methods that exploit differing chemistries to enable efficient and effective production of specifically-tailored bioactive materials.

Like silicon, phosphorous and vanadium precursors can be used as network-formers within the sol–gel process [44,46,50,51]. However, the σ–π double bond common to the latter two substrates reduces the expected coordination number and further produces repulsion between the oxygen atoms coordinated under adjacent σ bonds. This difference in network connectivity results in a more relaxed network structure when compared to silica based networks [52], as silicate is able to share all 4 oxygen atoms with neighboring cationic groups [53]. This in turn increases the range and quantity of species that are able to be included, but such flexibility comes at the expense of stability, as the high electronegativity of the =O bond leaves the network open to hydrolysis. As with conventional melt-derived materials, solubility can be controlled by the combination of network modifiers, as can the release of active agents or tailoring of other physical properties of the material in question.

Nandy et al. [43] exploited the effects of steric hindrance on basic ammonium catalysts to control the textural properties of mesoporous silica. The approach of these authors was to reduce the catalytic

effect of NH_3 on TEOS hydrolysis with the use of primary, secondary and tertiary amines. Like silanes, the addition of further organic groups on the amine reduces its capacity to act as a Lewis base. However, the steric effects of bound organic groups also prevent the nucleophilic base from entering a reactive field with the substrate; hence, sterically hindering catalytic activity. More directly, the concept that steric properties can influence nucleophilic reactions is well known in a number of fields [55]. As a result, the Tolman cone angle has been proposed as a means by which the reactivity of a complex can be predicted [56], although this is not to say that such a measure can be applied to the sol–gel process as whole. As noted above, a number of factors are able to influence the process with respect to the steric properties of the ultimate leaving groups and represent only one aspect of the system.

The solvent itself also plays an important role in determining the rate of gelation reactions [37,45,54,57]. This solvation effect can occur in two ways: through viscosity and hydration effects. For example, NiO_2 particle size was successfully directed by Talebian and Kheiri [45], who by employing a series of solvents with increasing viscosity, were able to increase the particle size in a controlled manner. However, the solvent was also shown to alter the NiO_2 crystalline structure, which serves to highlight the need for experimental confirmation as, with such a variety of avenues available to exploit, comes as set of variable that must also be controlled. The effects of viscosity, or more precisely the dielectric constant, have also been recently described by Han et al. [54]. These authors made use of non-contingent esterification between the solvent (an alcohol) and sulfuric acid to provide water for polymerization of the titanium-based network. In doing so, results were confounded through the porogenic nature of water itself. However, what was demonstrated clearly was the influence of the solvent on the physical structure of the particles produced. A more definitive explanation was put forward by Nabavi et al. [44] who identified the ability of metal alkoxide to exchange leaving groups under solvation. By altering the solvent species from that of the alkoxide itself, the substrate can become coordinated with a mixture of alkoxy groups. Undoubtedly, this would affect polymerization in a way that is dependent on specific combination of coordinated groups present on network-forming substrates throughout the solution.

2.2. Colloidal sol–gel methods

Colloidal solutions can be defined as solutions containing discrete particles that do not settle, but remain suspended for several years, unless induced to do otherwise [31]. Depending on the size of the colloid particles, (which usually range from 1 nm to 1 μm), those with a density greater than that of the solvent can be maintained in suspension through the effects of Brownian motion alone; however, factors specific to the surface chemistry of the colloids themselves also make a significant contribution. Work within this area first began in the 1900s and was initially followed by efforts that aimed to control both particle size in absolute terms and the uniformity of the sols that could be produced. Today, methods of producing uniform particle sizes are further understood [36,48] with colloidal sol–gel methods remaining an active area of research.

Ludox® was the first commercial colloidal suspension of silica available on the open market. This product offers a range of potential applications; the most pertinent to biomedical application is its ability to form condensed silica networks upon drying. This property results from condensation of –OH groups present on adjacent silica particles. The initial Si–O–Si bridges that are formed can be further strengthened by passive deposition of silica on the initial bridge as a result of the equilibrium silicic acid ($Si(OH)_4$) and the silica making up the mass of the colloids. It is important to note the delineation between this process and Ostwald ripening; the latter being influenced by a propensity to increase the thermodynamic stability of the system and thus showing a preference to enlarge the size of discrete particles. Furthermore, colloidal sol–gel methods are not limited to silica or silica-based systems [50].

The applicability of the colloidal methods is based on two key aspects of the process: stabilisation of the colloidal particles within the sol and coalescence or flocculation to form the gel. With particles that possess the same electrostatic charge, colloidal suspensions are maintained by the ζ-potential, which in turn reflects the magnitude of the electrical double layer present on charged particles in solution. As noted above, the removal of the solvent is one method by which the aggregation of colloidal particles can be achieved. Alternatively, altering the pH, salinity or temperature can induce depeptisation,

whereby the electrical double layer is reduced to a point that the ζ-potential is no longer strong enough to prevent attractive van der Waals forces and flocculation takes place [31,50].

Despite the potential of colloidal methods to provide much thicker, more structurally resistant films and deposits than methods that rely on *de novo* synthesis, this route has seen the least number of applications within biomedical research. This is not to say that the methods have fallen out of fashion completely. Based on the need to retain protein conformation, Liu and Chen [33] explored the use of colloidal Ludox® SM-30 to encapsulate cytochrome C, myoglobin, haemoglobin and catalase using an acidified solution of water glass (Na_2SiO_3) to enhance network formation between the silica particles already present within a colloidal suspension. These authors were able to show an enhanced preservation of protein conformation in comparison to direct synthesis from alkoxide precursors. The gelation rate correlated well with the structural stability of the encapsulated proteins and served to demonstrate an ability to circumvent conditions that would otherwise damage sensitive molecules. For certain applications however, the colloidal sol–gel method does not provide the degree of protection required. For example, living cells are extremely sensitive to their immediate environment. Aside from pH, temperature, nutrient availability, and specific growth factors, salinity alone can rupture cellular walls resulting in immediate death of the organism. Colloidal methods offer a further benefit over alkoxide based systems in that the majority of the network is already present in the sol. Adaptations such as the introduction of osmoprotectants can therefore be applied without significantly interfering with the integrity of inorganic capsule itself [58].

2.3. Metal chelation in the sol–gel methods

In aqueous solution, metal ions are coordinated by a hydration shell, the nature of which depends both on the valence of the specific metal in question and the pH of the solution [59]. The unique combination of the polar solvent coordination and the ability of hydrated metal cations to act as Lewis acids enable the processes of olation and oxolation to take place. This ultimately results in the formation of polymeric oxides in solution [60]. The exact series of reactions that take place are complex and may involve the formation of several aquo- $[M(H_2O)_n]^{z+}$, hydroxo- $[M(H_2O)_n(OH)_{m-n}]^{z+}$ and oxo-$[M(H_2O)_n(O)_{m-n}]^{z+}$ ligands or combination thereof. For a detailed description of the chemistry evolved in the polymerization of hydrated metal ions the reader is referred to Livage et al. [49]. In most basic terms, solvated metal ions ($[M(H_2O)_n]^{z+}$) are able to displace H_2O from neighboring complexes ($[M(H_2O)_n]^{z+}$). With the formation of a hydroxy-ligand ($[M(H_2O)_n(OH)_{m-n}]^{z+}$), –OH is able to act as a bridge between the two hydrated metal complexes. This results in the release of a proton into the aqueous medium and is followed by a subsequent deprotonation event to from a resultant M–O–M covalent bond.

From this brief description alone, the influence of pH on the process can also be deduced; an increase in pH favoring olation with lower pH inhibiting the process. As noted above however, the polymerization process seldom proceeds smoothly throughout aqueous media. Localized shifts in the immediate vicinity of the complex undergoing polymerization leading to the formation of heterogeneous ceramic aggregates, as opposed to an even dispersal that can be produced when sol–gel methods are applied [35,36]. For biomedical applications, sporadic synthesis is by no means ideal to the end function of the material (i.e., as biocompatible coatings, tissue scaffolds or novel composite materials).

Undoubtedly, materials composed of metal oxides exhibit a wide range of desirable properties [5,31,32,36,61] and as a result, a series of methods have been developed based on chelation of metal precursors in order to control the natural polymerization processes. Essentially, metal chelation sol–gel methods employ strong chelating agents (such as citric acid or EDTA) as a means of controlling the formation of the highly reactive hydrated complexes [36,59]. Although discussed here in terms of chelated inorganic precursors, chelation itself is not limited to inorganic processes. Such methods can also be applied to modify the polycondensation of metal alkoxides whereby the rate of reaction is reduced following the replacement of alkoxide leaving groups with a chelating ligand in more stable conformation [62].

In further discerning metal chelation methods from the alkoxide sol–gel route, the underlying principle is that polycondensation of the metal itself occurs through hydration processes described above

(Fig. 2.3) as opposed to the hydrolysis and condensation steps akin to the polymerization of organometallic precursors. Based on a system that made use of triethanolamine (TEA) as an Fe(III) chelating agent, El Haskouri et al. [63] were able to produce mesoporous iron-phosphate–phosphonate materials *via* a district metal chelation sol–gel route. The mesoporous nature of the material was achieved with use of a surfactant system involving TEA and cetyl-trimethylammonium bromide (CTAB); however, the incorporation of Fe(III) within the material itself was made possible through the chelation of the metal with the TEA aspect of the system. Furthermore, the viability of synthesis within a phosphate based network offers a pathway for the design of biomaterials that completely degradation in aqueous media such as biological fluids. Clearly, adjustments to these procedures would require careful planning of the factors that influence the process *ab initio*. Nevertheless, TEA is able to form chelation complexes with a wide range of transition metal elements [64] therefore offering a plausible route for further biologically relevant substitutions within the network.

The use of epoxides as gelation agents provides another useful synthesis pathway. Typically, epoxide routes are most effective when the formal oxidation state of the dopant cation is M^{3+} [34,57] although species that possess a lower valence may also be incorporated. In this instance, the epoxide does not act as a precursor *per se* rather the epoxide group is able to efficiently accept protons leading to the formation of hydrated oxo-ligands $[M(H_2O)_n(O)_{m-n}]^{z+}$. The pH of the reaction medium can therefore be adjusted to a range that favors the less reactive aquo-$[M(H_2O)_n]^{z+}$ coordination until deprotonation in the presence of an epoxide. Although not strictly a chelation-based method, parallels can be observed between this approach and those more typical chelation methods that aim to prevent natural polymerization processes until required.

2.4. Polymer-assisted sol–gel methods

In a natural extension from metal chelates methods are the polymeric sol–gel methods. Essentially, these methods involved the chelation of reactive inorganic gel-forming agents within an organic polymer network although, depending on the material to be produced, chelation is secondary to the stabilisation [65]. In more broader terms, gel-forming agents are maintained in a state of dispersion throughout the solution, thereby preventing the precipitation of aggregates within in the sol [36]. This method does however require subsequent heat treatment to remove the organic polymer following the formation of the inorganic gel. Recently, Yang et al. [66] successfully synthesized nanoscale $LiMn_2O_4$ particles using Pluronic P-123 as stabilising polymer and citric acid as a chelation agent. The nanoparticle exhibited a superior degree of porosity when compared with particles that were synthesized without the presence of the polymer network. Whilst not a biomedical application, the ability to control the textural aspects that influence functionality was clearly demonstrated.

Chemical properties, such as the biomimetic molar ratios of apatites, can also be achieved with polymer assisted stabilisation [65] due to the homogeneous elemental distribution of the gel network. For example, Valliant et al. [67] applied γ-glutamic acid polymers ranging in molecular weight between 30 and 120 kDa to control the spatial distribution of calcium within a typical silica sol–gel network synthesized *via* a TEOS precursor with 3-glycidoxy-propyl-trimethoxysilane as the covalent coupling agent. Their results showed a homogenous distribution of calcium in the silica network, and the larger polymers also appeared to show reduced degradation rates. Here, a biocompatible polymer was purposefully chosen so as to remain within the network and thus avoid processing complications encountered during thermal treatment.

Inorganic networks can also be formed *in situ* through the polymerization of organic precursors [36]. Originally patented by Pechini [68], this method involved the formation of a three-dimensional (3D) polyester network as a result of the reaction between ethylene glycol and citric acid; the citric acid acting as a chelation agent due an available bi-dentate binding mechanism followed by an esterification with ethylene glycol (Fig. 2.4). The organic network can then be removed as with *ex situ* polymers described above.

This route offers a robust and effective means of synthesizing materials that disperse poorly in viscous solutions or that would otherwise form reaction products prior to assembly into the required form. This is especially useful for the calcium phosphates (CaPs) which have a tendency to form a diverse range of minerals when present at low concentration in aqueous solution [69]. This family

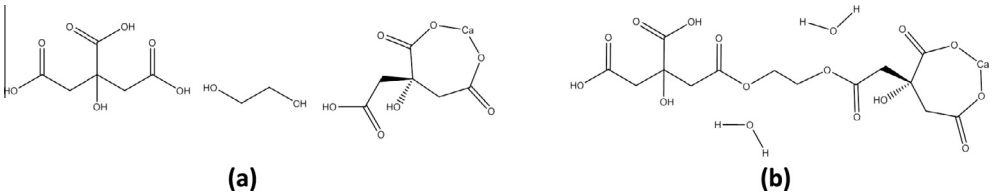

Fig. 2.4. Esterification (condensation) of ethylene glycol and citrate in the presence of a cationic ligand (calcium).

of minerals are extremely important from a biomedical perspective, as they allow for true hard tissue integration and bonding to take place and is utilized in orthopaedics and dentistry for direct implant bonding [48]. Effective production of both biocompatible ceramic-mineral composites [70] and apatites with predefined stoichiometry has been achieved [65,71] with polymer-assisted sol–gel methods. Such research may also have broader implications than in solving issues associated with biocompatibility as, with the advent of controlled deposition of inorganic mineral layers, abiotic hard tissue regeneration may also be within reach.

3. Sol–gel based materials

3.1. Silica-based materials

Silica-based sol–gel materials have been the subject of intense interest for the last three decades [19,32,43]. However, research on sol–gel processing of these materials is dated back to as early as mid-eighteenth century by Ebelmen and Graham [8,11,48]. These authors noticed that a solution of polysilicic or silicon alkoxide, such as TEOS is able to hydrolyze under acidic conditions and in the presence of H_2O. This yielded SiO_2 in the form of a "glass-like" material. Later works were able to obtain a clear film by spreading a colloidal solution of salicylic acid on a spinning substrate [72]. The process of reacting from the liquid allows these materials to be drawn into fibers, micro or nano-sized spheres, or as a thin film on a substrate [1,73,74]. In addition, because of the low processing temperature, there is a possibility to entrap most organic and biomolecules in the sol–gel network during the formation of the gel matrix [6,75]. Biomolecular encapsulation within sol–gel derived silica matrices was first introduced by Braun et al. [76] who successfully entrapped enzymes into TEOS matrices. Following that, Reetz et al. [77] reported sol–gel entrapped lipase enzymes with up to 100 times higher catalytic performance as compared to the free enzymes [77]. Other follow-up (?) studies confirmed the potential applications for encapsulating other biomolecules such as antibodies and phospholipids [78,79].

During the last few decades, silica-based materials have supplied successful solutions for soft and hard tissue regeneration [80]. These materials are highly biocompatible and the positive biological effects of their reaction products, make them an interesting group of materials for tissue regeneration [81]. Silica-based bioactive glasses (BGs) were first synthesized *via* a sol–gel technique by Li et al. [82] at lower processing temperatures compared to the melt-derived glasses. Pereira et al. [83,84] extensively researched sol–gel glasses based on the SiO_2–CaO–P_2O_5 system for biomedical applications. Silica-based sol–gel glasses exhibit many of the properties associated with an ideal material for tissue regeneration, such as high surface area and a porous structure, in terms of overall porosity and pore size that promote cell–material interactions and cell invasion [85]. Research on these glasses showed that the porous structure of these glasses brings higher surface area that exhibits higher tissue bonding rates [86]. Another study by Greenspan et al. [87] confirmed higher rates of HCA formation because of a greater release of soluble silica that nucleates HCA crystals compared to the melt-derived glasses of the same composition.

A sol–gel process, involving the foaming of a sol with the aid of a surfactant, followed by condensation and gelation reactions, has been used to prepare porous scaffolds of a few bioglasses (BGs), such as the glass designated 58S, with the composition (mol%): 60 SiO_2–36 CaO–4 P_2O_5 [88]. The

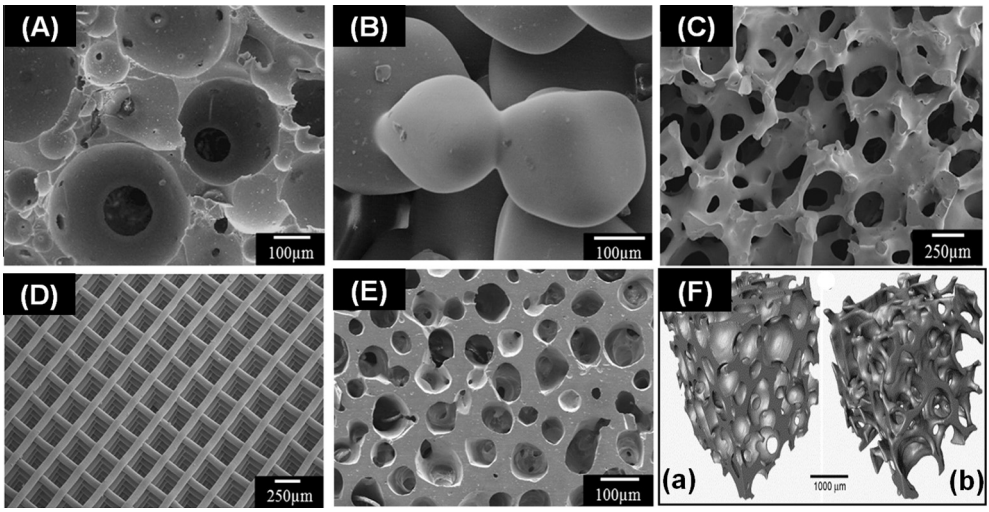

Fig. 3.1. (A–E) Porous structure of bioactive glass scaffolds created by sol–gel methods with different techniques, and (F) micro-computed tomography image of typical scaffold and human trabecular bone [89–92].

as-prepared scaffold had an overall microstructure similar to that of dry human trabecular bone, but the pore structure was hierarchical, consisting of interconnected macropores (>100 μm) resulting from the foaming process and mesopores (less than several tens of nanometers) that are inherent to the sol–gel process [89–92]. Fig. 3.1 illustrates the porous structure of the scaffolds made of bioactive glasses produced by means of sol–gel processes. This hierarchical pore structure of the scaffold is beneficial for stimulating interaction with cells as it mimics the hierarchical structure of many natural tissues (e.g., bone) and more closely simulates the physiological environment of mineralized tissues (?). Thanks to the nanopores in the glass, sol–gel derived scaffolds have a very high surface area (100–200 $m^2 g^{-1}$). As a result, these scaffolds degrade and convert faster to HA than those of melt-derived glass with the same composition. However, these sol–gel-derived scaffolds have a relatively low compressive strength (2–3 MPa) [93], and consequently, they are primarily suitable for applications focused on low load-bearing orthopaedic sites.

The discovery of mesoporous silica nanoparticles (MSNs) in 1992 was quickly recognized as a breakthrough that could lead to a variety of important applications [94]. These materials have uniform cylindrical pores with a diameter size range of 2–30 nm, along with a large surface area between 700 and 1500 $m^2 g^{-1}$ making them ideal for chemical separations, catalysis and biomedical applications [95]. In general, solution synthesis is carried out under a basic condition, which is similar to the traditional Stöber method for preparation of silica particles. Under basic conditions, a part of the silanol group (Si–OH) is deprotonated to form silanolate (Si–O$^-$). In order to match the negatively charged silica surface, cationic surfactants are normally used. Thus, the hydrolysis and condensation rates of the silica sources (e.g., TEOS) are highly associated with several factors such as pH, silica source, additives, and temperature. The effect of pH is critical as it affects nucleation and growth. For example, Lu et al. [96] demonstrated that the particle sizes of MSNs were controlled over a wide range, from 30 to 280 nm, by simply adjusting the pH value of the precursor solutions. As the pH decreased from 11.5 to 10.9, the particle sizes decreased gradually. On the other hand, Qiao et al. found that the particle sizes tended to increase from 30 to 85 nm, as the pH values decreased from 10 to 6.28 [97]. These previous reports hint that the minimum particle size can be obtained at around pH 9–10, indicating that the condensation rates, rather than the hydrolysis rate, of silica precursors highly affect the final particle sizes. In fact, Chiang et al. [98] demonstrated that pH had the largest influence on particle sizes of MSNs, rather than the amount of the silica source or reaction time.

There have been very few trials to prepare MSNs under acidic conditions [99,100]. One of the advantages of acidic conditions is the capability of using block copolymers, which have a templating

effect and allow larger mesopores (>5 nm). The condensation rate for the synthesis at pH 5–8 should be faster than at pH < 5. Since the condensation reaction solidifies the silica network, one can expect that a too rapid condensation reaction will create a cross-linked network faster than the mesostructure organizes. This explanation is based on a formation mechanism where the particle formation, silica condensation, and ordering of the pore system are considered as separate processes. Thus, in order to obtain an ordered material the rates of the different processes must be properly adjusted relative to each other [99]. However, compared with basic synthetic systems, it is difficult to obtain MSNs with uniform particle size less than 100 nm and with spherical morphologies, but the large surface area of the pores allows the MSNs to be filled with different biomolecules for biomedical applications [101].

3.2. Phosphate-based materials

Phosphate-based materials are inorganic polymers, based upon the tetrahedral phosphate anion which is linked to form a 3D network [102]. Despite many structural similarities between silica and phosphate-based materials, they exhibit very different chemical behaviors in solution [103]. As explained, the sol–gel chemistry of silica-based materials has been extensively studied, but very little research has been carried out on the sol–gel synthesis of phosphate-based materials and much fundamental work remains to be done.

The novelty of phosphate-based materials in biomedical applications is related to their solubility and controllable dissolution rate in aqueous media compare to silica-based sol–gel materials [104]. Researchers have reported that these materials can be applied as a third generation of biomaterials that are bioresorbable [104,105]. This property of resorption allows for a variety of new biomedical applications, such as temporary implants that can be replaced with natural tissue as the body repairs a wound or DDSs that allow local and sustained release of macromolecules at the implant site [104,106]. Moreover, the breakdown components are monovalent and divalent ions and oligophosphates, which can be easily metabolised in the body [107]. Studies on phosphate-based melt-derived glasses have found that the degradation rate can be easily altered *via* addition of different modifier oxides such as CaO, TiO_2, and Na_2O, thus allowing one to tailor the persistent of the biomaterial, which is an important parameter in many tissue engineering and drug delivery applications [104].

The idea of using phosphate-based sol–gel derived glasses for biomedical applications was first introduced by Knowles [104], and a few years later Carta et al. [108,109] successfully synthesized ternary P_2O_5–CaO–Na_2O and quaternary P_2O_5–CaO–Na_2O–SiO_2 phosphate-based glasses *via* a sol–gel route. Following studies by the same group confirmed that the structure of sol–gel synthesized glasses is comparable to the melt-derived glasses with the same composition, and similar bioactivity can be expected for a variety of biomedical applications [109]. Pickup et al. [41,46] developed the sol–gel technique to synthesize binary P_2O_5–TiO_2 and ternary P_2O_5–CaO–Na_2O sol–gel derived glasses at lower temperature. Later, these authors showed the potential drug delivery application of these glasses with the subsequent release of drug molecules into an aqueous solution [106].

Biocompatibility and degradation rate of phosphate-based melt-derived glasses has also been extensively studied, but is outside the scope of this review. The interested reader might see the review by Abou Neel et al. [52]. However, pertinent to the sol–gel process, the degradation rate of the ternary P_2O_5–CaO–Na_2O glass system was found to be too high (of the order of hours) for many tissue engineering applications, so oxide elements like titanium oxides are often introduced to reduce the degradation rates [104,110]. However, limits exit with conventional melt-quench techniques in that achieving a TiO_2 content above 8 mol% is generally infeasible. Conversely, the sol–gel approach enables TiO_2 contents to reach up to 15 mol%, therefore greatly increasing the potential range of applications for glass-based materials [26]. Moreover, the challenges associated with tailoring the morphology of melt-derived glasses for biomedical applications can be overcome through further development of the sol–gel route. One point to note is that mesoporous phosphate-based materials have yet to be synthesized by the sol–gel route, and it is likely that this is due to a very small processing window between the loss of organics from the structure and the softening temperature at which the glass collapses. This remains a significantly challenging area for future efforts.

3.3. Metal-based materials (Fe–O, Ti–O, Zn–O, etc.)

Considerable efforts have been spent in the development of iron oxide nanoparticles, particularly those with magnetic properties, i.e., MNPs, the understanding of their magnetic behaviors, and the improvement of their applicability within biomedical research [111,112]. MNPs possessing the appropriate physico-chemical and tailored surface properties have been extensively investigated for drug delivery, magnetic resonance imaging (MRI), tissue engineering and repair, biosensing, biochemical separations, and bioanalysis [111–113]. The ferrite colloids, magnetite (Fe_3O_4) and maghemite (γ-Fe_2O_3), are the main representatives of the MNPs. Due to their biocompatibility and biodegradability these materials have received considerable attention in the medical and pharmaceutical fields [111,114]. The range of applications speaks to the potential value of efficient synthesis methods and, as with the previous examples given, the sol–gel route is properly applicable.

Sol–gel is a facile and convenient way to synthesize iron oxides from aqueous iron-based salt solutions. Addition of a base under inert atmosphere prevents the formation of undesired oxides or changes in the oxidation state of the metal cation [115]. Further to this, the size, shape, and composition of the MNPs highly depends on the type of salt based precursors used, the Fe^{2+} to Fe^{3+} ratio, the reaction temperature, the pH value and ionic strength of the media [18–21]. However, as alluded to above, MNPs are unstable under ambient conditions, and are easily oxidized to maghemite or dissolved in an acidic medium. Since the iron species within maghemite are present in the 3+ oxidation sate, oxidation is of little concern and rather controlling the oxide content of the final ceramic network is most important to proper synthesis. However, both pH sensitivity and the propensity for oxidation to maghemite can be exploited through typical sol–gel means. In this instance, transformation is achieved by dispersing magnetite (a mineral possessing iron in both ferric and ferrous oxidation states) in acidic medium, then addition of ferric iron nitrate. The maghemite particles obtained are then chemically stable in alkaline and acidic medium [18–21]. However, even if the magnetite particles are converted into maghemite after their initial formation, further experimental challenges in the synthesis of Fe_3O_4 by sol–gel lies in control of the particle size and thus achieving a narrow or uniform particle size distribution. Since the blocking temperature depends on particle size, a wide particle size distribution will result in a wide range of blocking temperatures and therefore non-ideal magnetic behavior for many applications. At present, particles prepared by sol–gel unfortunately tend to be rather polydisperse [18–21]. However, it is well known that a short burst of nucleation and subsequent slow controlled growth are crucial to produce monodisperse particles [116]. Controlling these processes is therefore the key in the production of monodisperse iron oxide MNPs.

As one of the most common materials used in biomedical research, methods for the preparation and extended uses of titanium dioxide (TiO_2) have been the subject of interest for many years. Specifically biomedical applications of TiO_2 have motivated strong interest owing to its unique photocatalytic properties, excellent biocompatibility, high chemical stability, and low toxicity [117]. Advances in nanoscale science suggest that some of the current problems associated with alternative materials could be resolved or at least improved through applying TiO_2. For example, the TiO_2 content of phosphate-based glasses produced by the sol–gel route can be far higher than is possible by conventional melt-quench techniques [26]. Titanium itself naturally forms in four main phases: rutile, anatase, brookite, and monoclinic TiO_2. The relative stability of the four titania phases depends on particle size, with rutile being the thermodynamically stable form in bulk titanium but anatase being the most stable phase at sizes below 14 nm [118]. Brookite and monoclinic TiO_2 are metastable forms that are not commonly observed in minerals and are difficult to synthesize in pure form. It therefore stands to reason that the sol–gel approach would be able to improve the range of titanium-based materials that can be effectively produced and would thus enable exploitation of their respective beneficial properties [119].

In early examples, particle sizes obtained *via* the sol–gel method were several hundreds of nanometers. For example, Matijević et al. [120] described the preparation of uniform titania spheres by hydrolysis of $TiCl_4$ in highly acidic HCl solutions containing sulfate ions. This step was followed by aging for long periods of time (days or weeks). Similar uniform micrometer-size particles were prepared by Barringer and Bowen [121] through the fast hydrolysis of titanium ethoxide or isopropoxide precursors. The most important step in their preparation was the promotion of homogeneous

nucleation during hydrolysis and uniform growth of the nuclei by guaranteeing colloidal stability to the growing particles. However, porous and nonporous monodisperse spheres were reported more recently by a similar procedure but with addition of polymers to promote the pore formation [122]. Yet more recently, titania particle size was controlled to achieve smaller size regimes. Morales et al. [123] studied the hydrolysis of titanium ethoxide in the presence of hydrolyzing agents. These authors investigated the consequences of adding several acids and bases as additives during the synthesis and found some contradictory results. Use of HCl at mild acidic pH resulted in the isolation of crystalline particles containing all three phases of titania. On the other hand, use of oxalic acid or ammonium hydroxide caused the formation of mainly amorphous titania phase. In another report, in the presence of 0.1 M HNO_3 and titanium butoxide, 3.3 nm anatase particles are obtained [124]. From this brief history, a clear development in the sol–gel approach to the production of TiO_2 NPs can be seen.

One of the main problems faced in sol–gel chemistry is proper control of the hydrolysis and condensation rates when using titanium precursors. As described above, the metal chelating method can be an attractive way to overcome this issue by modifying the chemical activity of the precursors with complexing ligands that reduce the rate of or prevent hydrolysis. Scolan and Sanchez [125] used acetylacetone as such a ligand and conducted the hydrolysis in the presence of *p*-toluenesulfonic acid to obtain crystalline, dispersible anatase NPs (1–5 nm) whereas Khanna et al. [126] similarly used myristic acid to prepare 5 nm anatase nanocrystals with colloidal stability. Jiu et al. [127,128] used a combination of the surfactants F127 and CTAB to drive the hydrolysis of titanium tetraisopropoxide (TTIP) modified by acetylacetone. However, in this case, anatase particles of 3–5 nm in size were obtained only after calcination at 450 °C to promote crystallization.

In another variation of the classical sol–gel method, in the early 1990s Sugimoto and Sakata [129] developed the so-called "gel–sol" method. Originally applied to the preparation of α-Fe_2O_3 particles [129], it is based on the preparation of a metal hydroxide gel that is then aged to obtain a sol in which colloidal particles are dispersed. By this technique, colloidal dispersions of titania particles can also be produced by a combination of the sol–gel methods and an anodic alumina membrane (AAM) template. TiO_2 nanorods have also been successfully synthesized by dipping porous AAMs into a boiled TiO_2 sol followed by drying and heating processes [130]. By electrophoretic deposition of TiO_2 colloidal suspensions into the pores of an AAM, ordered TiO_2 nanowire arrays can be obtained [131]. Porous TiO_2 based films have been obtained by the sol–gel method using tetrabutoxytitanium and polyethylene glycol (PEG) as the precursor and template, respectively [132]. The morphology of porous TiO_2 was shown to be dependent on the amount of water, type of solvent, complexing agent(s), and the concentration and molecular weight of the template.

Metal oxide NPs, including ZnO, are versatile platforms for biomedical applications and therapeutic intervention, especially in the treatment and imaging of cancers. There is an urgent need to develop new classes of anticancer agents, and recent studies demonstrate that ZnO NPs hold considerable promise. The concentration of various chemical groups ($-ZnOH_2^+$, –ZnOH, $-ZnO^-$) on the surface of ZnO NPs is pH dependent [133] and the availability of these reactive groups lends ZnO NPs to antibody/protein functionalisation *via* N-hydroxysuccinimide/1-ethyl-3-(3-dimethyl-aminopropyl) carbodiimide (NHS/EDC) coupling chemistry [134], as well as other standard coupling approaches which can further improve cancer cell targeting.

ZnO NPs have also been shown to exhibit strong protein adsorption properties, which can be exploited to modulate their cytotoxicity, metabolism or other cellular responses [135]. The sol–gel method proposed by Spanhel and Anderson [136] in 1991 is commonly used to obtain ZnO nanometer-sized particles to prepare nanoparticulate films with strong visible luminescent properties, which are useful for optical and imaging methods [137]. Otherwise, the choice of acid or basic catalysis and the temperature was pointed out to play a key role in the rates of the hydrolysis–condensation reaction and in the equilibrium concentration of dissolved Zn^{2+} species, leading to changes in the size and shape of ZnO-based NPs [138].

The favorable optical properties of NPs obtained by the sol–gel method have also become a common topic of research as reflected in numerous scientific publications [136–138]. Benhebal et al. [139] prepared ZnO powder by sol–gel method from zinc acetate dihydrate, oxalic acid, using ethanol as solvent. Yue et al. [140] also obtained ZnO by the sol–gel method. High-filling, uniform, ordered ZnO nanotubes have been successfully prepared by sol–gel method into ultrathin anodised aluminum oxide

membranes. Integrating the ultrathin anodised aluminum oxide membranes with the sol–gel technique may help to fabricate high-quality 1D nanomaterials and to extend its application as a template for nanostructures growth.

Sol–gel routes are regarded as the optimal method for modifying ZnO quantum dots (QDs), because the synthetic reactions proceed near room temperature and do not harm the structure of the nanomaterial [141]. Previously reported ZnO NPs with various capping groups, including polyvinylpyrrolidone [142], oleic acid together with diethanolamine [143], polyethylene glycol methyl ether [144], and polymethylmethacrylate [145] among others. These materials tend to possess a series of surface associated ligands that effectively link drugs within a stabilizing steric shell. For example, the core–shell model based on ZnO NPs enables drug loading, although further modification of the shell itself can also be achieved *via* the sol–gel route [146]. The addition of folate groups to the NPs allows for preferential localization toward cancerous tissue which, for the majority of cancers, tend to have a relatively higher proportion of folate receptors in comparison to non-cancerous tissues [147]. Thus, the specific design of the NP system can be tailored to localize agents to a given site and deliver payloads with far greater efficacy with reduced systemic effects [148]. Beyond targeting cell surface receptors, these materials may also be engineered to enter cells through intercellular endocytotic pathways and release drugs to specific intracellular target sites [149].

3.4. Calcium phosphate based materials

Calcium phosphate (CaP)-based ceramics are widely used in medicine as bone substitutes, implants, and coatings on dental and orthopaedic prostheses [150]. Because of their chemical and structural similarities to the inorganic phase of human bone, hydroxyapatite (HA) and other calcium phosphates such as α- or β-tricalcium phosphate (α- or β-TCP) show excellent biocompatibility. In the last decade, HA/β-TCP biphasic materials [151] as well as silicon-substituted HA have been incorporated into clinical practice [152,153]. Most of the relevant application properties of these materials, including their biological influence on tissues and especially their biodegradation behavior, are determined by their chemical composition, morphology and surface topology. Therefore, proper material design offers numerous possibilities for the use of CaP materials in hard tissue replacement or regeneration, and, depending on the processing and formulation, drugs can either be incorporated during the ceramic processing or be surface associated at the end of the synthesis process [154,155]. These uses demonstrate further versatility of the sol–gel process.

The CaP system represents one of the most complex families of materials due to the existence of a myriad of phosphate compounds. Furthermore, the stability of each of the phosphates is affected by not only small compositional changes but also by the variations in pH and the reaction. Some of the CaP compositions like α-TCP and tetracalcium phosphate (TTCP) are able to harden in aqueous solution, allowing for cement applications, such as injectable biomaterials to treat bone defects. Among the phases possible within a hydrated system composed of calcium and phosphate only, HA is the most similar to natural tooth and bone. This is also the most stable mineral phase in aqueous solution, meaning that aqueous degradation of CaP-based materials including CaP cements ultimately results in the formation of HA crystals. It is this complexity that makes this family of materials unique and one of the most interesting class of inorganic biomaterials.

Understandably, sol–gel synthesis of HA ceramics has recently attracted much attention [15,16,156–166] as this method offers a molecular-level mixing of the calcium and phosphorus precursors and is capable of improving chemical homogeneity of the resulting mineral composite in comparison with conventional solid state reactions [167], wet precipitation [168,169], and hydrothermal synthesis [170]. As alkoxide-based routes maintain a largely anhydrous medium, precipitation of undesirable CaP phases can be minimized and the molar concentration of the reactive species can be raised to a point that favors the desired mineral form before initiation of the reaction. Likewise, this same degree of control is afforded through the prevention of precipitation by chelation-based sol–gel methods.

The synthesis of pure HA requires a correct molar ratio of 1.67 between calcium and phosphate in the final product. Besides the difference in chemical activity of sol–gel precursors, it appears that the temperature that is required to form the apatitic structure depends largely on the chemical nature of

the precursors. For instance, Gross et al. [160] used calcium diethoxide ($Ca(OEt)_2$) and triethyl phosphate ($PO(OEt)_3$) to form pure HA phase at temperatures above 600 °C. These authors also found that an ageing time longer than 24 h is critical for the solution system to stabilize its crystal structure and improve the stoichiometry of the resultant mineral [160]. In a similar fashion, Jillavenkatesa and Condrate [164] synthesized a mixture of HA and CaO at 775 °C using calcium acetate ($Ca(C_2H_3O_2)_2$) and triethyl phosphate as precursors although further hydrochloric acid leaching was required in that process to eliminate CaO, and obtain a pure HA phase. Conversely, Brendel et al. [159] obtained HA at temperatures as low as 400 °C using calcium nitrate ($Ca(NO_3)_2{\cdot}4H_2O$) and phenyldichlorophosphite ($C_6H_5PCl_2$) as precursors. However, the resulting HA phase produced by Brendel et al. [159] exhibited low purity with a poor degree of crystallinity in the hexagonal unit cell. As expected, further increases in the synthesis temperature resulted in a pure, well-crystallized HA phase. Several other examples exist which serve to illustrate this same point; i.e. although plausible avenues exist for the sol–gel synthesis of CaP-based materials this area is yet to reach fruition. As noted above, one of the most promising aspects of sol–gel methods is the lower synthesis temperatures that lead to a greater range of compatible substrate materials and lower economic costs. Whilst sol–gel methods do generally require lower reaction temperatures, further work is needed in order to produce HA coatings as viable option.

Phosphorus alkoxides have frequently been used as the phosphorus precursors for sol–gel HA synthesis in recent years. Triethyl phosphate and triethyl phosphite are major precursors among them [15,16,156–160,164,166]. However, the hydrolysis activity of the triethyl phosphate is relatively poor and a higher solution temperature together with a prolonged time period are needed to form the HA phase [171]. Alternatively, triethyl phosphite offers a much higher set of reaction kinetics [172,173]. Recent studies also revealed a valence transition from P(III) to P(V) upon ageing with calcium precursors to form HA within 24 h [160]. This indicates a nucleophilic addition of negatively charged OH^- groups to the positively charged metal P, leading to an increased coordination number of the phosphorus atom, which is essentially an indication of the polymerization reaction [174]. After subsequent protonation of the alkoxide ligands (–OR) and removal of the charged ligand $(-OR)^+$, P–(OR) hydrolyzes to form P–(OH) [167,175] following interaction with Ca precursor to develop the apatitic structure.

In general, the shape, size and specific surface area of the apatite NPs appear to be very sensitive to both the reaction temperature and the reactant addition rate [176]. Both Han et al. [177] and Liu et al. [24] were able to synthesize HA *via* non-template-mediated and a template-mediated sol–gel techniques, respectively. Liu et al. [178] used triethyl orthophosphate and calcium nitrate as the initial chemicals for nanosized HA synthesis. This process did however require a high temperature and produces a multi-phase powder. However, a relatively simple sol–gel process using ethanol and/or water as a solvent has also been reported to obtain stoichiometric, nanocrystalline single-phase HA [179]. Nanocrystalline HA powder was also synthesized at a low calcination temperature of 750 °C by the citric acid sol–gel combustion method [177]. The attractive features of this method were that it synthesized materials with a high purity, a better homogeneity and a high surface area within only a single step.

At present, for all those clinical applications where load-bearing properties are required, most of the implants used are metallic, with subsequent and serious problems due to: the large differences in mechanical properties between the artificial implant and the natural bone, giving rise to ruptures, the presence of ions that, released from the artificial implant, could be toxic or harmful and provoke pains, and the impossibility to regenerate natural bone. An alternative option is therefore to coat the metallic implant with bioactive ceramics. This technique is currently being used both for dental implants and hip joint prosthesis. The ceramic coating process on a metallic substrate is, however, quite complicated, and several methods are available in this sense. A great deal of the clinical success depends on this coating, since the quality and durability of the interface attachment greatly depend on the purity, particle size, chemical composition of the coating, layer thickness and surface morphology of the substrate.

The versatility of the sol–gel method thus creates great opportunities to form 'thin film' coatings. Whilst somewhat high temperatures are often required, the approach provides significantly milder conditions for the synthesis of HA films. This result in a much better structural integrity whereas

the defects that originated from thick coatings *via* a conventional plasma spraying can be largely avoided [180]. Furthermore, the lower temperature synthesis particularly benefits the metal substrates where the mechanical degradation or phase transition of the underlying Ti or Ti-alloy (i.e. α to β phase transition) can be prevented. However, thermal treatment of HA sol–gel films under vacuum environment is frequently required to avoid metal oxidation. This leads to structural instability of the HA coating as a result of the evolution of water during thermal treatment. Therefore, from both the economic and practical points of view, thermal treatment of the HA coating should be performed in air, and below the transition temperature of the substrate. In order to minimize oxidation of the underlying substrate, a thermal treatment temperature should be selected at a minimum level that still assures sufficient quality of HA film, in terms of crystallinity, film integrity, and adhesion to the substrate. For examples, at temperatures below 500 °C, oxidation of the underlying Ti or Ti-alloy is negligible due to the presence of a natural, dense oxide layer on the metal implants [181,182]. This means that, for the purposes of coating Ti-based metal implants, temperatures below 500° are preferable. Optimization of the film deposition has also been carried out [183]; single phase HA coatings were deposited on Ti_6Al_4V by the sol–gel dipping technique from aqueous solutions containing triethyl phosphite and calcium nitrate. In order to obtain homogeneous and monophasic HA coatings, the ageing time and temperature of the sol were the variables studied. The pH measurement is also a valuable tool to evaluate the best conditions of sol–gel deposited coatings. The higher the sol temperature, the shorter the ageing time needed to obtain pure HA after coating annealing. When the ageing parameters or the annealing temperature are not adequately controlled, additional phases or poor surfaces are obtained. The conditions to obtain the best coatings have been related with the pH decrease on the aqueous sols observed during the ageing, according to the polymerization reaction between calcium and phosphorous. In order to obtain homogeneous, crack-free coatings, the annealing temperature and thickness of the coatings should also be controlled. Films roughness is related with the viscosity of the sol-precursor used to do the deposition, as well as with the number of coating layers. Thus depending on the exact application, various parameters of the coating that is applied can be adequately controlled.

3.5. Organic and inorganic hybrid materials

Organic and inorganic hybrids are the materials composed of intimately distributed organic and inorganic phases. Each phase of the hybrid materials has scale from 1 to 100 nm and the types of hybrid materials range from molecular level donor–acceptor complexes to fiber-reinforced nanocomposites according to the dimension of each phase. In the late 20th century, the current concept of organic–inorganic hybrid materials, so-called functional hybrid materials, have been developed based on soft chemistry. In the biomedical field, the inorganic–organic hybrids have also gained much interest because each component can complement each other's features including mechanical properties, biological properties and hydrophilicity. Meanwhile, there are also numerous cases of organic–inorganic hybrid structures in nature, including bone and nacre. This also suggests that the organic–inorganic hybrid materials have high potential in biomedical field.

The inorganic–organic hybrid materials might be sorted by means of the predominant phase, i.e. organic–inorganic or inorganic–organic materials. However, this is not generally accepted because there are many intermediate cases. The hybrid material can be distinguishable from general nanocomposites because it is not a physical mixture and there are chemical reactions between each phase. Thus, the classification of the hybrid materials is usually made according to the nature of interaction between organic and inorganic phases [184,185]. Class I indicates hybrids which do not contain covalent or ionic-covalent bond between the organic and inorganic phases. Instead, each component interacts by only weak interactions, such as hydrogen bond, van der Waals bond, π–π interaction or electrostatic forces. Maya blue, mentioned above, belongs to this class. Contrast with Class I, Class II hybrids refers to materials in which a part of organic and inorganic components are linked to each other by strong chemical bondings such as covalent or ionic-covalent bonds.

Class I hybrids can be produced by several approaches including hydrolysis–condensation of alkoxides in organic polymers and mixing alkoxides and organic components. Some hybrids made in this approach include homogeneously dispersed composites including polyphosphazene–metal oxide

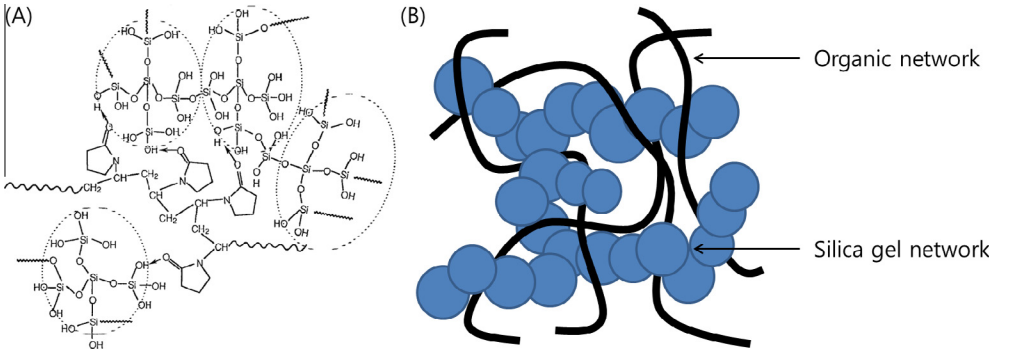

Fig. 3.2. Schematic diagram of (A) molecular structure of PVP-silica hybrid and (B) hybrid with interpenetrating SiO_2 and organic gel networks structure.

(Si, Ti, Al and Zr) [186–188], silica–PDMAAm [189], silica–PVP composites [190], PDMS–SiO_2 [191], Poly(n-butylmethacrylate)–titanium oxide [192] and PMMA–silica hybrids [193]. Fig. 3.2A shows the representative scheme of PVP–silica hybrid material. This class of materials can form hydrogen bonds between hydroxyl groups of sol–gel oxides and amide, carboxyl or carbonyl groups that exist in polymer chains, and can show improved mechanical properties and flexibility compared to those of materials composed of a single polymer component. The second approach is to make hybrids with interpenetrating inorganic and organic substance networks [194,195]. Fig. 3.2B shows the schematic diagram of hybrid material, which has interpenetrating SiO_2 and organic gel network structure. The interpenetrating 3D networks are formed by simultaneous gelation of organic and inorganic components. Because the polymer phase is often precipitated in water–alcohol based solvents, cyclic alkenyl monomers, which polymerize by ring opening metathesis or unsaturated alcohols which polymerize by a radical mechanism were selected as organic component. Through this approach, elastic hydrogel, flexible rubber and hard glass with mesoporous networks are obtained, which are highly biocompatible, show reduction of shrinkages and good physiochemical stability [196]. From a biomedical perspective, the most useful inorganic component of organic–inorganic hybrid materials is bioactive glass (BG). The BG usually has SiO_2–CaO–P_2O_5, SiO_2–CaO or SiO_2–CaO–Na_2O systems. For example, calcium-containing hybrids like the PDMS–CaO–SiO_2 reported by Kokubo et al. [197] revealed HA-forming ability in SBF solution.

For biomedical purposes, well-known degradable synthetic or natural biopolymers, including PVA [198,199], poly(ε-caprolactone) (PCL) [200,201], gelatin [202] chitosan [203–205] and PEG [206] have been used. Typically, these types of hybrid materials were prepared by mixing of polymer solution with silica-based sol and then gelation. Very recent work has also investigated TiO_2–PCL hybrids [207]. Very recently, ZrO2/PCL hybrids have also been investigated as an implant coating [208]. Although these materials are classified as Class I, the organic and inorganic components are sometimes connected by covalent bonds. Pereira et al. [198] reported that C–OH bonds in PVA were converted into C–O–Si bonds by esterification reactions, which were observed by infrared spectroscopy. Because of the good electrospinnability, these hybrids have frequently been obtained as electrospun nanofiber membrane forms which are known to promote desirable cellular behaviors [201,202]. Furthermore, since the process is carried out under mild conditions at low temperature, these hybrids materials can also be used for delivering of biomolecules such as drugs and growth factors [204,209] which would otherwise degrade under harsh synthesis conditions.

In Class II hybrid materials, a part of organic and inorganic components are connected by covalent or ionic-covalent bonding. To obtain this type of material, organically modified alkoxysilanes precursors such as R′nSi(OR)$_4$-n or (OR)$_4$-nSi-R″-Si(OR)$_4$-n (with n = 1, 2, 3) are firstly prepared and then the hybrid materials formed through hydrolysis and condensation process. In the hybrid, the organofunctional group, R′, affects the networks depending on their chemical structure. If R′ is nonhydrolyzable group it will act as a network modifier. On the other hand, if R′ can react with itself or with additional

polymerizable monomers, it will act as a network former. In similar ways, mixing of di- or tri-functional alkoxysilanes will tune the mechanical and functional properties of produced hybrid materials. Along with Class I hybrid materials, the organic components of Class II hybrid materials should be biocompatible for biomedical use. The representative organic components used in the fabrication of these hybrids are synthetic polymers (PEG, PCL) and natural polymers including proteins (gelatin) and polysaccharides (chitosan). Yamamoto et al. [210] developed PEG–SiO_2 ormosil using triethoxysilyl-terminated PEG and TEOS. To obtain triethoxysilyl-terminated PEG, allyl-group terminated PEG was reacted with triethoxysilane with hexachloroplatinic acid as a catalyst. Due to the presence of silanol groups [211], the fabricated hybrid material showed excellent bone-like apatite forming ability in SBF. The PCL–silica ormosil was also prepared in similar way by Rhee et al. [212]. For the sol–gel reaction the PCL molecules were end-capped with TEOS. This functionalised PCL was then reacted with TEOS containing calcium nitrate tetrahydrate as Ca source. As expected, this hybrid sample showed remarkably improved apatite forming ability in SBF. The natural-origin organic molecules also can be modified by TMOS or TEOS for enhancing their reactivity. Gelatin–SiO_2 systems showed enhanced apatite-forming ability [213] and osteoblast biocompatibility [214]. Meanwhile, chitosan–siloxane hybrid revealed enhanced apatite-forming ability with interesting photoluminiscent properties [215].

Most recently, new materials called cerasomes were reported by Ariga et al. [216] which served to mimic natural liposomes. These nanostructures were synthesized by a dual process of sol–gel and self-assembly of organic chain containing organoalkoxysilanes [217]. Two structural types of supramolecular materials, of either a lamellar or hexagonal long-range periodicity, could be obtained in a controlled way depending on the amount of silica involved during the synthesis. The intratubular swelling of these materials is related to the flexible nature of the silica walls. The procedure of self-templating synthesis works for cationic surfactants bonded to silica, but it is also expected to work with both neutral (polyoxyethylene-based) or anionic (long-chain carboxylate-, phosphate-, or sulfonate-containing alkyl-based) surfactants. The new compounds could serve to prepare new mesoporous silica materials and also as models for biological membranes and, in particular, for investigations of the diffusion of ions and lipophilic substances through them [217]. These new hybrids are able to incorporate different organophyllic substances, having a high potential for application in DDS [218,219].

4. Physical, chemical and biological properties

4.1. Mesoporous structure

4.1.1. Mesopore generation

The porous structure of sol–gel materials is usually formed during synthesis or by subsequent treatment. Depending on the predominant pore size, the porous materials are classified following the IUPAC system: microporous materials, having pore diameters up to 2.0 nm; mesoporous, having pore sizes intermediate between 2.0 and 50.0 nm; and macroporous materials, having pore sizes exceeding 50.0 nm [220]. The pores are either isolated or interconnected that may have similar (homogenous) or dissimilar (heterogeneous) shape and size distributions. Furthermore, the pore shape can be roughly approximated by any of the following three basic pore models: cylindrical, ink-bottled, and slit-shaped pores [221–223].

These mesopores presenting ordered structures of subnanometers to tens of nanometers in scale could be built from the sol–gel processes, and the templating through a supramolecular chemistry. Overall, a meso-scaled hybrid phase is produced in the first stage composed of inorganic building blocks and an entrapped organized supramolecular template. This step is followed by a template removal, which leads to the actual mesoporous structure. The formation of the first meso-scaled hybrid phase is critical in obtaining a reproducible mesoporous material with tailored features [224]. A complex co-assembly of inorganic and organic building blocks that gives rise to well-defined framework walls and pore template regions takes place during the precipitation or gelation of the system. Control of this first step is essential to define the characteristic interaction lengths that control the nascent meso-phase. The main driving forces toward obtaining organized templated

meso-phases have been presented in the literature and the relevant thermodynamic and kinetic factors have also been analyzed in detail [225,226]. However, the interactions between the inorganic components and the organic template are among the most important thermodynamic drivers, and usually determine the feasibility of meso-structure formation as well as its resultant topology.

Organic–inorganic interactions are in turn determined by the composition of the initial systems, and the adequate size and hydrophilicity of the inorganic building blocks, in order to properly locate both kinds of building blocks in space. Regarding the kinetics, the cooperative formation of an organized hybrid meso-structure is a result of the delicate balance of phase separation and organization of the template and inorganic polymerization. It has been proposed that processes linked to phase separation and organization at the hybrid interface between the inorganic building blocks and the template must be faster than the inorganic condensation that leads to "freezing" of a continuous matrix [227]. Winning this "race toward order" leads to highly organized meso-phases. In the event that the rate of inorganic condensation takes over that of template assembly, or co-assembly at the hybrid interface, poorly ordered meso-phases will result [226,228]. With insight as to processes that govern pore generation, opportunities to exploit are also presented. This has ultimately led to successful manipulation of the synthesis route.

4.1.2. Controlling pore structure

Pore size depends on the chain length of the surfactant employed during synthesis but also on other parameters of the synthesis process. Different methods have been developed to control pore size by adding auxiliary organic molecules, which are solubilised in the hydrophobic micellar region, thus increasing the micellar, and in turn pore size [229,230]. These particular methods not only create the possibility of incorporating larger molecules, but also influences the release rate of molecules as pore size also affects the diffusion of loaded drugs to the delivery medium [231]. However, other factors such as pore ordering [232], particle morphology [233] and the macroscopic form [232] can also determine adsorption and drug release kinetics. In a natural extension from this, the use of binary surfactants of different molecular weights in the synthesis of surfactant-templated meso-structure can also lead to the formation of dual-mesoporous materials. For example, Niu et al. [234] synthesized core–shell structured MSNs with bimodal mesopores consisting of smaller pores (2.0 nm) in the shell and larger tunable pores (12.8–18.5 nm) in the core. This was achieved by utilizing an amphiphilic block copolymer (polystyrene-b-poly(acrylic acid), PS-b-PAA) and CTAB as co-templates. In an aqueous ammonia solution, the hydrophilic PAA blocks of rod-like aggregates could couple with the CTAB micelles *via* electrostatic interaction between CTA^+ and PAA^- to form composite rod-like micelles. After the subsequent silicate deposition on the rod-like micelles, and cooperative self-assembly between the rich CTAB and additional TEOS, core–shell dual-mesoporous MSNs were obtained. Wiesner and co-workers also synthesized highly aminated MSNs with cubic Pm3n symmetry and successfully controlled the sizes of particles. In contrast to previous studies, it is worth noting that using ethyl acetate in the aqueous ammonia solution could effectively elevate the amount of aminosilane incorporated in the MSNs, while still maintaining the meso-structural ordering [235].

Although the pore size of sol–gel based materials could be controlled somewhat by varying the chain length of the surfactants used, the range is rather limited (1.8–2.3 nm). It would be desirable to further expand the pore size of MSNs to accommodate larger biopolymers. However, this is often difficult as most synthesis conditions for MSNs are tuned for surfactants such as CTAB. Recently, Fuertes et al. [236] used DMHA and TMB as swelling agents to synthesize pore-expanded MSNs that were able to adsorb a large amount of protein. Likewise, Kim et al. [237] synthesized MSNs using TMB and a sol–gel method to obtain large pore sizes of MSNs for gene delivery whereas Zhang et al. [238] used TMB and decane to synthesize pore-enlarged magnetic MSNs as DNA carriers. An alternative way to make MSNs of larger pore size is to use block-polymers as templates. Whichever the specific way these feats are achieved, their purposes are similar; that is, to increase the loading capacity of the MSNs and to expand the range of agents that can be loaded.

In many applications, pore size can be controlled to meet the given requirements (Fig. 4.1). Moreover, organic functional groups should be kept unchanged throughout the preparation process. MSNs with uniform pore size and a long-range ordered pore structure were first reported in the early 1990s [94,239]. With the abundant availability of various types of surfactants, MSNs with different

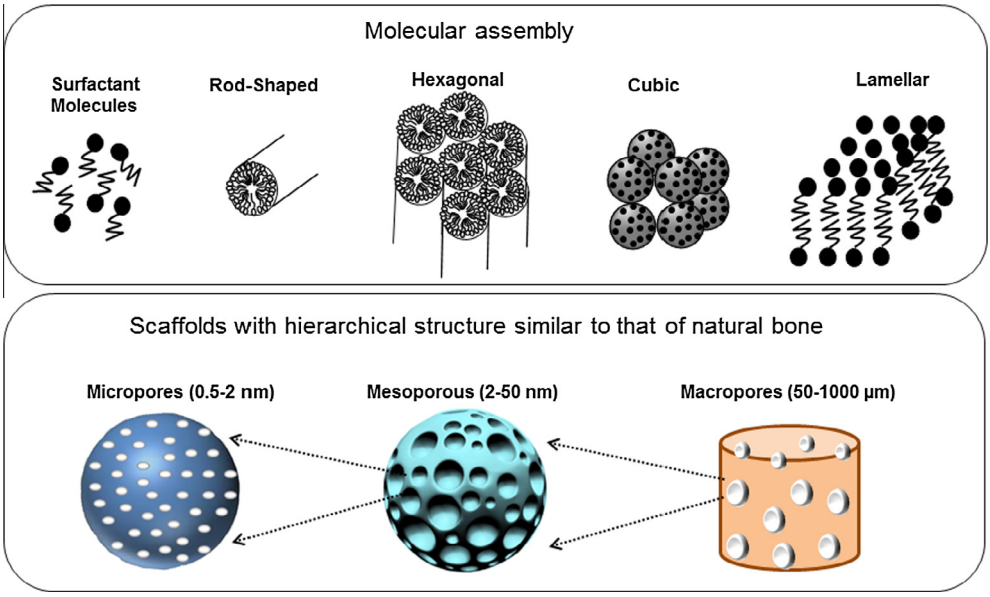

Fig. 4.1. Molecular assembly of the structural hierarchy and the different pore levels generated to form scaffolds targeted for bone repair.

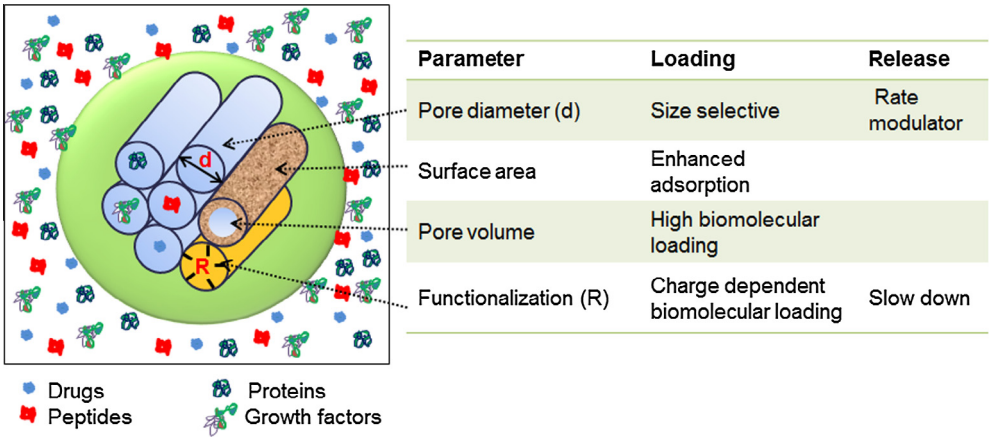

Parameter	Loading	Release
Pore diameter (d)	Size selective	Rate modulator
Surface area	Enhanced adsorption	
Pore volume	High biomolecular loading	
Functionalization (R)	Charge dependent biomolecular loading	Slow down

Fig. 4.2. Parameters that govern the loading capacity and release rate of biomolecules (drugs, proteins, peptides, and growth factors) in mesoporous materials.

structures have since been developed. However, the defining properties of any mesoporous materials are typically the pore structure and size.

Pore structure can be measured by low angle powder X-ray diffraction and by transmission electron microscopy whereas pore volume is usually measured by nitrogen gas sorption. Wall thickness, on the other hand, is usually determined by a combination of the X-ray diffraction data and the pore size distribution obtained from nitrogen gas sorption analysis. The most common meso-phases in silica with pore sizes between 2 and 5 nm are the 2D hexagonal *p6m*, the 3D cubic *Ia3d* and the lamellar

p^2 corresponding to MCM-41, MCM-48 and MCM-50 materials, respectively [240]. For silica materials with larger pore sizes SBA-15, with 2D hexagonal *p6mm* structure, was firstly synthesized in highly acidic media using amphiphilic triblock copolymer of poly(ethylene oxide)–poly(propylene oxide)–poly(ethylene oxide) ($EO_{20}PO_{70}E_{20}$, P123) as a template [241].

4.2. Morphology and shape

Materials in a variety of different shapes and morphologies can be produced at the micro-and macro-scale with the use of sol–gel methods. Thin films, bulk glasses, porous foams, fibers, microspheres and nanoparticles are but some examples. However, there is also an obvious prolonged interest in research on coatings for biomedical devices. Such coatings are thought to provide a high degree of biocompatibility and promote the healing response without causing severe reactions [242]. Thin or thick films can be made by spray, spin, and dip coating techniques and used on medical implants. For example, silica nanosols doped with silver are well suited as a simple antimicrobial coating [243]. As with mesoporous NPs, sol–gel derived films can also be used as drug delivery carriers by controlling the thickness and the pore-size distribution of the coating [244]. These materials can have a huge impact as a dressing for wound healing or by preventing wounds from further injury, bacterial invasion, and promoting natural healing process. Biodegradable silica fibers have been shown promise to act as a scaffold for cells with controlled release of drugs and antibacterial properties to promote wound healing [245]. Mesoporous materials are also able to encapsulate relatively large amounts of bioactive molecules. These materials with their high surface area, large pore volume and tunable pore size with a narrow distribution are suitable for various controlled drug release applications. The drug release rate can be designed to range from very slow, by materials with lower total porosity and smaller average pore size, to very fast with higher total porosity and larger average pore sizes [246].

The 3D foam scaffolds based on sol–gel route are considered an important class of biomaterials for tissue engineering that can be processed to achieve hierarchically structured macro- and meso-pores found in many tissues. Recently, some attempts at fabricating multi-scale sol–gel based scaffolds have been carried out by using proper sol–gel precursors and processing techniques in which the pore size and arrangement were carefully controlled and designed. The purpose of such scaffolds is twofold, as they combine the properties of traditional glass-derived scaffolds with the unique features supplied by mesoporous materials. Therefore, the development of highly porous 3D scaffolds with the BG compositions proven in repairing bone tissue can take the benefits of bioactive composition and porous morphology. In particular, the well-defined multi-scale porous 3D scaffolds, compared to the conventional porous scaffolds, can provide advantages for bone regeneration, with their micro- or meso-pores having the capacity to incorporate therapeutic molecules while the macro-pore channels (mostly above 100 μm) allow for cell migration, nutrient delivery, bone ingrowth, and eventually vascularisation [247–250].

The mesopores in the BG compositions are generated in a similar way to those in MSNs, through the supramolecular chemistry in sol–gel process. In fact, the mesoporous BG (MBG) materials can be produced either by melt-quenching or via a sol–gel route [91,247,250–253]. Compared to melt-quenching, sol–gel methods enable a broader range of compositions and mesopore structures. Furthermore, the macro-pore channels can be given to the sol–gel MGB materials by introducing foaming agents (e.g., hydrogen peroxide, surfactants) or porogen materials (e.g., polystyrene spheres, polyvinyl alcohol, polyethylene glycol, etc.) [254–257].

Although the MBGs have the advantages of tunable chemical composition, higher specific surface area and pore volume, and uniform mesopore size, studies on 3D porous scaffolds based on MBGs have just begun [258,259]. Yun et al. [260] prepared hierarchical mesoporous–macroporous MBG spheres with a size of several hundred micrometers in a hydrophobic solvent (chloroform) by the triblock copolymer templating and sol–gel technique. The spheres had interconnected pore structures and excellent *in vitro* bioactivity. Mesoporous hollow BG microspheres with a uniform diameter range of 2–5 μm and a mesoporous shell (500 nm) can be prepared by a sol–gel method using polyethylene glycol as a template [261]. In this strategy, the incorporation of structure-controlling agents (e.g. CTAB, P123 and F127) is essential for obtaining well-ordered structures. Currently, the structure-controlling agents for preparing MBG mainly include CTAB, Pluronic F127 (EO106–PO70–EO106) and P123

(EO20–PO70–EO20). It has been found that the structure-directing agents play an important role in influencing the mesopore shape, mesopore size, surface area and pore volume of MBG. Generally, CTAB-induced MBG have a smaller mesopore size (2–3 nm) than P123- or F127-derived MBG (4–10 nm). P123 induced a two-dimensional hexagonal (p6mm) mesopore structure whilst F127 induced a wormlike mesopore structure [262]. Therefore, it is still a challenge to find much more convenient approaches to prepare MBGs scaffolds and related materials, and to investigate their *in vitro* and *in vivo* potential for drug delivery and tissue regeneration.

Fibers are another interesting form of scaffolds that have been widely used for cell culture and tissue repair. A growing interest in scaffold-based tissue engineering is the use of electrospinning techniques to create nanofibrous scaffolds of biodegradable polymers, which mimic the fibrous structure of the extracellular matrix [263,264]. The technique is also being applied to the formation of fibers with submicron or nanoscale diameters, and to nanofibrous scaffolds of bioactive glass [265,266]. Because of their high surface area, bioactive glass nanofibers degrade rapidly and can convert to HA. As in the case of sol–gel derived bioactive glasses, the bioactivity of these glass nanofibers is maintained over a larger SiO_2 compositional range when compared to melt-derived glasses. Nanofibrous scaffolds of bioactive glass have been prepared by electrospinning organic–inorganic solutions. A mixture of tetraethyl orthosilicate and calcium nitrate, for example, is typically used as the starting solution for the preparation of 70S30C glass (70 mol% SiO_2, 30 mol% CaO) by the sol–gel process [265,266]. After the electrospinning step, the as-prepared nanofibrous scaffolds are heated to 600–700 °C to decompose residual organic or inorganic groups (e.g. ethyl, nitrate). Bioactive glass fibers with diameters in the micron to sub-micron range, prepared from a melt-derived glass, are available commercially. This material, which is very pliable and has a rapid degradation rate because of its fine fiber diameter, has potential applications in the regeneration of non-loaded bone defects and the healing of soft tissue.

While the individual sol–gel derived mesoporous nanomaterial can be utilized for the loading and release of biomolecules, external modification like the combination of other nanomaterials can provide the ability of stimuli-responsiveness thanks to the so-called gatekeeping concept. Basically, diverse chemical entities are employed to reversibly close the pore entrances to regulate the encapsulation and subsequent release of drug molecules [267]. Thus, these systems acquire the ability to control the biomolecule release on demand in response to different stimuli, such as temperature, pH, ultrasound, light, magnetic field, redox systems, peptides, enzymes, or antibodies [268]. The great advantage of these capped drug delivery NPs is the protection of the drug against any possible degradation and/or inhibition of premature release; the latter of which is of vital importance when the cargo to be delivered can give rise to side effects. Thus, a so-called "stair-case" release profile can be obtained, which is one of the most important characteristics of stimuli-responsive systems: the drug release can be tailored to be provided on demand. Advances made in this respect are detailed in Section 4.5 of this review.

4.3. Mechanical properties

In general, inorganic materials, including ceramics, have relatively higher hardness, tensile strength and elastic modulus when compared to other materials available [269]. These properties are due to their molecular structure composed of ionic and covalent bonding, which is much stronger than metallic bonding. Since dislocation motion is difficult in these bonding structures, the strength of the materials increases. However, the materials also become brittle because the stress concentrated at flaws in the structure cannot be released [270]. In this kind of brittle fracture, called 'catastrophic fracture', the cracks propagate rapidly without any predictable sign or appreciable amount of plastic deformation. Most sol–gel derived inorganic materials also show this same degree of brittleness. Moreover, because they are, for the most part, highly porous structures, particularly for aerogels (80–98%) [271], the mechanical properties of the sol–gel derived materials can often be much lower than that of dense materials. For instance, the flexural strength of the TMOS-derived silica aerogel with 95% porosity is 0.02 MPa [272], which is 0.0002% of that of the dense silica material [273]. Therefore, in order to use the sol–gel based materials in bulk or coating state, not only analyses of the mechanical properties but also developments of methodologies for improving the mechanical properties are important.

The mechanical properties of sol–gel based materials are significantly influenced by network properties. These in turn can be altered by adjusting the process parameters including the water to precursor molar ratio, pH, type of precursor as well as doping agents. When water content increases, hydrolysis reactions are accelerated; however, the density of the material also decreases because the concentration of reactants decreases. Murtagh et al. [274] reported the effect of water content on the elastic modulus of TEOS-based silica gel. They prepared the silica aerogel with various water contents and evaluated the elastic modulus by ultrasonic analysis. Their results showed that the elastic, shear and bulk moduli of the silica gel decreased from 9.95, 3.95 and 6.53 GPa to 6.55, 2.83 and 3.51 GPa, respectively, when the water content increased from 4:1 to 24:1. In instances where such elastic or tensile moduli closer to that of natural tissues are required to maintain adequate axial forces and, hence, prevent loss of bone mineral density, the parameters of a material can thus be manipulated in whichever direction is necessary though simple control of water content during the gel formation stages of the sol–gel process.

As stated above, the pH of the sol directly affects hydrolysis, however indirect effect on the mechanical properties of the resultant materials also occurs. Sol–gel based materials can fail to meet specification due to internal stresses resulting from shrinkage during the drying process, and this can be related to the pH of the synthesis solution. For example, Woignier et al. [275] observed shrinkage of TEOS-based gel decreased from 15% to 1.5% when the pH of the sol increased from pH 1.5 to pH 9. The authors concluded that the network of silica gel is built by larger particles when the pH of the sol is high and these large particles make the silica branches stiffer and reduce the overall shrinkage during the drying process. Understandably, internal stress can cause a decrease in the initial and long-term mechanical stability of these materials [276].

The type of precursors used during synthesis influences not only the reaction, but also the final material mechanical properties. For example, TMOS- and TEOS-based silica xerogels that were prepared from a solution with a 16:1 M ratio of water to Si had a porosity of 50% and showed strengths of 20 MPa and 10 MPa, respectively [277]. These issues with brittleness, limit the wider applications regardless of the relatively high strength or moduli. However, flexible silica aerogels derived from hydrophobic precursors have recently been reported. Rao et al. [278,279] developed a superhydrophobic and flexible silica aerogel using alkylalkoxysilane precursors such as MTMS and MTES by a two-step process. These types of coatings are covered in a recent review by Yu et al. [280]. Since the alkyl group of the alkylalkoxysilane did not participate in the network formation and the inter-chain cohesion in the silica is minimized, the result was networks with increased flexibility.

Substitution of the Si or O in the silica network with other elements also improves the mechanical properties of the sol–gel derived silica. Li et al. [281] prepared silica, which has a composition of 45S5 bioactive glass by sol–gel method, and observed the effect of the additives on the mechanical properties by adding small amounts of MgO, TiO_2 or CaF_2 to substitute Mg^{2+}, Ti^{4+} for Ca^{2+} or F^- for O^{2-}. The mechanical properties of the glasses as evaluated by 3-point bending test were improved for all cases. The Dietzel's ionic strength of Mg^{2+} ion is stronger than that of Ca^{2+} ion. Therefore the substitution of Mg^{2+} for Ca^{2+} makes the glass network stronger due to decreased bond lengths [282], although the biocompatibility decreases slightly. Like the Si^{4+} ion, the Ti^{4+} ion is able to connect with four O^{2-} ions. Ti^{4+} ions substituted for Ca^{2+} ions thus make the glass network stronger by connecting with more O^{2-} ions [283]. As a result, Mg and Ti substituted glass showed improved bending strength, fracture toughness and hardness. In contrast, the fluorine ions due to the substitution of CaO by CaF_2 disrupted the glass network, with an increased tendency to crystallization. Therefore, the CaF_2-doped 45S5 lacks favorable mechanical properties.

Mechanical properties of sol–gel derived gels can be enhanced by reducing the pore size during the sintering process [273]. One of the advantages of sol–gel derived materials is the ability to release therapeutic agents including drugs and growth factors in controlled manner by loading during sol preparation process [284]. For most DDSs, however, the final sintering processes cannot be used as heat can damage many therapeutic agents and so the materials remain in a weaker form. Therefore, hybridisation with organic materials is considered a more promising technique for toughening sol–gel based inorganic materials applied to DDSs. For biomedical applications, biocompatible and biodegradable polymers, including collagen [285,286], gelatin [286], chitosan [204], PCL [287], PLLA [288], have been hybridised with silica. For example, Lee et al. [204] reported a hybrid system of silica xerogel and

chitosan. In this instance, the authors prepared TMOS-based silica xerogel with differing chitosan contents. After hybridisation with 50 vol% of chitosan, the final compressive strength and elongation of silica xerogel increased from 10 MPa to 70 MPa and from almost zero to 10%, respectively. This hybrid material also exhibited sustained release of a pre-loaded drug, the antibiotic Vancomycin. Tailored release of the drug was also achieved by altering the chitosan content. These same authors also developed a silica–chitosan hybrid membrane for guided bone regeneration [203] and a coating system [289] with the same improved mechanical properties, therefore demonstrating the aforementioned flexibility of inorganic–organic hybrid systems for the production of sol–gel based biomaterials.

4.4. Chemical properties

4.4.1. Surface chemistry

4.4.1.1. Surface functional groups. As mentioned above, sol–gel materials can be synthesized with different structural features. It was also indicated that by altering their structures or surface functional groups, the physical and chemical properties of sol–gel based materials can easily be tuned. The ease with which tuning their surface properties can be achieved has also extended previously assumed limits of biocompatibility and drug carrying capacity. Surface-functionalisation of sol–gel based materials are widely used in biological applications because many such materials, especially those containing judiciously chosen functional groups, have improved adsorption capacities for loading of bioactive molecules or drugs, and increased binding affinity to deliver these molecules to specific cell and tissue targets, along with enhanced overall biocompatibility [3]. The surface functionalisation of mesoporous silica based materials, for example, is typically achieved by introducing functional groups either on the external surface of the material or the inner surface of the pore or, indeed, both. This can be accomplished through one of two basic synthetic strategies: stepwise synthesis (post-synthetic grafting) or one-pot synthesis (co-condensation method). The presence of a high density of surface silanol groups capable of being functionalised using a wide variety of entities represents one of the great advantages of MSNs [290–292]. When nanomedicine applications are required, the surface functional groups of MSNs can play diverse roles, such as tailoring the surface charge of NPs, allowing the grafting of functional molecules inside and outside the pores, or facilitating the capping of the nanopore openings to prevent premature release of entrapped drugs [290].

Adjustment of the polarity of the pore surfaces by the addition of organic building blocks considerably extends the range of materials that can be used in biomaterial applications [293]. Equally useful is modification with organic functionalities such as C–C multiple bonds, alcohols, thiols, sulfonic and carboxylic acids, and amines. These allow for localized organic or biochemical reactions to be carried out on a stable, solid inorganic matrix. As a consequence of the functionalisation, organic–inorganic hybrid materials are obtained which can adsorb drug molecules through weak electrostatic interactions. Functionalisation with hydrophobic functional groups is a good alternative to increase the loading capacity of most non-polar drugs. This strategy is also employed to delay the release of certain drugs from mesoporous channels in aqueous medium by manipulating the wettability of the material surface [294]. On the other hand, there are other situations in which pharmaceutical molecules can be confined into the mesoporous channels. However, higher loads and slower release kinetics can be achieved if the mesoporous silica wall is functionalised with different functional groups [295].

Thus, the capability to cross cell membranes, avoid endosome capture and similar undesired intracellular binding processes, can make the MSN's more effective These properties are often necessary so that they can reach their desired target with the maximum drug payload intact. Among these processes, the endosomal escape of MSNs constitutes a crucial step or checkpoint, which can be significantly improved by proper functionalisation of the external MSN surface [296–298]. For example, Serda et al. [298] used polycations (such as poly-L-lysine, PEI, polyamidoamine dendrimers, and natural chitosan) along with endosome-disrupting peptides to coat the outer surfaces of silica based NPs and thus dictate cellular uptake and trafficking responses. Furthermore, as alternative molecules such as branched chain PEI contain a high density of amine groups, the positive charge imparts a so-called "proton sponge effect" and can serve as an excellent buffering agent during endosomal encapsulation [296]. Due to this high endosomolytic activity, PEI-coated MSNs exhibit an improved ability to deliver

nucleotides and drugs to intracellular or even nuclear sites [297]. It is the precise manufacture of these materials that is made possible by the sol–gel process.

4.4.1.2. Sol–gel processed surface chemistry. Given the interests in the potential biological applications of silica based materials, sol–gel methods that make silica based materials as biocompatible as possible are necessary. In this regard, surface modification of silica based materials is very important as it may result in enhanced cellular uptake and endosomal escape, and reduced collisions with some undesired organelles during cellular trafficking of the NPs themselves. This can be best exemplified by the work performed by Lin and co-workers, in which a variety of surface-functionalised MSNs were found to be internalised differently into human cancerous HeLa cells expressing folate receptors [299]. The different surface-modified MSNs were synthesized by functionalising MCM-41 with 3-aminopropyl (AP), guanidinopropyl (GP), 3-[N-(2-guanidinoethyl)guanidine] propyl (GEGP), and N-folate-3-aminopropyl (FAP) groups. All these organic-functionalised MSNs exhibited lower surface areas and pore volumes compared with their parent MCM-41 [91]. Interestingly, the degree of particle uptake by the HeLa cells increased in the same trend as their surface charges, (i.e., in the order of parent MCM-41 < AP-MCM-41 < GP-MCM-41 < 0 mv < GEGP-MCM-41 < FAP-MCM-41) [91]. Furthermore, among these materials, the FAP-modified MSNs were internalised to a greater extent by the folate receptor-expressing cells, indicating that the chemical affinity of functionalised particles to cells could play more significant roles than physical properties in determining the degree of endocytosis of MSNs. The mechanisms for endocytosis of particles, except for GEGP-functionalised MSNs, were also included in the study, and they were reported to vary from material to material [299]. The authors concluded that the parent MCM-41 MSNs were ingested through a clathrin-mediated pathway, whereas the AP- and GP-grafted MCM-41 MSNs were internalised into cells *via* a caveolae-dependent mechanism, and the FAP-MCM-41 MSNs were engulfed by both clathrin and folate receptor-mediated endocytosis followed by greater confinement of positively charged particles inside endosomes [299]. These results clearly showed the effects of surface properties on the cellular uptake of MSNs and their subsequent endosomal escape. Notably, a particular surface chemistry, surface charge determined by surface functional groups, may not only help one of the steps in the given biological process, but may also inhibit the others in the process. Therefore, all the steps in a given biological process need to be taken into account when rationally designing and synthesizing sol–gel based nanomaterials for biological applications.

By using HA NPs with similar particle size, shape, and crystallinity but different surface charges, Liang et al. [289] recently showed that differently charged NPs underwent different cellular uptake in murine osteoblasts *in vitro*. The particles with positively charged surfaces accumulated inside cells more so than their negatively charged or neutral counterparts. This result is consistent with a previous report on the uptake of differently charged MSNs by HeLa cells [300]. Interestingly, the cells even with highest particle uptake (i.e., those containing positively charged HA NPs) maintained their membrane integrity, viability, and normal replication, with no difference compared to those containing fewer intracellular particles [289]. This result was unprecedented, considering the fact that substantial residues of nanomaterials remained inside the cells or tissues and that such materials are traditionally expected to result in severe injury or toxicity based on previous findings on the internalisation of HA NPs in other cells (e.g. fibroblasts or hepatic cancer cells) and their cytotoxicity and cell growth inhibitory effect [289]. Nonetheless, this again corroborated the results that surface charge on MSNs could play a major role on cellular uptake of materials and subsequent cell viability. Moreover, the results showed that the degree of uptake of the functionalised MSNs and their subsequent biological effects and biocompatibility could depend on the cell type.

The most often used method for the loading of small drugs into the pores of MSNs is physical adsorption from solution. In this instance, the presence of surface silanol groups on the silica surface means that, in the absence of specific ion adsorption, the silica surface is negatively charged under biologically relevant conditions. Therefore, electrostatic adsorption of positively charged adsorbates is an attractive method for incorporating water-soluble cargos onto siliceous MSNs. The extent of adsorption can be further increased by introducing functional groups, very often weak acids and bases like carboxylic acids or amines, which can then be used to tune the effective surface charge under given pH conditions and also provide the possibility for additional specific adsorbate–adsorbent

interactions. Hydrophobic drugs are typically adsorbed from organic solvents, followed by vacuum drying in order to remove the solvent. Naturally, pore size effects do play a role for the extent of adsorption if the molecular size of the drug is in the range of the pore diameter.

Balas et al. [301] reported amino-functionalised MCM-41 and SBA-15 mesoporous silica-based materials containing alendronate for bone repair or regeneration. Alendronate belongs to the bisphosphonate family, which inhibit bone resorption by osteoclasts. In both systems, the surfaces of the pore walls were organically modified with amino groups. After 24 h in an aqueous alendronate solution, the amino-modified materials showed a drug loading almost 3 times higher than that of the unmodified materials. This different behavior could be explained by the different chemical interaction between the phosphonate groups in alendronate with the silanol groups in the case of the unmodified materials and with the amino groups covering the surface of the mesopore walls of the modified materials. Song et al. [302] also reported the functionalisation of MCM-41 and SBA-15, respectively, with amino groups as an effective method to control drug release. The ionic interaction between the carboxy groups in drug molecules and the amino groups on the matrix surface allows the release rate of the drug from amino-functionalised MSN to be effectively controlled.

4.4.2. Bulk chemistry

The microstructure of sol–gel derived silica is closely related with the chemical properties of itself. For example, many acid-catalyzed sol–gel derived silica materials have fractal structures as shown in Fig. 4.3A. This fractal structure is formed by agglomeration of particles with a diameter of 4–6 nm (secondary particle), which are also composed of small particles with a diameter of 1–2 nm (primary particle) [303]. West et al. [304] estimated the size of primary particles using an intermediate neglect of differential overlap (INDO) molecular orbital model. This approach led them to first propose two silica structures: one is a ring structure (Fig. 4.3B), and the other is chain structure (Fig. 4.3C). In each structure, each silicon, except those at the end of the chain, is bonded to two bridging oxygens and two non-bridging oxygens. Each non-bridging oxygen is bonded to hydrogen for terminating the structure and balancing the charge. The INDO energy *per* silica tetrahedron of ring structured silica was about −55.8 AU regardless of the number of silica tetrahedra. On the other hand, the INDO energy *per* silica tetrahedron of chain structure silica was initially lower than that of ring structured silica, but increased with the number of silica tetrahedra [48]. Based on their data, the difference in the INDO energy *per* silica tetrahedron between the two structures becomes zero when the number of tetrahedra is between 10 and 12. This means that the silica initially grows in a chain structure and converts to

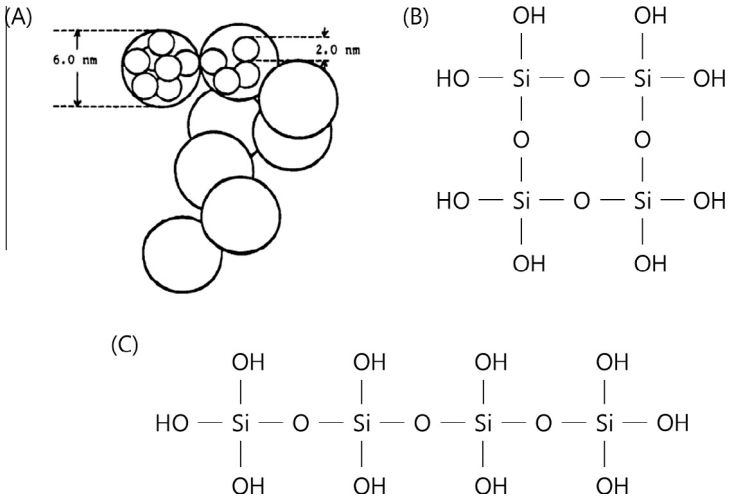

Fig. 4.3. Schematic diagrams of (A) fractal structure acid-catalyzed sol–gel derived silica gel network, (B) ring structure of 4 silica tetrahedra and (C) chain structure of 4 silica tetrahedra.

a ring structure when the number of silica reaches 10 or 12, because the driving force to produce ring structure becomes more favorable, and this conversion to a ring structure of the primary particles results in the development of fractal structure. The size of primary particles estimated by this model is similar to the radius of gyration of the primary particle calculated by SAXS analysis [303]. Meanwhile, the molecular energy of silica with ring or chain structures was recalculated by Davis et al. [48] using AM1. In their calculation, extra water molecules in the chain, as compared to the rings, were considered, and the energies were corrected for zero-point energy with subsequent conversion to enthalpies at 25 °C. Due to these corrections, the number of silica tetrahedral where the chain-to-ring conversion occurs moved from 10–12 to 3–4. This calculation suggested that the primary particle might be built with a 3- or 4-membered ring structure. Moreover, the size of 3- or 4-membered ring corresponds very closely to the 1–2 nm primary particles.

Because many properties of sol–gel derived materials are affected by their chemistry, the investigation of chemical reaction and chemical structure of the sol–gel materials is central to their development and optimization. Generally, the chemical properties of the sol–gel networks are analyzed by infrared [305–308], Raman [305,306] and/or nuclear magnetic resonance spectroscopy [306,309–311]. In infrared spectroscopy, silica exhibits three major absorption bands at ~460 cm^{-1}, ~800 cm^{-1} and ~1100 cm^{-1}, which respectively correspond to the rocking motion of oxygen perpendicular to the Si–O–Si plane, symmetric stretching motion of oxygen along the bisector of the Si–O–Si bridging group and asymmetric stretching motion of oxygen parallel to the Si–O–Si line [307]. Because these main peaks resulted from the Si–O–Si backbone of sol–gel derived silica, when the network is disrupted by network modifiers the spectra would be changed significantly.

For example, Ca^{2+}, an abundant element in human body, has been used for making the bioactive glasses because it promotes bone regeneration. In the silica network, the Ca^{2+} ion acts as a network modifier, which disrupts the glass network by breaking Si–O–Si bond and generating non-bridging oxygen species. As shown in Fig. 4.4A, as increasing Ca content in the glass, the intensity of absorption bands corresponding to symmetric and antisymmetric motions decreased and the peak corresponding to Ca–O formed at ~1220 cm^{-1}. Moreover, the bands of Q^0, Q^1, Q^2 and Q^3 which respectively indicate symmetric stretching motion of silicon with 4, 3, 2 and 1 non-bridging oxygen atoms [312] were detected, suggesting that the addition of Ca ions disrupted the polymeric structure of silica [305]. This kind of information related to molecular motions can also be obtained by Raman spectroscopy. Raman spectroscopy is a sensitive analysis method in which the scattering of the visible near infrared or near ultraviolet light is measured, while the absorbance or transmittance of the light is measured in IR spectroscopy. In the Raman spectrum of sol–gel derived silica, the main peaks are detected at ~980 cm^{-1} (Q^a), ~493 cm^{-1} (D_1) and ~606 cm^{-1} (D_2), which respectively correspond to Si–O stretching in the silanol group, vibration motions of oxygen atom in 4- and 3-membered rings [313]. It is noteworthy to point-out that these kinds of peaks are not detected in crystallized silica such as quartz [305].

The addition of network modifier cations, such as Ca^{2+}, also affects the Raman spectra of silica. Fig. 4.4B shows the Raman spectra of sol–gel derived silica with Ca contents ranging from 0 to 40 mol%. The D_1 and D_2 peaks were not influenced by Ca addition, but shifted when the Ca content reached 40 mol%. In addition, new bands corresponding to Q^2 and Q^3 appeared at ~980 cm^{-1} and ~1050 cm^{-1}, respectively [305]. Meanwhile, NMR is one of the most useful tools for investigating the chemical reaction during the sol–gel process. The terms Q^n (n = 0–4) were originally used in ^{29}Si NMR spectroscopy [305,311] where solid-state ^{29}Si NMR allows one to observe the connectivity and degree of condensation of sol–gel derived materials by comparing the intensities of Q^n signals [311]. Homogeneity of the element is one of the main advantages of the sol–gel technique when making the composite or compound. However, if the process is not sufficiently optimized, so that the self-condensation between the same precursors is more dominant than co-condensation between the different precursors, phase separation will occur and desirable properties cannot be obtained.

Energy dispersive spectroscopy or X-ray photoelectron spectroscopy is a more accessible way to investigate the chemical composition of surface layers, although it is difficult to investigate chemical reactions using these methods. Although ^{29}Si NMR gives much information about silica network, such as D_1, D_2, Q^0–Q^4, it does not give information about the reaction between different precursors, while ^{17}O NMR is more valuable in this respect [310]. Fig. 4.5 shows (A) ^{17}O NMR spectra of (A) prehydrolyzed TEOS sol and (B–D) mixture sol of TEOS and $Ti(OBu^n)_4$ with 1:1 M ratio at (B) 15 min,

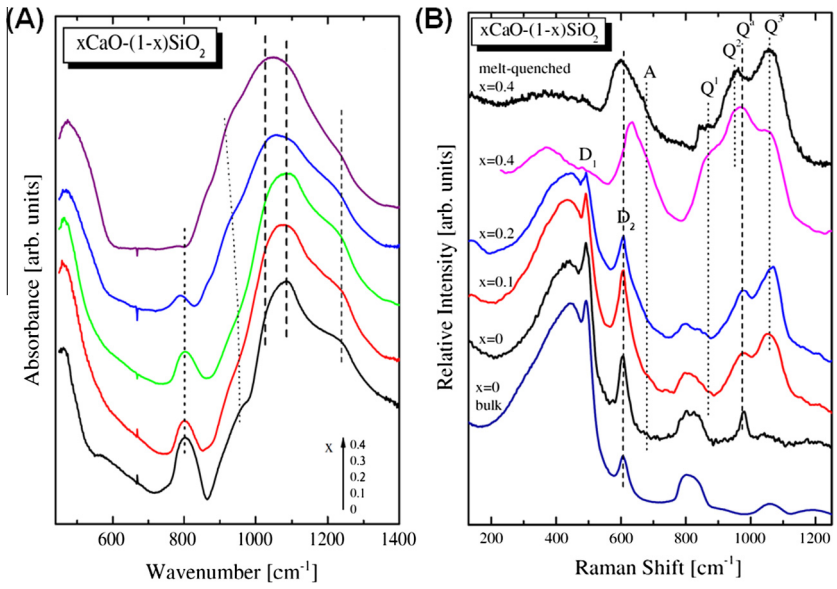

Fig. 4.4. (A) IR [312] and (B) Raman spectra of xCaO–$(1-x)$SiO$_2$ glasses (x = 0–0.4) [305].

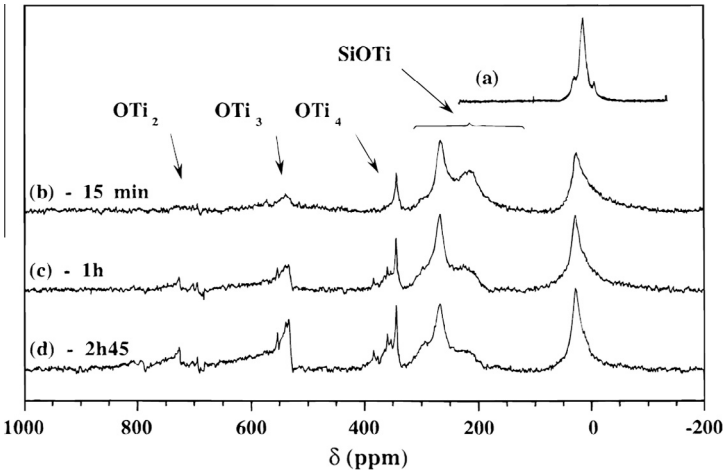

Fig. 4.5. ^{17}O NMR spectra of a prehydrolyzed solution of TEOS aged during 4 h, (a) before and (b–d) after addition of Ti(OBu^n)$_4$: (b) 15 min, (c) 1 h, and (d) 2.75 h (TEOS/H_2O/EtOH 1/1/4 (pH = 1.6); Ti/Si = 1) [310].

(C) 1 h and (D) 2.75 h. The bands indicating Si–O–Si, Si–O–Ti and Ti–O–Ti are clearly detected without any overlap [310] suggest that ^{17}O NMR may help to optimize the conditions of sol–gel processing.

The sol–gel derived silica materials have chemical structures based on the Si–O–Si backbone; thus, it would stand to reason that the many properties of sol–gel derived silica might be significantly affected by the elements which influence the network. The number of alkoxy groups in the precursor molecules is one example. TEOS/trimethylethoxysilane (TMES) system was prepared to functionalize the silica by using a hydrophobic precursor TMES. Since the TMES molecule has only 1 hydrolysable group, this mixture did not set when the molar ratio of TMES was higher than 0.6 [314]. For methyltrimethoxysiloxane (MTMS) or methyltriethoxysiloxane (MTES), these can set alone, because

they have three hydrolysable groups [279,315,316]. Due to the hydrophobic methyl group, the properties of silica aerogels derived from these precursors differ from silica aerogels derived from TMOS or TEOS. For example, MTES-derived silica aerogels showed flexible properties due to the flexibility of the final glass network [279,316] and also exhibited buoyancy in water because of the hydrophobic property imparted by the methyl group [316]. The incorporation of ions in the glass network also significantly affects the properties of sol–gel derived silica as described previously. The elastic modulus and strength of the glass decreased with increasing polymer content, because the stiffness of the Si–O network is reduced by incorporation of soft polymer molecules. However, the ductility and toughness of the glass increased [317,318].

Metallic ions also influence physicochemical properties, such as degradability. When Na_2O is substituted for CaO, the glass network became more disrupted because two Na^+ cations should exist between oxygen for charge balancing [319]. Furthermore, Na^+ ion can be released from the network more easily because the bond energy between Na^+ and O^{2-} is lower than that between Ca^{2+} and O^{2-} [320]. Thus, the chemical stability of Na-substituted 58S decreased compared to 58S glass. In the 58S glass system, Ti^{4+} substituted for Ca^{2+} results in covalent O–Ti–O bonding because the electrostatic field strength (z/a^2, z: cation charge, a: internuclear distance between cation and oxygen) of Ti^{4+} (1.05×10^{-20} m^{-2}) is higher than Ca^{2+} (0.36×10^{-20} m^{-2}) [321]. Put more simply, the lower difference in electronegativity between Ti and O (in comparison to Ca and O) favors covalent character between these elements. Since Ti has the same valence as Si, Ti can assist Si in forming the glass network. The Ti^{4+} cation is also known to strengthen phosphate glasses by cross-linking the chains effectively [322]. Therefore, Ti-substituted 58S glasses exhibit decreased degradability. As the composition of the glass becomes complex, it is difficult to predict the effect of each component on the degradability. Hill et al. [323,324] have suggested a systematic method to estimate the relationship between the dissolution rate of the glass and composition using split network or network connectivity (NC) models. NC is defined as the average number of bridging oxygen atom per network forming element and is a measure of glass structure polymerization. The network connectivity also affects bioactivity by modulating the rate of HCA layer formation [40]. When the NC value is too high (>2.4), the glass is insoluble and has decreased bioactivity. On the other hand, when the NC is too low, the glass degrades very quickly. Hill et al. [323,324] recommended an optimum range of NC from 2.0 to 2.4 for biomedical materials based on the percolation theory by Philips and separately by Thorpe [325,326].

Since many trace elements (such as Sr^{2+} [327,328], Mg^{2+} [329,330], Zn^{2+} [331,332], Fe^{3+} [333,334], B^{3+} [335,336], and Co^{2+} [337,338]) present in the human body are known for their anabolic effects on physiological processes such as bone metabolism [339,340], new approaches for enhancing bioactivity of the sol–gel BG-based materials are continually investigated by introducing such therapeutic ions into the structure. As indicated above, the subsequent release of these ions after exposure to a physiological environment is believed to favorably affect the behavior of human cells and to enhance the bioactivity of scaffold materials. Thus, research efforts are devoted to incorporate these ions in different implant materials. Furthermore, these substitutions often result in altered dissolution behavior and modified biological performance. In addition, single inorganic ions such as calcium [341,342], phosphorous [343], and silicon [344,345] are known to be involved in bone metabolism and to play a physiological role in angiogenesis, growth and mineralization of bone tissue. However, the variations in dissolution behavior are testament to effects on the chemical structure of the materials produced. This can, in some cases, mean that synthesis conditions are also altered. For example, borosillicate glasses dissolve much slower than unsubstituted silicate glasses [335]; however, significantly higher synthesis temperatures are also required to produce these glasses. For the purposes of coating implant materials, sol–gel approaches may be far more efficacious although, at present, sol–gel approaches have yet to be fully developed for this particular synthesis pathway.

4.5. Biological properties

4.5.1. Biodegradation

One of the most important properties that can be exploited in some sol–gel derived materials is their biodegradability. Compared to non-degradable materials, biodegradable materials show higher reactivity, which can have a close relationship with formation of an HCA layer [323]. However, as

noted above degradation is intrinsically linked to NC and this relationship does appear to show some optimum range with upper and lower limits [40]. Nevertheless in many applications, degradable materials are more ideal than permanent implant materials because they can be resorbed into the body and replaced with regenerated tissues [346] or one a drug payload has been delivered [284,347]. However, the controlling the rate of degradation is complex, excessive degradation rates must be avoided because the materials have to maintain space during the healing process with appropriate mechanical properties and Bioglass® can degrade at an excessively fast rate which can detrimental affect cellular local conditions [348]. Therefore, the understanding of the degradation mechanism and the factors which influence the degradation rate of sol–gel based materials is required. In this section, the ionic degradation by reaction with aqueous solution will be covered for biological applications.

In general, the dissolution tests are carried out by immersing the materials into solutions such as simulated body fluid (SBF) [67,349,350], tris buffer solution [67,350,351], phosphate buffered saline [347,350], and cell culture media [349], and measuring changes at pre-determined periods. Among the various ways to investigate the dissolution rate, measurement of weight loss is the simplest method. Other ways to examine the dissolution of the materials is measuring the concentration of released ions. The pH of the solution is another index of dissolution of the materials. For example, when the glass with network modifier such as Na^+ or Ca^{2+} is dissolved, ion exchange occurs between protons from the solution and the modifier ion from the glass and the pH of the solution increases [349,352]. The change in pH is closely dependent on the buffer capacity of the solution (or local environment *in vivo*) [349,350]. In most cases, dissolution tests are performed in static condition, where the fixed volume of solution is refreshed periodically, but the dissolution is significantly inhibited if the released ions are saturated in the solution. This complication means that, in some cases, that perfusion systems are highly valuable to investigate dissolution behavior of sol–gel materials in dynamic conditions [352,353].

When silica-based glass is immersed into aqueous solution, the following reactions occur simultaneously: (i) the penetration of water into the glass, (ii) hydrolysis of M–O bonds to form hydroxyl groups and (iii) ion-exchange reactions between protons and network modifier ions. The water molecules can penetrate into the glass matrix by diffusion through voids between oxygen atoms or by hydrolysis and condensation reactions. Usually the latter case is dominant when the water molecules are incorporated into the glass matrix, because most glass structures do not contain the voids which are large enough for water diffusion [354]. During the hydrolysis reaction, the SiO_4^{4-} sites in the glass structure are attacked by a nucleophile such as OH^- and five-coordinated intermediates are formed. These intermediates are highly reactive and easily decompose to facilitate the breakage of Si–O–Si bonds [355].

Since the breaking of the Si–O–Si network is a major part of the reaction of dissolution of silica glass, the dissolution rate is closely related to variables that influence the glass network, and the chemical composition of the materials is one of the main factors, which can affect the network structure. For pure silica, the hydrolysis reaction is inhibited because high connectivity of the glass structure makes the formation of five-coordinated intermediate difficult. The addition of network modifiers disrupts the network connectivity and forms the non-bonding sites, which decrease network stability. In general, the reactivity of silica decreases as network connectivity goes from Q^1 to Q^4 [354]. In the NC model, the role of the network modifier on the dissolution rate is systematically summarized [323,324]. As noted above, materials which have an NC value between 2.0 and 2.4 [324] or 2.6 [356] are recommended for biodegradable materials due to their appropriate dissolution rate and bioactivity. Furthermore, the network modifiers can be released from the network faster than Si ions that are bonded, leading to void development, which helps the diffusion of water molecules into the matrix. Therefore, the dissolution rate increases with increasing ionic radii of network modifier ions. For instance, in the case of alkali metal network modifiers, the effect of ions on the reactivity of the glass follows the trend K > Na > Li [357].

The dissolution reaction occurs at the interface between the material surface and solution. Thus, the specific surface area can be an important parameter which influences the dissolution rate [358]. Due to the larger surface area, the dissolution rate of mesoporous sol–gel derived glasses is higher than that of melt-derived glasses, which are relatively dense [349]. Moreover, when the pore size

increases the circulation of solution in the pore becomes easier, resulting in increased reactivity [358]. Meanwhile, sol–gel derived materials are often heat-treated to remove the organic phase [359] or increase the stability [360]. The heat-treatment process affects not only the materials porosity but also the crystallinity of the materials. Li et al. [361] compared the reactivity of silica with the same composition but different crystallinity using SBF solution. Results revealed that sol–gel derived silica had the highest reactivity among all the samples tested. The silanol groups (Si–OH) which are more abundant on the surface of amorphous silica gel may also affect the reactivity of the silica in providing a site for ion exchange or HCA nucleation [211]. In another example, the dissolution rate of sol–gel derived 45S5 subjected to different heat-treatment temperatures was evaluated. These investigations found that crystalline phases were detected when the heat-treatment temperature was 1100 °C, and this bioglass (BG) showed much slower dissolution behavior than glass which was treated at 700 °C [362]. As expected, these findings can be traced back to a lower degree of crystallinity within glasses when subjected to lower heat treatment temperatures.

The dissolution behavior of sol–gel derived materials is affected not only by the intrinsic conditions described above but also by environmental conditions such as solution temperature, pH and composition. First, the probability of activation of the hydrolysis reaction, as well as the solubility of $Si(OH)_4$ phase in the aqueous solution, increases with increasing temperature [354]. Thus, the solution temperature significantly influences the dissolution behavior of sol–gel derived silica materials. This trend is also shown in phosphate-based glass system [363]. The pH of the solution also affects the dissolution behavior of sol–gel based materials. For silica glass, the dissolution rate increases as pH increases because Si–O–Si bonds are broken by nucleophilic attack of OH^- in aqueous solution [364]. From a thermodynamic point of view, the solubility increases with pH when the pH is above ~8, while the solubility shows a small dependencies on pH within a range of 2–8 [364]. Alternatively, a kinetic view of dissolution shows that the rate increases with increasing pH from 2 to 8.5 and further increases above pH 8.5 because more soluble ions ($SiO(OH)^{3-}$) are formed above pH 8.5 [39,365]. The composition of the solutions is also an important factor, which determines the dissolution rate of the materials. There is no Ca or P source in Tris-buffered solution; thus, the apatite layer is formed only by the Ca and P ions released from the materials. On the other hand, in SBF or PBS solution, formation of an HCA layer is accelerated and the further dissolution is inhibited because a number of calcium or phosphate ions are contained in these solutions [350]. Furthermore, the biomolecules in the solutions also affect the dissolution behavior. Sepulveda et al. [349] compared the dissolution behavior of sol–gel derived 58S glass in SBF solution and culture medium. ICP results showed the dissolution rate of 58S glass is slower in culture medium than in SBF due to serum proteins. These positive-charged proteins can adsorbed on the materials surface and suppress the dissolution of glass. Thus, it is important to bear in mind the limitations of non-biological *in vitro* model systems when considering materials that will ultimately be applied *in vivo*.

From the above, a consensus view that bioactive materials should be tested for their biocompatibility with the physiological environment upon their implantation is without question [366,367], although factors pertaining to degradation of the material itself are but one facet. The bioactivity, or influence, of the material on its *in vivo* environment is equally important to consider. Critical levels of the ions released by bioactive glasses regulate genes in osteogenic cells, which can initiate a self-repair mechanism for tissue regeneration [368,369]. In other words, dissolution products of bioactive glasses should not be detrimental to the tissues of the host. As yet, bioactive glasses have been implanted in many mammalian species and no evidence of toxic effects have been found [370]. However, just as the release of ionic species can prove beneficial, so too can the release of potentially toxic agents be detrimental. An illustration of this process lies in the 45S5 Bioglass® composition. These granules have been implanted in rabbits to determine the pathway of silicon released during the degradation of glass *in vivo* [371]. After 7 months of implantation, histopathological analyses of tissues indicated the excretion of silica through urine in soluble form. Although 45S5 is the standard bioactive material, it has certain limitations such as its slow degradation rate and conversion to HCA-like material [372,373]. Hence, the rate at which new tissue formation takes place is not in equilibrium with the rate at which scaffold degrades, thus providing a distinct example of the pervasive nature inherent in the use of biomaterials and the care that should be taken in ensuring that secondary complications are avoided.

4.5.2. Possible interactions with molecules

With the versatile and tunable structures, mesoporous silica-based materials have been proven to be capable of loading a variety of guest molecules including pharmaceutical drugs, therapeutic peptides, proteins, and genes. MSNs have been used as DDSs for various kinds of pharmaceutical drugs with different hydrophobic or hydrophilic properties, molecular weights, and biomedical effects. This includes commonly used agents such as ibuprofen [374], doxorubicin [375], camptothecin [376], cisplatin [377], and alendronate [295]. Peptide and protein drugs have been developed as potent therapeutic agents in many medical applications including cancer therapy, vaccination, and regenerative medicine. However, protein delivery is difficult, in part related to their intrinsic properties of large molecular weight and a fragile structure that must be maintained for activity [378,379]. Attributed to the porous and stable nature, MSNs as DDSs can protect biomolecules against such premature degradation.

The release of the drug from the mesoporous matrix would take place through diffusion of the pharmaceutical molecule into pore channels. However, when targeting a truly controlled release, it is necessary to design stimuli-responsive systems. The use of different external or internal stimuli such as pH, temperature, ultrasounds, and light among others has been employed in order to achieve a controlled release of drugs trapped inside mesoporous silica NPs [268]. Different aspects should be considered for the development of an effective stimuli-responsive system to retain the drug until reaching the target zone and also releasing only the required dose. The combination of supramolecular chemistry with material science may open up excellent opportunities to achieve this goal. In 2001, the Vallet-Regi research group described for the first time that it was possible to load and release different drugs from a mesoporous silica matrix [374] and identified that these materials could host many different molecules. The performance of the silica nanocarriers was monitored employing a reporter molecule. Reporter molecules should present a convenient and relevant size that allows it to enter and exit through the pore, an adequate electrostatic charge and solubility in the environment (usually aqueous solutions) and finally, the molecule should be easily detected (e.g., fluorescent molecules). The next step is to achieve a controlled release of the trapped drugs in such a way that it only happens in the presence of certain stimuli. The system has to be able to transport a cargo to specific places in the body without premature release during transport and release the payload by the application of the trigger stimuli once reaching the target zone. Other potentially useful properties include switchability [380], which means that a capacity to be repeatedly activated by the trigger stimuli after reaching the targeted cells or tissues can be integrated into the delivery system.

Ibuprofen, a common anti-inflammatory drug and also a useful marker as it is readily measured, was the first to be confined inside of MCM-41 type mesoporous materials by using MNPs with different pore sizes and with subsequent release in SBF [374]. Since then, the interest in this field has grown exponentially as reflected by the number of research papers concerning mesoporous materials as DDSs [381,382]. Factors such as textural parameters and the functionalisation of the pore surface by organic molecules have been shown to influence the loading and release rate of biologically active molecules (Fig. 4.2). Commonly, pore diameters larger than the drug molecule dimensions (pore/drug size ratio >1) are enough to allow the adsorption of drug inside the pores. As can be expected, one of the most important characteristics of mesoporous materials is that the pore diameters can be tuned from a few nanometers to several tens of nanometers by changing the chain length of the surfactant, employing polymeric structure-controlling agents, or solubilising auxiliary substances into micelles [383,384]. Therefore, the loading capability of mesoporous materials can be large, ranging from small molecules up to macromolecules such as proteins [302,385,386]. Moreover, pore size has also been demonstrated to influence the release rate of molecules since this parameter affects drug diffusion to the delivery medium [231,387]. Finally, it must be highlighted that the cornerstone in the development of silica mesoporous materials as DDSs has been organic modification of the surface or functionalisation. As described above, functionalisation of the surface through organic groups provides numerous possibilities to control drug adsorption and release [294,388]. For this purpose the surface is functionalised with chemical groups that are able to link to the drug molecules through ionic bonds or through hydrolytically degradable ester groups and thus, to enhance the loading and release properties *via* increasing the guest-matrix affinity.

Surface area and pore diameter are critical factors for drug adsorption and release in implantable drug-delivery systems. In this case, the outermost mesopore surface of virtually insoluble porous frameworks is responsible for the interaction with the loaded drug, and the first approach in achieving this involves manipulating the amount of surface available for the drug molecules. So long as the pore size allows the drug to enter the matrix, the higher the surface area the higher the amount of drug adsorbed. However, weak drug–drug interactions can result in under loading conditions and can lead to the pores filling before reaching maximum capacity. In this case, the pore volume is a key factor in determining the amount of drug adsorbed. It was recently reported that several consecutive loadings of drug in ordered mesoporous materials lead to larger filling of the mesopores, which is attributed to the increased drug intermolecular interactions within the pore voids whereby larger pore volumes may result in greater drug loading [389].

In many clinical situations however, the administration of therapeutic compounds is hampered by impaired drug absorption or tissue-unspecific delivery [390,391]. Further to this, in clinical fields such as oncology, the high toxicity associated with currently employed cytotoxic drugs can create an unmanageable situation with respect to risk. In this particular field, the development of nano- or micro-particles able to deliver different therapeutic agents and release them in a controlled manner in the affected tissues has emerged as one of the most groundbreaking applications in nanomedicine today [392–395].

4.5.3. Possible interactions with cells and intracellular delivery

Advances in nanotechnology research have generated a growing list of contrast agents, therapeutics, scaffolds, and delivery vehicles. Many colloidal suspensions of NPs produced by sol–gel methods, which typically have at least one dimension in the 1–100 nm size range, are engineered as DDSs. Beginning with this aspect, the consequent cellular events can depend on the various physical and chemical factors of the nanomaterials (Fig. 4.6). Hence, evaluation of the combined effects of all the material variables in a series of biological processes, which consist of membrane trespassing, vesicular coating, endosome development, and lysosome degradation, are necessary for one to determine how exactly the cellular trafficking of MSNs occurs.

Considering cellular transport in more detail, the intracellular milieu is physically segregated from the environment by the plasma membrane, an elastic lipid bilayer embedded with domains of lipids, carbohydrates, and membrane proteins. In order to deliver NPs into cells and to their subcellular targets, NPs must first be able to traverse this plasma membrane, which is not always feasible. For example, it was previously found that quaternary amine-functionalised MSNs tended to adhere to negatively charged components of cell membranes rather than penetrating the cells and entered the cytoplasm [396]. This effect was most likely due to the non-polar tail region within the cell membrane lipid bilayer preventing further transport of the MSN. This, in turn, would also suggest that functionalisation of the MSNs surface to the point of introducing larger non-polar domains may prove advantageous.

Aside from passive diffusion, NPs may also be internalised either directly by interacting with membrane-embedded receptors or indirectly by associating with the lipid bilayer. In the first approach, NPs are functionalised with ligands that bind to receptors on the cell with high affinity and specificity. Ligands can be selected or engineered to target over-expressed receptors on healthy and diseased cells [397]. Internalisation of the resulting receptor–ligand complexes then leads to receptor-mediated endocytosis of the NPs. Alternatively, NPs can interact with the membrane *via* hydrophobic and electrostatic interactions and be taken into the cell through pinocytosis, a form of fluid-phase uptake where cells take in the local extracellular environment through invagination [398]. The variety of pathways available adds a further level of complexity in predicting the activity of such DDSs however with this complexity come further avenues for research.

Controlling the route of NP uptake is important for mediating their intracellular fate and biological response. An increasing number of mechanistically distinct and highly regulated endocytic pathways are used by cells to traffic the extracellular cargoes to different intracellular locations and interactions [399–401]. However, recent studies show that the endocytic processes not only function to internalize nutrients and membrane-associated molecules but orchestrate the spatio-temporal dynamics of cell signaling circuitry [402], meaning that a deep understanding of the cellular uptake mechanisms of

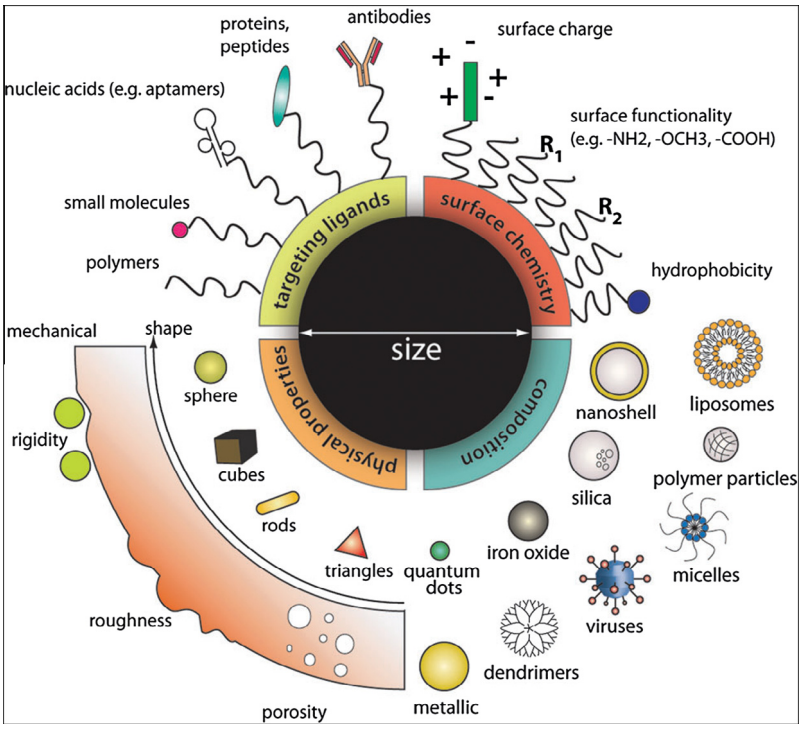

Fig. 4.6. Designing NPs for intracellular applications. NPs can be modularly assembled from different materials composition with different physical and chemical properties and functionalised with a myriad of ligands for biological targeting [398].

NPs is necessary to determine what and how they would modulate signaling and the subsequent molecular response of the cell [403–405]. In order for a material to be taken up efficiently by non-phagocytic cells, for example, the particle size of the material needs to be on the sub-micron scale [400,406]. For intracellular drug and gene delivery applications, this limitation has led to extensive research efforts on different designs of materials with precise control of the particle size (Fig. 4.7). Furthermore, it is important for the drug carrier to have proper surface properties and favorable interactions with the drug molecules to achieve high loading. This would allow the release of the drug with high local concentrations at the site of interest intracellularly.

Cellular uptake of molecules is often facilitated by the specific binding between the molecule in question and membrane-bound receptors (e.g., LDL or transferrin receptors). In contrast, delivery systems aimed at cells lacking receptors can still be taken up by constitutive "adsorptive" endocytosis or by fluid phase pinocytosis [400,407]. Silica particles are known to have a great affinity for the headgroups of a variety of phospholipids [408]. Therefore, the high affinity for adsorbing on cell surfaces that eventually leads to endocytosis is not surprising. Similarly, chitosans, poly(alkyl acrylic acids), and anionic amphiphilic peptides (derived from viral fusion peptides), which are protonated in response to pH decrease, can also be tethered on MSNs' surfaces *via* covalent bonding or electrostatic interaction. This functionalisation can help MSNs accumulate with high charge density when acidity increases during endosome development, destabilising the endosomes' membranes [298]. In addition, surface modification of MSNs with functional groups, such as photosensitive porphyrins, have been used to develop a novel MSN-based delivery system for photo-induced endosomal escape in living cells [409]. After entering cells *via* endocytosis and binding to endosomal membranes, photosensitised MSNs can be excited by light and further quenched by a triplet oxygen moiety to produce a singlet oxygen species [409]. The singlet oxygen species then damaged the endosomal membranes, thus releasing the cargo-loaded MSNs.

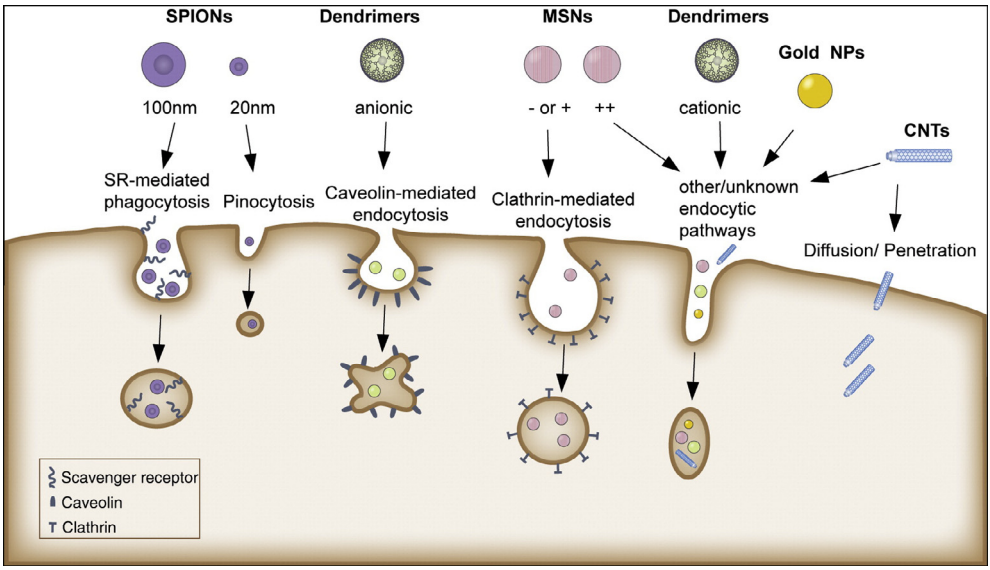

Fig. 4.7. Pathways of cellular internalisation of NPs. Several different pathways are implicated in the cellular uptake of NPs, and the main determinants are thought to be size and surface properties of the particles as well as the nature and activation status of the engulfing cell (macrophage, endothelial cell, etc.). However, the details of the routes of different nanoparticle uptake remain to be elucidated [410].

Although few studies have been conducted on exocytosis, there have been some reports on exocytosis of MSNs in a number of cell lines. PEG has been widely utilized for these purposes as it has the ability to improve the surface hydrophilicity of MSNs, reduce their protein adsorption, and shield them from nonspecific binding [411]. Compared to their naked counterpart, PEGylated NPs (including PEGylated MSNs) have been shown to have much higher dispersion and stability in biological media and much lower adsorption of serum proteins with less uptake by macrophages [411–413]. PEGylated MSNs with enhanced biocompatibility could be produced more easily by applying PEGs with molecular weights >10 kDa on the NPs and by ensuring homogeneous surface coverage and optimal PEG density on the NPs' surfaces rather than by increasing their chain lengths [411–413]. In addition, properly performed PEGylation could also help the mesoporous structures of MSNs remain intact [413,414]. Furthermore, PEGylated MSNs were shown to exhibit significantly lower effects toward hemolysis of human RBCs, possibly because the PEG groups shielded the silanols on the surfaces of MSNs and prevented the latter from possibly generating ROS that could damage cell membranes. This was confirmed both with *in vivo* and *ex vivo* mouse model studies in which the distributions of PEGylated MSNs in various tissues following intravenous injection were probed. PEGylated NPs exhibited longer retention times in the bloodstream and lower accumulation in the spleen, liver, kidney, and urinary bladder, compared to their parent MSNs or their carboxylated or hydroxylated counterparts with similar particle sizes [415,413,416]. In addition, PEGylation prolongs the blood circulation time of MSNs by reducing RES organ uptake, bypassing renal and hepatobiliary clearance, and thus enhancing permeability and retention of the NPs. Hence, the surface modification of MSNs, using PEG or other similar functional groups, not only improves the biocompatibility of MSNs but also promotes the ability of the MSNs to deliver drugs or biomolecules to desired sites in a sustained manner.

4.5.4. Possible interactions with cells and morphological traits

One of the main advantages of sol–gel synthesized materials over other materials is the tunability of the process to shape different morphologies, including films, fibers, foams and particles. Among these, the nanoparticulate form of sol–gel materials hold unique properties derived from the

morphological trait. In this section, we focus on this aspect of sol–gel materials and discuss briefly the possible effects of size and shape of NPs on pertinent biological responses.

4.5.4.1. Particle size. As discussed above, NPs are promising candidates for DDSs, contrast agents for imaging, and other biomedical applications [417–419]. The high surface area of NPs can also be modified by various functional groups for targeting a variety of biomedical applications. Particle size is also considered to be one of the most important properties of nanomaterials including interactions with cells and tissues. Although it is still uncertain as to what the exact relationship is between particle size and potential toxicological effects of nanomaterials [420], size is certainly a property that can be exploited

For the biotranslocation of MSNs, Lee and co-workers investigated the influence of particle size on the cellular uptake of MSNs by HeLa cells [421]. The cellular uptake amount is size-dependent in the order 50 nm > 30 nm > 110 nm > 280 nm > 170 nm and this may be due to statistical variation. The cellular uptake amount of 50-nm NPs was about 2.5 times higher than that of 30-nm particles. This result is consistent with the trend of other NPs systems that showed 50-nm particles led to maximum cellular uptake [422,423]. It suggests that 50-nm MSN may be the most effective in drug delivery from the perspective of cellular uptake. The distribution in the liver and spleen increased with the increase of particle sizes from 80, 120, to 200 nm at 30 min post-injection, but the particles with a diameter of 360 nm exhibited a different effect, being localized in the spleen [415]. Importantly, particles of smaller size had longer blood-circulation lifetimes. The excretion from urine also increased with increasing particle size, which may reflect the *in vivo* degradation rates and the excretion amount of degradation products. Research on the cytotoxicity of spherical MSNs with particle sizes of 190, 420, and 1220 nm found that cytotoxicity is strongly correlated with particle size [424]. 190 nm and 420 nm MSNs showed significant cytotoxicity at concentrations above 25 mg ml^{-1}, while microscale particles of 1220 nm showed slight cytotoxicity due to decreased endocytosis. Others have reported that MSNs with sizes of 150 nm, 800 nm, and 4 μm showed a size-independent toxicity *in vivo*, and instead there was a significant dependence on route of administration [300]. Clearly, further work is needed to decipher role of particle size on both cellular and systemic levels, although what is certain is that sol–gel approaches to the production of such NPs will provide the degree of control and homogeneity needed to produce safe and effective treatments with the efficiency and the flexibility required.

4.5.4.2. Particle shape. In the past few years, particle shape has gained increasing attention [425,426] due to the possibilities that arise with being able to fabricate sol–gel based materials with different shapes and similar composition, structure, diameter, or dispersity. This control enables research into shape effect on nanotoxicity, biodistribution, and performance for drug delivery. Until now, research on the shape effect of sol–gel based materials has mainly focused on *in vitro* cellular uptake. As reported, cellular uptake of spherical (size from 80 to 150 nm) and tube-shaped (600 nm in length and 100 nm in width) MSNs by Chinese hamster ovarian (CHO) cells and human fibroblast cells was both morphology- and cell line-dependent [427]. For CHO cells, the endocytosis rates for both MSNs were similar and rapid, whereas endocytotic rate of sphere MSNs was significantly faster than that of rod-like MSNs by fibroblast cells. Another study by Yu et al. [428] reported on the cytotoxicity of MSNs with diameter of 80–150 nm and aspect ratio of 1, 2, 4, and 8 showed that aspect ratio had no significant effect on the particles' acute cytotoxicity, proliferation inhibition, plasma membrane integrity, and cellular uptake to murine macrophage, human lung carcinoma cells, and human erythrocytes. However, the hemolytic activity was shape-dependent: MSNs with higher aspect ratio showed lower hemolytic toxicity. The different cellular uptake behavior of MSNs with similar aspect ratios in this respective study is likely due to the difference in other parameters including diameter of MSNs, selection of cell line, and existence of serum protein in the research systems. With controllable synthesis of MSNs and fluorescent counterparts with aspect ratios from 1 to 10, the interaction between A375 human melanoma cells and MSNs with diameter of about 100 nm and aspect ratio of 1, 2, and 4 [429] also were examined. Overall, particles had a greater impact on different aspects of cellular functions including cell proliferation, apoptosis, cytoskeleton formation, adhesion and migration with the increase of the aspect ratio (Fig. 4.8B) [429], which may result from the accelerated cellular internalisation rate and increased uptake amount (Fig. 4.8C) [429]. In addition to cellular behavior, the protein

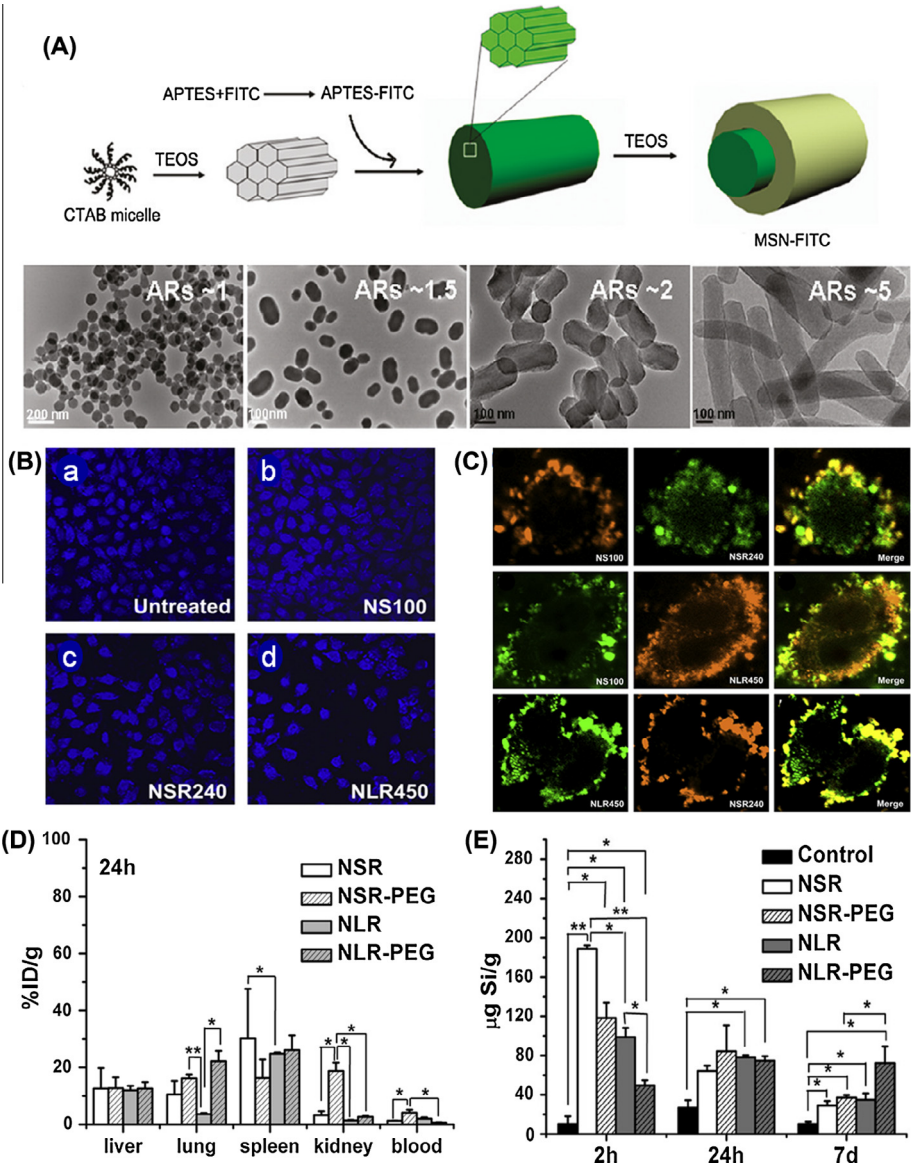

Fig. 4.8. Controlled fabrication of MSNs with different aspect ratios and their effect on the *in vitro* and *in vivo* behaviors. (A) Illustration of the fabrication of MSN–FITC with aspect ratio from 1 to 5 and the TEM images of NPs [416]. (B) A375 cellular adhesion was influenced by nanoparticle with different aspect ratios. (a) Negative control, (b) sphere MSN, (c) short-rod MSN (aspect ratio = 2), and (d) long-rod MSN (aspect ratio = 4) [429] Copyright 2010, Elsevier. (C) A375 cellular uptake simultaneously incubated with two kinds of MSN labeled with different fluorescence. (a) Sphere MSN (RITC-labeled, red), short-rod MSN (aspect ratio = 2; FITC-labeled, green), and merge fluorescent image; (b) sphere MSN (FITC, green), long-rod MSN (aspect ratio = 4; RITC-labeled, red) and merge fluorescent image; (c) long-rod MSN (aspect ratio = 4; FITC-labeled, green), short-rod MSN (aspect ratio = 2; RITC-labeled, red) and merge fluorescent image. FITC: fluorescein isothiocyanate; RITC: rhodamine B isothiocyanate. Reproduced with permission from Ref. [429]. Copyright 2010, Elsevier. (D) Relative silica contents in liver, spleen and kidney at 24 h post intravenous injection of short-rod MSN (aspect ratio = 1.5) and long-rod MSN (aspect ratio = 5). Reproduced with permission from Ref. [416]. Copyright 2011, American Chemical Society. (E) Si content in urine at 24 h post intravenous injection of short-rod MSN (aspect ratio = 1.5) and long-rod MSN (aspect ratio = 5). Reproduced with permission from Ref. [416].

expression related to cell adhesion (e.g., cell adhesion molecule-1 (ICAM-1) and melanoma cell adhesion molecule (MCAM) at the protein and mRNA expression level) were investigated. The influence of particle aspect ratio on protein expression followed the same trend as the cellular behavior. The different cellular uptake pathways would finally determine the intracellular fate of the NPs as DDSs.

Clearance, *in vivo* biodistribution, and biocompatibility of MSNs and PEGylated counterparts with aspect ratios of 1.5 and 5 and diameters of 110–150 nm has also been shown to be dependent on both shape and the degree of surface modification [430]. At 2 h post-intravenous injection, short-rod MSNs (NSR) were easily trapped in the liver, while higher amounts of the long-rod MSN (NLR) were distributed in the spleen (Fig. 4.8D) [416]. PEGylation can decrease the RES sequestration by the liver and spleen for both shaped MSNs. In terms of the circulation time of particles in blood, the long-rod MSN (NLR) and short-rod MSNs (NSR) did not show detectable concentration differences in blood at 2 h after administration. At 24 h, the Si content of NSR in blood significantly decreased, whereas that of NLR maintained at a similar level as that of 2 h, indicating that NLR has a longer blood circulation time than NSR. These results also showed that short-rod MSNs had a more rapid clearance from urine and feces than long-rod MSNs in both excretion routes (Fig. 4.8E) [416]. All these findings may provide useful information for the rational design of efficient drug delivery nanocarriers and therapeutic systems and provide further insights into nanotoxicity.

Understanding the shape effect of sol–gel derived HA microparticles on cellular behavior is important for enabling new kinds of biological and biomedical applications. Yang et al. [431] prepared sol–gel HA microparticles with different shapes and investigated the interaction between the particles and bone marrow mesenchymal stem cells (BMSCs). The results revealed that the shape of HA has a strong influence on cellular behavior, and that the sphere-like particles performed better than the rod-like particles. Moreover, the HA microspheres performed better than the microrod particles for promoting osteogenic differentiation of BMSCs.

To confirm the influence of shape of MSNs more precisely, more rigorous research is needed. Currently, evidence clearly shows that the shape does have an important influence on the cell–nanoparticle interaction and *in vivo* particle biotranslocation. In a recent study [432], it was found that a rod of 15 nm diameter and 54 nm length (CdSe/CdS quantum dot (QD) coated with silica shell) penetrated tumors 4.1 times faster than 35-nm diameter spheres (CdSe QD). This result serves as a reminder that MSNs with large aspect ratios and suitable diameters may have longer circulation time and more efficient tumor accumulation than the spherical ones, which may significant enhance the therapeutic efficacy of nanoparticulate DDSs [433]. However, techniques to produce particles with different shapes using biocompatible materials are limited [434]. Regarding their effect on endocytosis, a theoretical model was proposed in 2005 to compare cell membranes containing diffusive mobile receptors that wrap around ligand-coated cylindrical or spherical particles [244]. In this model, the concept of "wrapping time" was introduced to explain the faster endocytosis of spherical particles than the cylindrical counterpart. To some extent, these models provide useful guidance for the consideration of shape in designing DDSs. However, other approaches have focused on adjusting the concentration and the molar ratio of specific aspect of the system more directly. For example, by adjusting the CTAB and NaOH concentrations, Huang et al. [416] were able to precisely control the aspect ratio of MCM-41 from spherical to rod-like structure with constant diameter. With the ability to tailor any one of the parameters of diameter, aspect ratio, pore size, and geometry while keeping other parameters constant (Fig. 4.3a), the effect of certain chemo-physical properties on biocompatibility and performance in drug delivery of NPs can be more easily investigated.

4.5.4.3. Structure and surface area. Structure is one of the greatest contributors to the properties of sol–gel materials; however, this area of research has been given little attention with respect to biocompatibility. The high specific surface area may be advantageous for encapsulating guest molecules, but may pose an increased risk and hazards with higher reactive and oxidative activity [435]. It is now generally accepted that the specific surface area is positively correlated with the toxicity of NPs. NPs with large surface areas and abundant silanol groups have the ability to generate reactive oxygen species (ROS) which in turn play a significant role in nanomaterial-related injury [435]. It has also been demonstrated that MSNs can inhibit cellular and mitochondrial respiration [436] and cause oxidative stress [437], which itself is not surprising given the correlation between ROS and available

surface moieties. However, comparison of the toxicity of porous and non-porous silica NPs results in differing opinions. The reason is deduced as follows: the "cell-contactable surface area" of NPs dictates the nanoparticle–organism interaction. Although the surface area is higher for porous silica than the nonporous counterpart, the "cell-contactable surface area" (the area which cell membrane, cell-bound proteins, and cell-associated molecules can interact) is lower for porous silica NPs instead [438].

Two independent groups also showed that MSNs exhibited less hemolytic activity compared with their dense silica counterparts possessing sizes similar to those of the MSNs but no mesoporous structures in them [439,440]. The authors attributed this difference in the hemolytic effect exhibited by these two materials to the differences in their surface silanol density and overall cell-contactable surface areas. MSNs with fewer silanol groups on their cell-contactable surfaces were considered to trigger the hemolysis of RBCs at a lower rate than their nonporous silica counterparts containing higher density of cell-contactable surface silanol groups [413].

As introduced above, MSNs can be synthesized with different mesostructures such as hexagonal, cubic, and worm-hole. Besides sizes and shapes, the type of mesostructures existing in MSNs was also found to affect the MSNs' biological activities as illustrated with the following examples. The first example deals with MSNs' catalytic activity toward the oxidation of epinephrine. As mentioned above, both MCM-41 and SBA-15 MSNs were shown to catalyze the oxidation of epinephrine; however, the two materials exhibited different catalytic activities toward this reaction, which was attributed mainly to their differences in mesostructures [441]. In another example, whereas SBA-15 type MSNs impaired cellular respiration and mitochondrial electron transport chain in cells when incubated *in vitro*, MCM-41 type MSNs at the same dosage barely resulted in any noticeable effect [436]. In addition, the MCM-41 type MSNs generally produced milder toxicity than SBA-15 type MSNs [442]. Although these two types of MSNs have similar hexagonally ordered mesostructures, they have some subtle differences. For instance, in contrast to MCM-41, SBA-15 has a unique porosity as it possesses pore interconnectivity between the ordered cylindrical channel pores; this in turn, contributes to a substantial part of total surface area and leads to a different catalytic activity from MCM-41 [441]. Thus, some different biological effects exhibited by these two types of MSNs can be explained based on these structural differences. The relatively larger surface area and smaller pore diameter of MCM-41 can make these nanoparticles thermodynamically more favorable for cellular ingestion, according to the proposed model regarding nanoparticle endocytosis [414].

Studies on 3D porous scaffolds confirmed that surface area, volume, and size of the pores have a considerable effect on cell adhesion, growth, and proliferation [242]. An ideal scaffold needs to mimic the extracellular matrix of the tissue that is being replaced and act as a template for cells to attach, proliferate, migrate and function [73]. The pores should be interconnected with minimum diameters of 100 μm for cell penetration, tissue ingrowth and vascularisation, and with the passage of nutrients to the center of the regenerating tissue [242]. The shape of the scaffold also has an effect on tissue cells and sharp edges may elicit more of an inflammatory response than spheres [443]. The biocompatible scaffold structure provides a 3D environment which promotes cell attachment and proliferation [444]. Apart from being 3D, the scaffold should be made from a biocompatible degradable nontoxic material and should be highly porous to permit the diffusion of nutrients, oxygen, and waste products [445]. This is where nanotechnology can have a significant role to play, since nanotechnology permits the creation of a specialized scaffold structure that can be specifically designed for the particular cell or tissue type. Furthermore, the scaffold can be enhanced to provide the maximum environmental conditions for optimal cellular growth.

5. Biomedical applications

5.1. Scaffolds and matrices for tissue repair and regeneration

Sol–gel technology is a contemporary advancement in science that requires a multidisciplinary approach for its various applications. As noted previously, it is the process of making crystalline and amorphous materials at a relatively low temperature that allows doping of various inorganic,

organic and biomolecules during the formation of a glassy or more ordered matrices [74]. Among the matrix networks, silica-based systems and its combination with modifiers in the biocompatible ionic source categories have gained the greatest attraction in biomedical fields. This class of materials, known as silica-based sol–gel bioactive glasses (BGs) have unique merits as the BGs produced by conventional melt-quenching methods have been limited by the prerequisite of high temperature processes for many decades.

One area of profound impact of BGs relates to bone grafts. Bone grafts are used for augmenting or stimulating the formation of new bone in cases such as the healing of skeletal fractures or between two bones across a diseased joint, to replace and regenerate lost bone as a result of trauma, infection, disease or improve the bone healing response and regeneration of the tissue around surgically implanted devices. The high incidence of these conditions is evidenced by the 2.2 million bone grafts used in orthopedic procedures worldwide annually. The tissue regeneration capacity of these grafts is measured in terms of their osteogenic, osteoconductive, and osteoinductive potential [446]. The osteogenic potential of a bone graft is given by cells involved in bone formation, such as MSCs, osteoblasts, and osteocytes. The term osteoconductive refers to a scaffold or matrix, which stimulates bone cells to grow on its surface. Osteoinductive capacity of a bone graft is perhaps the most challenging property in bone healing, as it can refer to the stimulation of MSCs to differentiate into preosteoblasts and thus to begin the bone-forming process [446].

The properties required to actively stimulate cells and bone formation can be improved by the design of scaffolds as biomimetic (i.e. with an ability to simulate natural tissues) and often involves the delivery of osteoinductive factors (?). To design biomimetic bone scaffolds involves building a proper representation of bone, which, in turn, requires understanding of bone biology and clinical physiology. Bone can be seen as an open cell composite material composed of osteogenic cells, ECM proteins, growth factors, mineral in the form of HCA, and a complex vascular system. The cells that make up the bone represent about 10% of the total volume and include osteoprogenitor cells of mesenchymal origin. Pre-osteoblasts are bone progenitor cells located in the periosteum, endosteum, and Haversian canals that derive from MSCs and which are stimulated through specific growth factors. An ideal mimic for the bone matrix would be facilitated by the tissue engineering approach, a concept to engineer tissue equivalents through the use of scaffolding matrix and tissue forming cells. Tissue engineering has emerged as a promising approach for the repair and regeneration of tissues and organs lost or damaged as a result of trauma, injury, disease or aging [447]. It has the potential to overcome the problem of a shortage of living tissues and organs available for transplantation. In the most common approach, a biomaterials scaffold with a well-defined architecture serves as a temporary structure for cells to guide their proliferation and differentiation into the desired tissue or organ. Growth factors and other biomolecules can be incorporated into the scaffold, along with the cells, to help and guide the regulation of cellular functions during tissue or organ regeneration [448,449]. The overall purpose of this scaffold-based tissue engineering approach is to provide the temporary support structure for tissue forming cells to synthesize new tissue of the desired size and shape.

Scaffolds for tissue engineering are commonly constructed from biodegradable polymeric materials of both synthetic and natural origin [450,451]. However, for the regeneration of load-bearing bones, the use of biodegradable synthetic polymer scaffolds is challenging because of their low mechanical strength and lack of bioactivity. Attempts have been made to reinforce biodegradable polymers with a biocompatible inorganic phase, commonly HA [452,453]. Although brittle, scaffolds fabricated from inorganic materials such as CaP-based bioceramics and BGs can provide higher mechanical strength than polymeric scaffolds alone. Biodegradable metals are currently under investigation [454], but their corrosion behavior *in vivo* remains a key concern. In addition, the situations concerning load-bearing bone grafts often become more complicated from a tribological perspective in that mismatch between the compressive strengths or plastic deformation characteristics of the implant and the natural tissue can result in direct failure due to shear stress induced fractures. Likewise, inappropriate materials which absorb too high a degree of the longitudinal force can lead to a reduction in bone mineral density in the adjacent tissues, thus indirectly exacerbating the differential and increasing the likelihood of implant or joint replacement failure. Whilst the bulk properties of implant materials are outside the scope of this review, applied sol–gel coatings have the potential to provide a biocompatible barrier and therefore stand to increase the range of materials that can be used for their mechanical benefits

alone. The biocompatibility of such materials is therefore less of a concern as the interface between the natural tissue and the implant materials is mediated by the coating that is applied. In this part, we will focus on BGs and their hybrids with organic phases, and other sol–gel compositions for biomedical scaffolds and matrices to stimulate cells and proper bone formation.

5.1.1. Sol–gel bioactive glasses and hybrids

Among the sol–gel compositions, silica-networked glasses have been the most widely studied. In fact, the greatest commercial success of BGs is the silica-based bone graft known as 'Bioglass 45S5' (45% SiO_2, 24.5% NaO_2, 24.5% CaO and 6% P_2O_5 in weight). This material is processed using melting temperatures in the range of 1300–1450 °C followed by casting of bulk implants or quenching to allow formation of powders [455]. Since its discovery, a series of sol–gel compositions have been used to demonstrate *in vitro* bioactivity in SBF with up to approximately 90% SiO_2. These glasses have indeed shown the formation of a HCA layer. Moreover, the rate of surface HA formation for the 58S sol–gel derived compositions was higher than that for the conventional melt-derived 45S5 Bioglass most probably due to a greater surface area and surface reactivity achieved by the low-temperature route and the mesoporosity that is generated. These results encourage the pursuit of potential processing methods for molecular and textural tailoring of the biological behavior – a so called third generation of bioactive materials [456].

For the most part, bioactivity results in the formation of a bond between the tissue and that material, of which two kinds of bioactive materials can be classified according to the tissue response: Type (A) or osteoinductive (which have and connective tissue bone bonding properties and enhance bone formation) and type (B) osteoconductive which are able to bond to bone but at slower rate than the previous Type A and they lack the ability to bond to soft tissue [457]. In other words, these sol–gel derived glasses are considered as bioactive glasses because they have the ability to regenerate bone, and to release ionic stimuli that promote bone cell proliferation by gene activation [242]. Specifically, these properties are thought to be related to the formation of an apatitic surface layer; [458] however, the balance of apatite formation, degradation rate and the presence of extraneous ions are currently the subject of active research.

For the case of sol–gel processed BGs, the effects of ions present in the glass compositions have been substantially researched [459,460]. The presence of major ions, like silicon and calcium, has already shown significant influence on the proliferation and differentiation of cells including osteoblasts and MSCs [461]. Furthermore, some recent attempts have been made to alter the composition of glasses, i.e., incorporating different ionic elements such as phosphate, magnesium, strontium and zinc, in partial replacement of calcium [459,461,462].

Kaur et al. [463] demonstrated the substitution of calcium with phosphate in sol–gel derived glasses with four different compositions, and it was found that the increase in phosphate content led to an increase in the formation of an HCA crystal layer. Moreover, it was found that the growth in this layer increases with glass solubility, and the acidity when immersed in SBF has a direct relation with phosphate content and that there is an association between the decline in cell toxicity with the increase in crystallization. Olmo et al. [464] prepared three different types of sol–gel derived glass compositions $[(SiO_2)_{0.75-X}(CaO)_{0.25}(P_2O_5)_X]$ when $X = 0$, 2.5, 5 and found the rate of HCA layer formation coincided with the high phosphate percentage. In addition, osteoblast cell attachment and spreading were the highest at the highest phosphate composition in comparison to the other compositions in the experiment [464]. Substituting magnesium as (MgO) into (SiO_2–CaO–P_2O_5) sol–gel systems in different percentages showed that replacing the magnesium with calcium led to a decrease in the formation rate of HCA layer, and led to the formation of a thicker HCA layer along with a second whitlockite like layer that attached to the apatite layer formed on the surface of bioactive materials when exposed to physiological solutions. This caused an increase in foam surface area and pore volume with little decrease in pore size [465,466]. In addition to that, adding magnesium to sol–gel derived glasses showed them to be biocompatible and had the ability to stimulate human fetal osteoblastic cells (HFOB) growth [467]. Strontium addition led to strontium traces in the HCA layer formed after immersing it in SBF. In addition to this, the MTS viability assay showed that there was no cytotoxic effect of the added strontium to bone cell viability and calvarial bone cells were seen to colonize the strontium-modified BG. Also examination of osteoblast differentiation markers:

Collagen I and ALP both of which are associated with osteoblast differentiation displayed levels significantly increase over the culture experiment time, and the Runx2, Osterix (Osx) and Dlx5 genes, which are three transcription factors strongly involved in skeletal formation and bone repair, were highly expressed [468,469]. On other hand, zinc-modified sol–gel derived glasses were found to form a thick mineral layer after immersion in SBF and little decline in silicon and calcium dissolution rate was noticed with incubation for seven days. Culturing extracted rat bone marrow mesenchymal stem cells (MSCs) in zinc-modified glass granules resulted in clear increases in the ALP level in relation to zinc concentration and bone sialoprotein (BSP) secretion which is an indicator osteogenic differentiation, were evident especially around the glass granules. This enhanced osteogenesis (?) was significantly enhanced by the zinc BG granules in comparison to that in the zinc-free BG granules after examination by immunofluorescent staining. In addition there was some evidence of increased cell mineralization in the zinc containing samples when viewed by using Alizarin Red S (ARS) staining [470].

As explained above, ionic substitutions have been proposed as an effective tool to improve the biological performance of sol–gel based inorganic materials. Several inorganic materials have been shown to be bioactive and resorbable and to exhibit appropriate mechanical properties, which make them suitable for bone tissue engineering applications. However, the exact mechanism of interaction between the ionic dissolution products of such inorganic materials and human cells are not fully understood. What is certain is that for such materials it is necessary they degrade *in vivo* so that the trace elements can be released. Further to this, release rates should be maintained at a safe level so as to avoid complications that may arise from toxicity. Hoppe et al. [459] describe a schematic overview of biological responses to ionic dissolution products of sol–gel based biomaterials (Fig. 5.1). However, inorganic dissolution products are by no means the only active agents that can be delivered from sol–gel materials. As discussed above (Section 3.5), the production of organic–inorganic hybrid materials is particularly akin to the sol–gel route.

One of the first hybrids reported was based on PMMA–SiO_2 [210]. This material provides a good environment for cell attachment, proliferation, and differentiation for mouse calvarial osteoblast cell cultures when seeded on these silicate BG surfaces. This observation is possible for two reasons: the

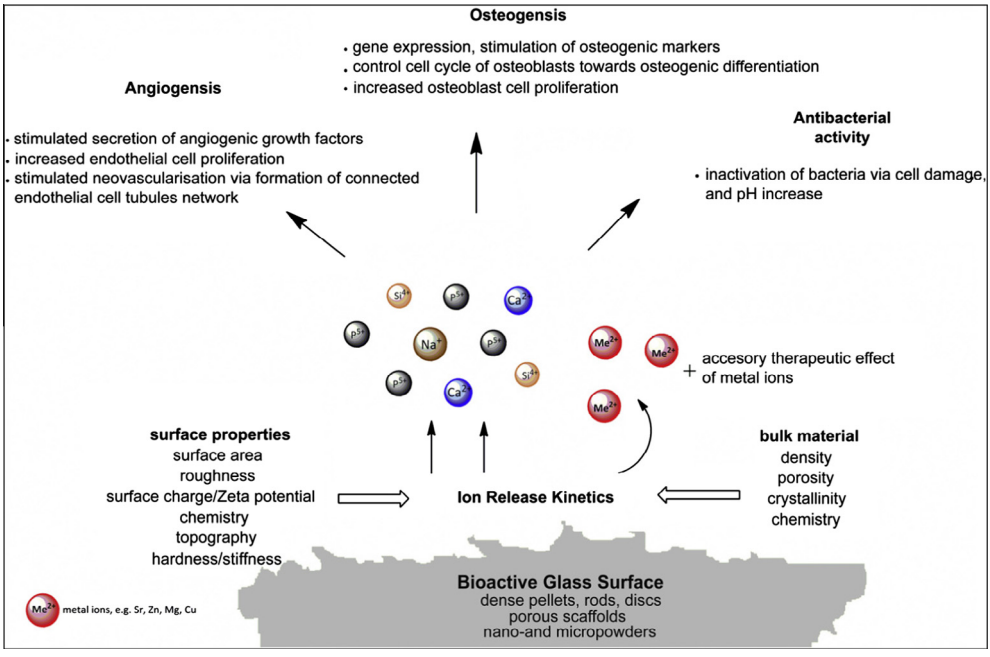

Fig. 5.1. Overview of biological responses to ionic dissolution products of sol–gel based bioactive glasses [459].

PMMA–SiO_2 materials retain the ability to nucleate a favorable CaP surface layer in cell culture media whilst they also release silica (as silicic acid), which itself can aide in osteoblast mineralization. In another example, Chen et al. [317] explored the effects of calcium within a PDMS-modified $CaO–SiO_2–TiO_2$ system. Here, surface calcium was shown to stimulate an apatite-like phase on their surface when immersed in SBF for 12–24 h. As a result, the mechanical properties of the immersed material were increased by PDMS incorporation while the calcium served to promote HCA formation by both providing physical sites for HCA nucleation and through contribution of the crystal growth thermodynamically; the net result being an increase in *in vitro* bioactivity. In instances where hydrophobicity is an issue, other less hydrophobic organic components may also be added [471].

The hybrids of sol–gel BGs with natural polymers including collagen, chitosan and gelatin, have also been researched targeting bone matrix and even for eluting drugs. Several characteristics have been suggested for the tissue-engineered constructs, including porosity, suitable pore size and shape, fiber alignment and orientation, fiber density, internal and external architecture, hydrophilicity, and hydrophobicity, including water uptake, binding, and delivery [472,473]. Regardless of the composition of the scaffolds, the abovementioned characteristics are crucial for their osteoconductive properties [474]. Since the materials should be eventually substituted by new bone, another important criterion is their resorbability. Degradation of the polymers is based on enzymatic or hydrolytic pathways [474,475]. Polymeric scaffolds have unique properties, such as biodegradation. Natural polymers are considered as the first biodegradable biomaterials, while synthetic biodegradable polymers can be produced under controlled conditions [474,476]. Bioactive ceramics, such as HA, TCP (TCP is more quickly biodegraded than HAP), and BGs, react with physiological fluids [476]. However, their biodegradability is often insufficient, limiting their potential clinical use. This issue can be overcome by blending synthetic and natural polymers or using composite materials that improve the scaffold properties such as biodegradability. These products are often named 'hybrid' materials [477–479]. Recently, a novel nanocomposite hydrogel made of collagen and mesoporous BG nanoparticles with surface amination has been developed [480]. The addition of BG nanoparticles into the collagen hydrogel significantly increases the bioactivity of the scaffold and improves its mechanical properties; this novel strategy would therefore be suitable for bone tissue engineering applications [480]. Moreover, the BG foam produced by sol–gel method is an osteoinductive material with a network of interconnected macropores necessary for cell colonization. It has been shown that BG can differentiate human adipose-derived stem cells into osteoblasts, *in vitro* [481]. When BGs were implanted, they bind to collagen, growth factors, and fibrin to form a porous matrix to allow infiltration of osteogenic cells [482].

BGs and their hybrid matrices exhibit unique properties for hard tissue regeneration due to their osteoconductive and osteoinductive behaviors. In addition to this, they also show an ability to bond to soft tissue [483,484]. The rapid formation of a thick HCA layer is responsible for the strong bonding between BGs and bone [483,484]. For soft tissue applications, the bioactive layer prevents the formation of fibrous encapsulation, thus enabling better integration between an implanted material and the tissue itself. More recently, it was observed that ionic dissolution products from 45S5 Bioglass® and other silicate-based glasses stimulate expression of several genes in osteoblastic cells [370]. Furthermore, some BGs were shown to stimulate angiogenesis both *in vitro* and *in vivo* [485,486], whilst possible antibacterial [487,488] and anti-inflammatory [489] effects of BGs have also been investigated. Increasing evidence in the literature indicates that ionic dissolution products from inorganic materials are key to understanding the behavior of these materials within the context of tissue engineering.

One of the more interesting aspects of materials produced by the sol–gel method is the relatively high surface area that results from condensation of the gel network. As noted above, sintering is often applied in order to produce a more condensed material. However, this high surface area may also present significant benefits concerning the release of desired ionic species. With adequate control over the dissolution rate as a whole, the efficiency of the material as a vehicle for the delivery of active agents would be far greater in materials produced *via* sol–gel methodologies. Some of the recent studies have shown the potential of the sol–gel BGs and BG-based hybrids with organic materials in eluting drug molecules that have therapeutic actions [476,477–482]. Since studies have only just begun to emerge, more exciting areas in tissue repair and regeneration are warranted for further investigation and should be explored in the near future.

5.1.2. Matrices with other sol–gel compositions

The development of bone implant devices has resulted in an increase in our understanding of the microenvironment where the replacement has occurred. This evolution can be measured by defining three different generations [105]. First generation bone graft substitutes required the biomaterial to match the physical properties of the tissue to be replaced while maintaining a degree of inertness with the tissue microenvironment. These include metals such as stainless steel, titanium, and alloys; ceramics such as alumina and zirconia; and polymers such as silicone rubber, polypropylene, and poly(methyl methacrylate). A common occurrence for all these biomaterials when implanted, is the formation of fibrous tissue at the biomaterial–tissue interface. This eventually encapsulates the entire implant and can subsequently lead to aseptic loosening. This occurs as a non-specific immune response to a material that cannot be phagocytosed and an inflammatory response persists until the foreign body becomes encapsulated by fibrotic connective tissue, shielding it from the immune system and isolating it from the surrounding tissues [490]. To avoid this non-specific immune response, second-generation bone graft substitutes were developed with bioactive interfaces to elicit a specific biological response (i.e. osteoconduction) and to avoid the formation of the fibrous layer and improve osseointegration. The overall strategy has been to modify first generation biomaterials with coatings that are bioactive or biodegradable. This bioactivity is provided by a surface chemistry that allows either mineralization through heterogeneous nucleation and crystallization of HA or covering of the biomaterial surface with bioactive ceramics such as HA, β-TCP, or bioactive glass. Another type of second-generation bone graft substitutes has been designed as biodegradable with the aim that the rate of degradation matches the healing rate of the injured bone tissue. These materials are based on the use of synthetic or natural polymers that can provide a controlled chemical breakdown under physiological conditions into inert products that can be resorbed by the body. Third generation bone graft substitutes aim to get closer to the autograft standard by using biomaterials capable of inducing specific cellular responses at the molecular level by integrating the bioactivity and biodegradability of second generation devices. This type of bone graft is based on the concept of bone tissue engineering which focuses on creating devices that enhance bone repair and regeneration by incorporating bone progenitor cells and growth factors to stimulate cells into a scaffold made of various natural or synthetic biomaterials or combination thereof, and with sufficient vascularisation to allow access to nutrients to support this process [491]. This method of bone regeneration is osteoconductive in which MSCs are recruited and stimulated to differentiate into pre-osteoblast and depends on the microenvironment.

From a material science perspective, scaffolds are an important area in tissue engineering and can be divided into two main categories including biological (natural or organic) and synthetic (artificial) materials [490–493]. However, for the regeneration of load-bearing bones, the use of biodegradable polymer scaffolds is challenging because of their low mechanical strength and lack of biological activity. Attempts have however been made to reinforce the biodegradable polymers with a biocompatible inorganic phase such as HA [494–497]. Although brittle, scaffolds fabricated from inorganic materials such as calcium phosphate-based bioceramics and bioactive glass can provide higher mechanical strength than polymeric scaffolds. Biodegradable metals are currently under investigation [498], but their corrosion behavior *in vivo* remains a key concern.

To produce a scaffold, important information can be gained by deconstructing biologic tissues to their basic components and then reconstructing the critical component according to the tissue engineering goals [499,500]. Such constructs are specific for one or two materials (e.g., collagen + hydroxyapatite, collagen + chitosan) and therefore have low antigenicity compared with cadaveric grafts [499,501]. Human primary osteoblasts have been seeded onto innovative collagen–gelatin–genipin–HAp scaffolds. *In vitro* attachment, proliferation, and colonization of human primary osteoblasts on col lagen–genipin–HAp scaffolds with different percentages of HA (10%, 20%, and 30%) all increased over time in culture, but comparing different percentages of HA, they seemed to increase with decreasing HA content [502]. A tricomponent osteogenic composite scaffold made of collagen, HA, and poly(L-lactide-*co*-ϵ-caprolactone) has been recently developed, and this composite scaffold was combined with human osteoblast-like cells. The composite was highly porous and enabled osteoblast-like cell adhesion and growth [503]. Jung et al. [504] elucidated the role of collagen membranes when used in conjunction with bovine hydroxyapatite particles incorporated with collagen matrices for lateral

onlay grafts in dogs. This strategy leads to superior new bone formation and bone quality compared to bone graft alone.

CaP ceramics, specifically β-tricalcium phosphate (β-TCP) and synthetic HA, have recently been used in composites and in fibrous composites formed using the electrospinning technique for bone tissue engineering applications. CaP ceramics are often sought because they can be bone bioactive, so that apatite forms on their surface, facilitates bonding to bone tissue, and is osteoconductive [505]. In a recent study, the bioactivity of electrospun composites containing CaPs and their corresponding osteogenic activity was investigated. Electrospun composites consisting of (20/80) HA/TCP nanoceramics and poly(ϵ-caprolactone) were fabricated, and the results demonstrated that after seeding the hybrid scaffold with human MSCs, the cells not only showed greater osteogenic differentiation but also proliferated and produced more bony matrix *in vitro* [505].

5.2. Nanocarriers to deliver biomolecules

The goal of an ideal drug-delivery system is to deliver the therapeutic amount of a drug to the proper site in the body to achieve promptly, and to maintain, the desired drug concentration [75]. Drug-delivery carriers have attracted interest during the past decades, since they can deliver low-molecular-weight drugs, as well as large biomacromolecules such as proteins and genes, either in a localized or in a targeted manner. Many newly designed drugs are also based on biomolecules such as peptides, proteins, and DNA. These molecules are by and large chemically unstable, thus encapsulating and protecting them can be useful in order to deliver drug molecules to the target tissues. Various drug delivery carriers such as micelles, dendrimers, liposomes, emulsions, and porous materials have been showing great promises [506–508]. In particular, porous materials that can be easily processed by the sol–gel approach have attracted greater attention because of their high surface area, stability, uniform porous structure, and tunable pore size [509,510]. In this part, we discuss how sol–gel nanocarriers are evolving as DDSs targeting the repair and regeneration of tissues and the treatment of diseases like cancer.

The essential function of DDS is the ability to increase drug solubility, securing the biological activity from harsh environmental factors like acidic and enzymatic degradation; as well carriers can change drug metabolism and pharmacokinetics to increasing drug accumulation in the targeted location and decrease the off-target distribution and unwanted toxicities. Incorporation of drugs into mesoporous silica materials was introduced as early as 1983 and developed by Kortesuo et al. [284] who reported a sustained release of toremifene citrate from implanted silica sol–gel glass discs with no tissue irritation at the site of the implantation over 42 days. In a logical development from this, mono-dispersed mesoporous silica microspheres were produced by Grun et al. [101]. Following this, increasingly narrow size distributions were developed by fine-tuning the reaction conditions and using various surfactants [511,512]. The uniformity of these materials was identified at an early stage of development in order to ensure a controlled rate or dose of drug release, however, the exact nature of the material must also be controlled. As noted above, particle size can influence both drug release kinetics and the entire loading capacity of MNPs and sol–gel formulated mesoporous nanocarriers have shown excellent capacity to deliver genetic molecules intracellularly, including small interfering RNA (siRNA), micro-RNA (miRNA), messenger RNA (mRNA), and plasmid DNA (pDNA), etc. Compared with viral carriers, non-viral gene delivery systems are much safer and exhibit low-immunogenicity, but the main roadblock of current non-viral carriers is their low gene transfection efficiency. MSNs are considered to be promising candidates for high efficiency gene delivery. The mesoporous structure and tailorable pore size provide space to accommodate gene molecules. Sterically protected in the mesopores, these payloads can escape from nuclease degradation during delivery [513].

To increase the loading capacity of electronegative nucleic acids, well-established surface chemistry allows easy surface modification of MSNs with polycationic groups. Polycation polymers including PAMAM [514], PEI [515], and mannosylated PEI [516] have been functionalized onto MSNs for gene delivery. The positive surface not only increases electrostatic interactions between negatively charged genes, but also facilitates escape from intracellular endosomes through the "proton sponge effect". Xia et al. [517] found that non-covalent attachment of PEI to the surface of MSNs not only generated a cationic surface for DNA/siRNA constructs attachment, but also increased MSN cellular

uptake. Recently, direct packaging of siRNA or DNA within the mesoporous structure of MSNs has also been achieved without the need for surface modification [100,237]. In this case, the main driving forces for siRNA and DNA adsorption into mesopores were intermolecular hydrogen bonds instead of the electrostatic interactions that associated with surface functionalisation. Similar to the delivery of small pharmaceutical drugs, the loading of genes in MSNs can also be controlled by pore size [205,209]. For example, MSNs with large pores (≈23 nm) and functionalised with amino groups have been synthesized for the delivery of pDNA to human cells [209]. Large pores can protect the plasmid against degradation by nucleases in an intact supercoiled form, whereas plasmid vectors loaded in MSNs with 2 nm pores were completely released or degraded because the majority of the vector was loaded on the outer surface of the MSN particles [205].

Nel et al. [517,518] utilized PEI to improve the gene transfection efficiency of MSN because PEI is known to intra-cellularise effectively. PEI was first incorporated into MSNs, and siRNA and DNA subsequently adsorbed. Particle to nucleic acid ratios of 10:100 were needed for complete adsorption. As expected, the high positive charge density of the PEI layer was beneficial for adsorption and showed high transfection efficiency. With non-porous silica NPs, the surface modification showed also some effects on the DNA adsorption and the gene transfection, in which case however the DNA may not be fully protected against degradation by nucleases in the plasma [519,520]. Two main approaches can thus be proposed to enhance the adsorption of genes onto the mesopores of silica NPs: optimization of the loading conditions and increasing mesopore dimensions. In a recent report, Li et al. [209] demonstrated the exclusive adsorption of short salmon derived DNA (20–250 base-pairs with an average chain length of 50 nm) onto the mesopores of small-pore MSNs (pore diameter 2.7 nm) under chaotropic salt conditions where the diameter of the particles was about 70 nm and where the core was composed of a 10 nm super-paramagnetic iron oxide crystallite. Using longer calf thymus DNA (20,000 base-pairs) the maximum loading capacity was reduced to about 22 mg DNA/g MSN, ascribed to the stiffness of DNA under the conditions used. The same group also studied the packaging of siRNA into the mesopores of MSNs under the same conditions as those used for the adsorption of salmon DNA but virtually no adsorption of siRNA was observed [205]. However, performing the siRNA adsorption under more dehydrating conditions (66.7% ethanol) led to siRNA loadings of 13.5 mg siRNA/g MSN at an equilibrium siRNA concentration of 80 μg/ml regardless as to whether a negative control siRNA or expressed green fluorescent protein (eGFP) siRNA was used thus highlighting the importance of optimizing the adsorption conditions to the hydrophilicity of the cargo. The benefit of using MSNs with larger pores was also demonstrated by Solberg and Landry [521]. Using amino-functionalised MSNs containing much larger cage-like pores, with an inner diameter of 20 nm and a particle size of 70–300 nm, Gao et al. [100] were able to adsorb up to about 150 μg/g MSN of firefly luciferase plasmid DNA (5256 base-pairs) from PBS buffer. The surface amino-groups allowed for an attractive interaction with the negatively charged DNA. The adsorbed plasmid was protected against enzymatic degradation, although the exact location of the plasmid, inside the mesopores and on the outer particle surface, remained unclear.

However, many cancer drugs have poor solubility, instability and poor cellular uptake that hamper their therapeutic effects. Due to frequent occurrence of side effects, the therapeutic window of many drugs is narrow. Therefore, the development of delivery systems that can carry a high payload of drug, protect the drug from degradation, facilitate cellular uptake and target specific cell populations is necessary for the clinical applicability of many drugs. MSN-based carriers have thus been highlighted to be especially suited for delivery of small molecules with the advantage of being able to carry a high load of poorly soluble drugs [522]. As more than 40% of substances discovered through combinatorial screening programs have poor solubility in water [523] it comes as no surprise that MSNs based materials have attracted a high interest as drug carriers. The majority of studies to date have focused on the delivery of anticancer drugs such as DOX. Lee et al. [421] delivered DOX to tumor sites and observed DOX-originating fluorescence as well as apoptosis *ex vivo* in the harvested tumor cells 48 h post-injection. However, no free drug was used as control in this study, and hence, the therapeutic benefit of particle-mediated delivery remained unclear. Hillegass et al. [524] applied similar sol–gel based silica microparticles as carriers for DOX to treat malignant mesothelioma. DOX-loaded and empty microparticles were injected both subcutaneously and directly into the tumor or intraperitoneally in an *in vivo* mouse model. Particle-mediated delivery showed enhanced intracellular uptake of

DOX, improved therapeutic efficacy. Enhanced efficacy by incorporation of DOX in MSNs has also been demonstrated in Hep-A-22 liver cancer [525]. For example, Meng et al. [526] demonstrated enhanced particle-mediated DOX efficacy by PEG–PEI coated 50 nm MSNs after intravenous administration. Tumor regression was significantly higher as compared with free drug. Importantly the particle-encapsulated DOX demonstrated reduced systemic, hepatic and renal toxicity. The particles accumulated at tumor sites due to the enhanced permeability and retention effect. Active targeting achieved by specific tumor targeting ligands to the particles can further enhance therapeutic efficacy.

Along with genetic molecules, small drugs have also been delivered substantially through sol–gel NP systems. In particular, anticancer drugs have been the most potentially studied in this regime. Combination therapies with two or more therapeutic agents with complementary or synergistic effects have been used in a variety of diseases especially in cancer therapy. It has been one of the most promising areas in nanomedicine to develop efficient DDSs that could simultaneously deliver two or more kinds of therapeutic molecules in a coordinated manner. Because small-molecule drugs and macromolecular drugs differ greatly, conventional DDSs have difficulty in co-delivery. With tunable pore size, MSNs are excellent candidates for drug co-delivery systems [375,527,528]. They offer both interior pore and exterior particle surface for loading different guest molecules, which is particularly useful for controlling the release sequence of different cargos. Lin et al. [529] designed glucose-responsive double delivery system for both modified insulin and cAMP. These two kinds of molecules had a precise releasing sequence by immobilising gluconic acid-modified insulin (G-Ins) proteins on the exterior surface of MSNs as caps to encapsulate cAMP molecules inside the mesopores. The release of both G-Ins and cAMP from MSNs can be triggered by the introduction of saccharides, such as glucose. Chen et al. utilized MSNs to co-deliver doxorubicin and Bcl-2 siRNA into multidrug-resistant cancer cells to reverse drug resistance [375]. Zhu et al. designed enzyme-triggered drug and gene co-delivery systems by combining hollow mesoporous silica with enzyme degradable PLL polymer [528,530].

More recently, Ashley et al. [531] fused supported lipid bilayers onto MSNs to construct a "protocell" (Fig. 5.2A). The organic–inorganic hybrids were able to synergistically combine the advantage of MSNs with extraordinarily high drug loading capacity with liposomes for enhanced lateral bilayer fluidity. They enabled targeted delivery and controlled release of high concentrations of multicomponent cargos within the cytosol of cancer cells. The hybrids were used to deliver drugs and drug cocktails, siRNAs, and protein toxins (Fig. 5.2B). When delivering a cocktail of DOX, 5-fluorouracil and Cisplatin, the protocells had a 10^6 times higher killing effect on multidrug resistant cells over comparable liposomes (Fig. 5.2C and D). In one instance, by co-delivering Bcl-2 siRNA and DOX, the anticancer efficiency was increased 132 times for drug resistant human ovarian cancer cells compared with free DOX [375]. Lindén and co-workers have delivered γ-secretase inhibitors (GSIs) encapsulated into folate bioconjugated PEI coated MSNs to inhibit Notch signaling, which plays a significant role in tumor angiogenesis, maintenance and progression, and is a specific cancer stem cell signaling for maintaining stem cell characteristics [532]. They showed effective Notch inhibition and significantly enhanced breast tumor therapy efficacy [533].

One important concept in MSN-based DDS is 'gatekeeping', which hybridises another type of molecules or NPs (much smaller than MSNs) on the surface of MSNs. The gatekeeping material is primarily sensitive to internal or external stimuli to enable stimulus-responsive opening of mesopore gates to release drug molecules on demand. Acid-decomposable inorganic materials are examples of gatekeepers that are able to control drug release offering opportunities to design promising carriers for specific therapeutic agents (Fig. 5.3A). One of the more elegant examples of this was demonstrated by Rim et al. [534] who introduced inorganic CaP as a pore blocker through enzyme-mediated mineralization on MSN surfaces. This block could then be dissolved in intracellular endosomes as nontoxic ions to initiate drug release. The construction of the nanoparticle involves urease functionalisation of MSN surfaces and subsequent enzyme-mediated surface calcium phosphate mineralization in the presence of urea under mild conditions within a short time. For pH-controlled DOX release from mineralized MSNs, pH variation between physiological pH and low pH is employed. The results show that a large amount of DOX was released after 24 h under low pH conditions (Fig. 5.3B). Furthermore, the pH-dependent dissolution kinetics of HA-like coating support the DOX release profiles from CaP-capped MSNs (Fig. 5.3C), which confirms that the dissolution of pore blocks results in the opening

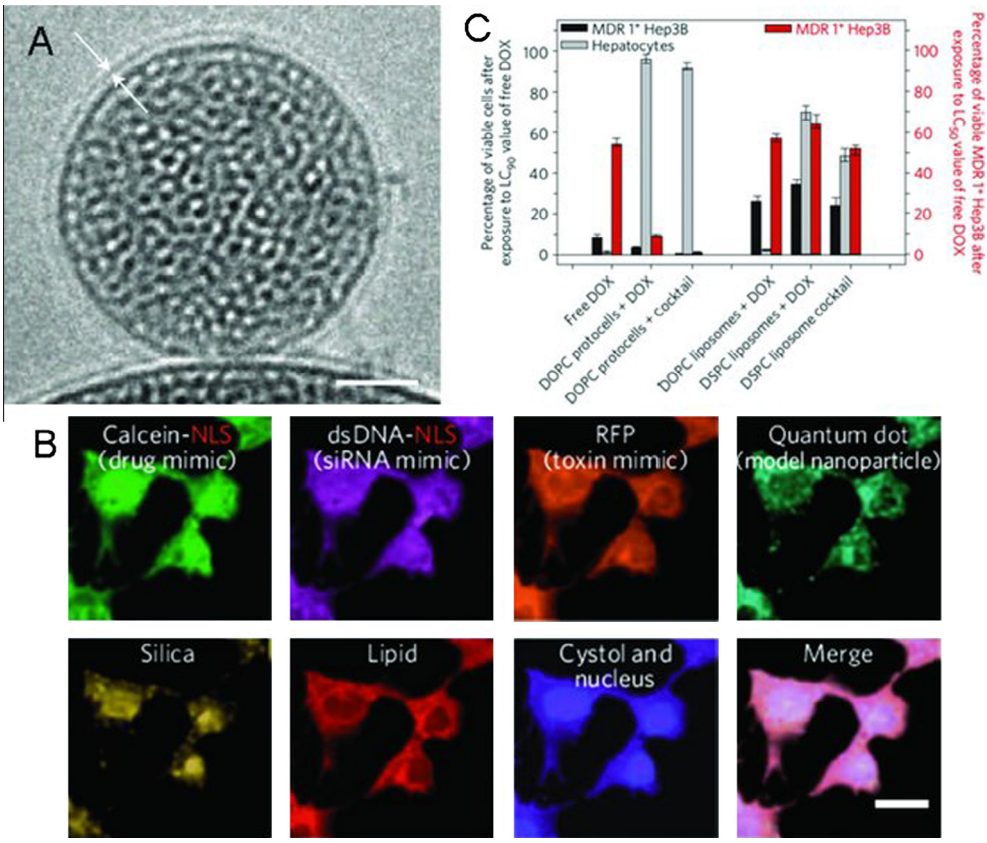

Fig. 5.2. MSN coated with lipid bilayer (called protocell) for multicomponent cargos. (A) Cryogenic TEM image of the protocell. (B) Targeted delivery of multicomponent cargos to the cytosol and nuclei of HCC cells. Alexa Fluor 532-labeled nanoporous silica cores (yellow) were loaded with a multicomponent mixture of four surrogate cargos: calcein (green), Alexa Fluor 647-labeled dsDNA oligonucleotide (magenta), RFP (orange) and CdSe/ZnS quantum dots (teal). Scale bar = 20 μm. (C) Concentration-dependent cytotoxicity of targeting peptide SP94-targeted protocells and liposomes encapsulating DOX. Left axis: the number of $MDR1^+$ Hep3B and hepatocytes that remain viable after exposure to 9.6 μM free DOX, protocell-encapsulated DOX or liposomal DOX for 24 h. Right axis: the number of $MDR1^+$ Hep3B that remain viable after exposure to 2.4 μM free DOX, protocell-encapsulated DOX or liposomal DOX for 24 h. Reproduced with permission from Ref. [531]. Copyright 2011, Nature Publishing Group.

of the pore and then triggers DOX release. In breast cancer MCF-7 cells, DOX-loaded mineralized MSNs carry DOX in nanopores effectively before endocytosis. DOX release can also be facilitated in lysosomes by the dissolution of mineral coatings (Fig. 5.3D).

An alternative strategy was also employed by Muhammad et al. [535]. These authors made use of acid-decomposable ZnO QDs to seal the nanopores of MSNs and inhibit premature drug (DOX) release. After internalization into HeLa cells, the ZnO QD lids are dissolved rapidly in the acidic intracellular compartments, therefore enabling intracellular drug release. In this pH-responsive DDS, ZnO QDs behave as a dual-purpose entity that not only serves as a lid but also imposes a synergistic anti-tumor effect on cancer cells. Another modification of pH-responsive MSNs, able to overcome drug resistance, was published by He et al. [536]. Their composite NPs consisted of MSN carriers still containing the porogen, CTAB, and DOX, where the surfactant served as a chemosensitizer, thus enhancing drug efficacies whilst also acting secondary offensive against multi-drug resistant cancers. It should also be noted that such pH-sensitive DDSs are not only of use in cancer research, but may also have applications in other circumstances where the diseased state can be delineated by a change in pH.

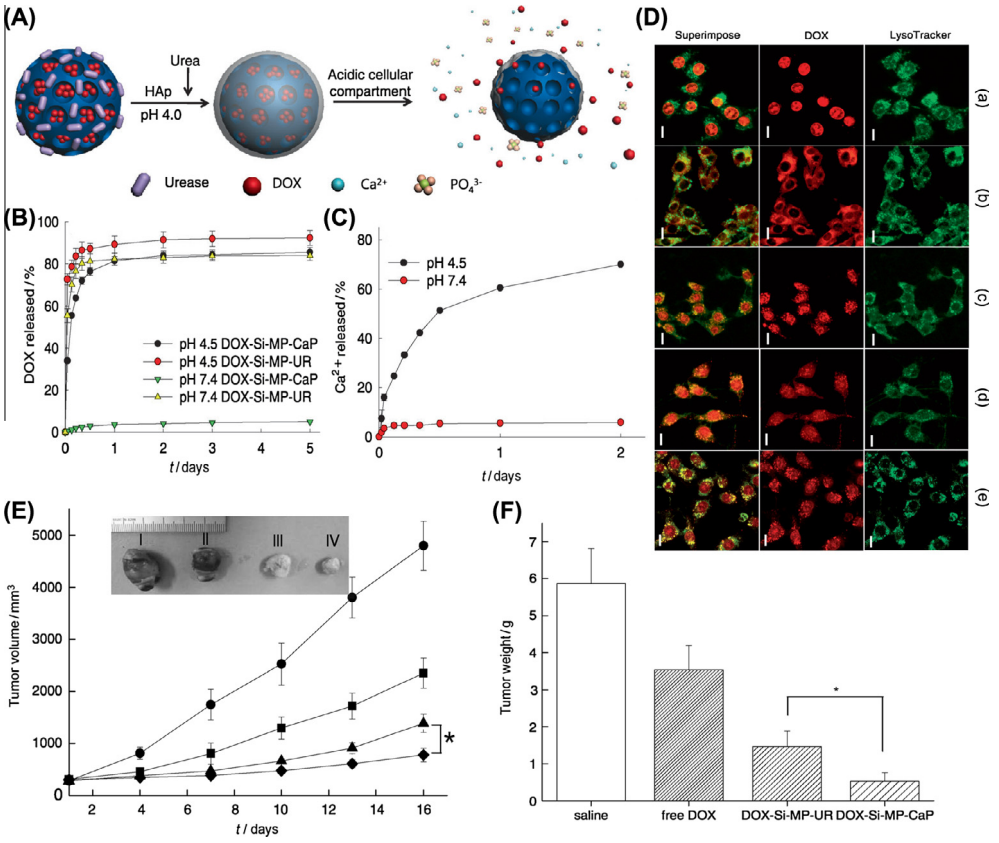

Fig. 5.3. (A) Graphical representation of pH-responsive MSNs with acid-decomposable inorganic gatekeepers. (B) DOX release profiles from DOX–Si–MP–UR and DOX–Si–MP–CaP under pH control. (C) Kinetics of calcium dissolution from DOX–Si–MP–CaP under pH control. (D) CLSM images of live MCF-7 cells treated with Lyso Tracker (50 nm), free DOX (5 μg/mL), and DOX–Si–MP–CaP (DOX = 5 μg/mL), thereinto, (a) free DOX for 1 h exposure; (b) DOX–Si–MP–CaP for 1 h exposure; (c) DOX–Si–MP–CaP for 5 h exposure; (d) DOX–Si–MP–UR for 1 h exposure; and (e) DOX–Si–MP–UR for 5 h exposure. (Green fluorescence is associated with Lyso Tracker; the red fluorescence is expressed by free DOX, released DOX, and DOX retained within MSNs. Scale bar: 20 μm.) (E) *In vivo* therapeutic efficacy after a single intratumoral injection of saline (●), free DOX (■), DOX–Si–MP–UR (▲), and DOX–Si–MP–CaP (◆) at a DOX-equivalent dose of 10 mg kg^{-1}. Inset: images of excised tumors after 16 days post-treatment. I: saline, II: free DOX, III: DOX–Si–MP–UR, IV: DOX–Si–MP–CaP. (F) Tumor weights after 16 days post-treatment [534].

5.3. Multifunctional sol–gel nanocarriers for diagnostic purposes

Diagnosis of diseases at an early stage is a key factor in medicine and improves the chance for a successful treatment. Successful diagnose is in turn dependent on the clinician ability to determine the exact nature of the diseased state. It therefore stands to reason that tools that are able to improve the clinician ability to make such deductions would aide treatment in their own right. Imaging modalities in the clinic generally include optical imaging, MRI, CT, ultrasound and PET or single photon emission computed tomography (SPECT). Fig. 5.4 shows the characteristics of these imaging modalities currently used in the clinical field [18]. Each imaging modality has its own unique advantages along with intrinsic limitations (such as insufficient sensitivity or spatial resolution) which make it difficult to obtain accurate and reliable information at the disease site [537]. To compensate for this problem, the combination of imaging modalities, such as PET and CT or PET and MRI, have gained attention to improve currently used imaging instruments for diagnosis. Multimodal imaging is a powerful method that can provide more reliable and accurate detection of disease sites. Some inorganic NPs also exhibit

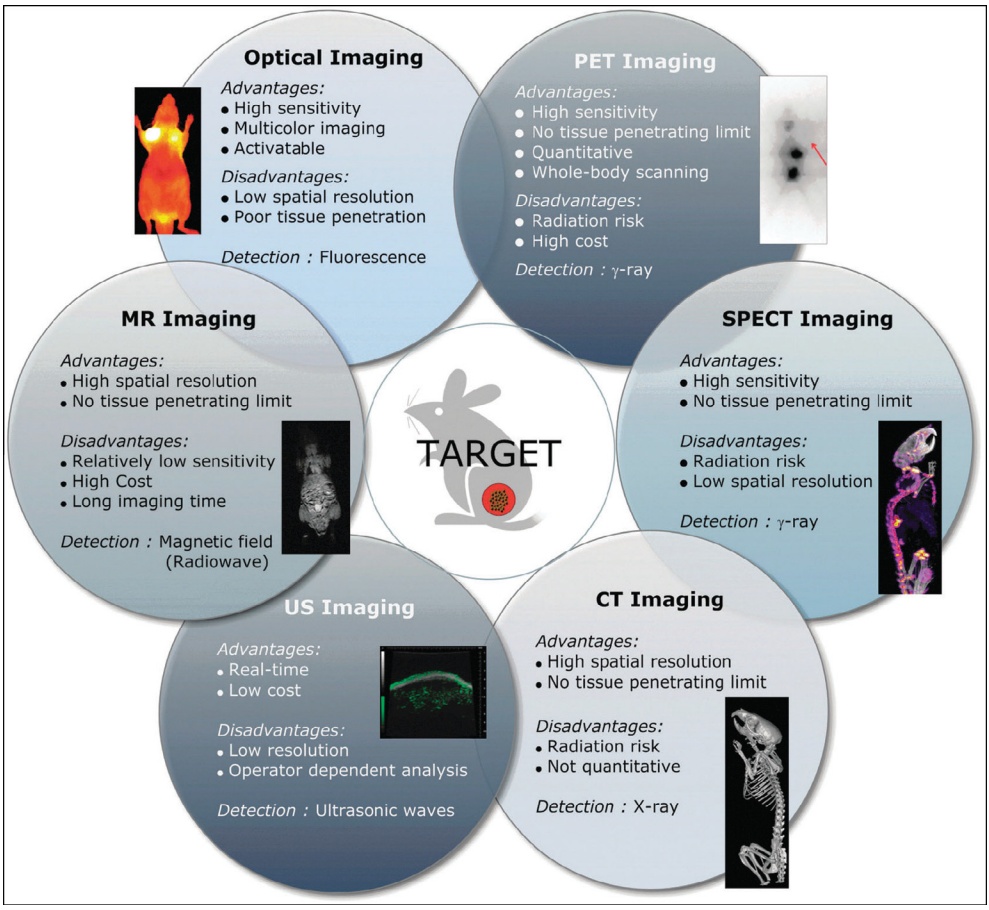

Fig. 5.4. Characteristics of imaging modalities currently used for biomedical applications [18].

intrinsic imaging abilities, such as MNPs for MRI, gold NPs for CT, and QDs for optical imaging. These can be combined with different imaging agents by co-encapsulation or conjugation to develop multimodal imaging platforms.

Commonly used imaging modalities have varying capabilities based on individual mechanisms of tissue contrast or function, specific sensitivity, spatial and temporal resolution in relationship to diseases, as well as biological processes. Multimodality imaging with two or more imaging modalities allows integration of the strengths of individual modalities while overcoming their limitations. Anatomical imaging technologies such as CT and MRI provide unparalleled structural detail whereas functional modalities such as PET and SPECT provide insight into morphological and functional behaviors. By incorporating anatomical and functional imaging in a common hybrid imaging platform, a synergism in the imaging capabilities can be achieved, thus making it possible to visualize and delineate precise structural and functional information. Multimodality imaging thereby ensures better elucidation of physiological mechanisms at molecular and cellular levels. Therefore, multimodality imaging has an immensely beneficial role for improved diagnosis and therapeutic planning of a disease. The field of multimodality imaging has seen rapid progress in the last decade, with its value having been demonstrated in numerous studies. Multifunctional NPs can thus enable multimodal imaging with the combination of two or more imaging modalities for simultaneous imaging and therapy. These techniques are expected to overcome the hurdles of traditional diagnosis and therapy through

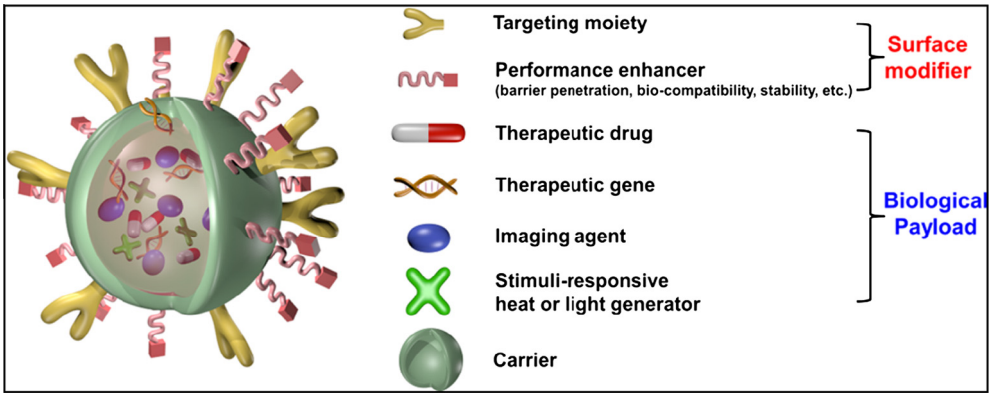

Fig. 5.5. Schematic illustration of a multifunctional nanocomposite [539].

optimized therapy called "theranostics". The sol–gel silica, with its abundant surface silanol groups, a mesoporous structure, and the facile sol–gel synthetic method, provides a matrix for integrating other NPs or chemicals to form nanohybrids.

Generally, silica NPs themselves do not have characteristics for imaging. Therefore, encapsulation with silica matrix is one of the most widely used methods for surface modification of inorganic NPs [538], because the unique properties of the NPs can be preserved by silica shells and various high quality NPs synthesized in organic media can be readily transferred to aqueous media. Controlled sol–gel reactions generate amorphous silica shell around the NPs as described in Fig. 5.5 for the carrier system.

The formation of mesoporous silica instead of a dense silica shell can impart additional drug delivery functionality onto silica-based nanocomposite NPs. Instead, they afford an excellent platform that allows facile loading of a broad range of imaging and therapeutic functions thus making them a good candidate for theranostic purposes. Aside from small molecules, NPs can also be easily incorporated into silica matrices and reports on using such technology to encapsulate inorganic materials (such as MNPs, gold NPs, and QDs) have been well documented [113,540–542]. Moreover, several functionalities can be encapsulated into a single silica particle simultaneously [113,541,542]. A theranostic NP can be dissected into at least three basic components, i.e. biomedical payload, carrier, and surface modifier, depending on their roles and physical locations (Fig. 5.5) [539]. Nanocarriers should provide sufficient physical protection for the biological payloads under physiological conditions during delivery to the desired target site. Various sol–gel based inorganic carriers have been developed. The carrier might be designed to become cancer-specifically disintegrated for better imaging or therapeutic efficacies. Finally, modifiers are attached to the surface of the carrier which are expected to provide theranostic nanomaterials with additional properties, for example, long circulation time, barrier-penetrating ability, and target-specific binding ability. The components for generating a theranostic nanoparticle along with material classifications and functions are listed in Table 5.1. Sathe et al. [543] utilized silica to encapsulate both MNPs and QDs, creating hybrids that retained both magnetic and optical properties. Koole et al. [544] reported a dual-function core–shell–shell nanoparticle, where silica NPs were loaded with both QDs and gadolinium complexes. Both of which served to illustrate this point.

One of the most widely studied theranostic hybrid NPs is magnetic-based because the MRI applications facilitate detection of even the earliest stages of disease, monitoring of tumor response to drug therapies, and tracking cell migration [21]. Surface modifications may be easily introduced through conjugation with targeting moieties, fluorescence dyes, genes, or drugs to provide multimodal functionalities [21,545]. For soft tissue imaging, researchers commonly employ gadolinium ions as chemical contrast agents. In addition to gadolinium, MNPs of elements such as iron, nickle, cobalt, manganese, chromium, as well as their chemical compounds are also used in MRI.

Table 5.1
Materials used in multifunctional NPs for biological imaging, DDSs, and tissue engineering.

Component	Material	Function
Biomedical payload	Imaging agents for optical, CT, MRI, PET, ultrasonic imaging (organic dye, QDs, UCNPs, magnetic materials, metal NPs with SPR, CNT)	Imaging enhancement
	Therapeutic agents (anticancer drugs, DNA, siRNA, hyperthermal/photodynamic materials)	Cancer cell death induction, gene up/downregulation
Carrier	Inorganic (hollow metal NPs, hollow metal oxide NPs, carbon nanostructures, porous Si or SiO_2 NPs)	Multifunctional (imaging ability added to above functions)
Surface modifier	Antibody	Molecular imaging
	Aptamer	Target specific delivery
	Peptide/protein	Uptake enhancement
	Small molecules	Penetration of barrier
	Charge-balancing molecules	Signaling transduction
		Stimuli responsiveness

Magnetic nanocrystals coated by hydrophobic surfactants cannot be used directly for biomedical applications, because intravenously injected nanocrystals tend to agglomerate thereby blocking blood vessels or resulting in nonspecific accumulation in nontarget organs. Many efforts have been made to avoid aggregation of NPs by increasing colloidal stability. Encapsulation by silica is one such example. In 2006, the Hyeon group reported a simple and general method for encapsulation of magnetic oxide NPs in mesoporous silica shell [546]. In this method, pre-synthesized uniform magnetic oxide NPs stabilised with oleic acid were transferred to aqueous media by capping with CTAB. Subsequent silica sol–gel reaction followed by the removal of surfactants resulted in the production of mesoporous silica spheres embedded with iron oxide NPs. This simple and highly reproducible synthetic process can serve as a standard protocol for the fabrication of uniform-nanoparticle possessing mesoporous-silica core–shell nanostructures for multifunctional theranostic applications.

Using this synthetic method, uniform iron-oxide–nanoparticle with mesoporous-silica core–shell nanocomposite NPs were synthesized for imaging and therapy [547]. Particle size strongly affects the efficiency of *in vivo* delivery and cellular uptake [548,549]. For effective systemic delivery, it is desirable to keep the size of therapeutic nanocomposite particles smaller than 100 nm because of their high colloidal stability in a physiological environment and long blood circulation time. The overall particle size could be controlled from 45 to 105 nm by varying the concentration of iron oxide NPs (Fig. 5.6A). The resulting core–shell NPs were monodisperse and maintained discrete form without aggregation, which is highly desirable for *in vivo* applications. Because these nanocomposite NPs are composed of superparamagnetic iron oxide nanoparticle core and mesoporous silica shell, they can be used not only as an MRI contrast agent but also as a drug delivery vehicle. Furthermore, organic fluorescence dyes such as fluorescein isothiocyanate and rhodamine B isothiocyanate can be readily immobilised in mesopores rendering them useful as fluorescent imaging probes. Surface modification with PEG imparted biocompatibility and colloidal stability under physiological conditions. Even after PEG-coating, the hydrodynamic diameter of nanocomposites was kept below 100 nm and they were easily internalised into cells by endocytosis. DOX loaded nanocomposite NPs were internalised by cancer cells and induced cell death (Fig. 5.6B). The applicability of nanocomposite for *in vivo* cancer imaging was also demonstrated. Fig. 5.6C shows *in vivo* MR and optical images of subcutaneously injected cancer cells labeled with magnetic iron oxide nanocomposites. The labeled cells appeared as dark contrast in the MRI scan due to enhanced T_2 relaxation, and intense red emission, due to rhodamine B isothiocyanate, was also observed in the fluorescence image. Such multimodal imaging capability is very useful for both noninvasive diagnosis and guidance to surgical treatment [550]. The small size and high colloidal stability of the nanocomposite NPs also enable systemic delivery to the tumors. When these NPs were administered to the tumor-bearing mice via intravenous injection into the tail vain, they were accumulated at the tumor sites and detected via MRI 2 h after the injection (Fig. 5.6D). The multifunctional capability of the nanocomposite NPs as MRI and fluorescence imaging probes, along with their potential as drug delivery vehicles, makes them novel candidates for simultaneous cancer diagnosis and therapy.

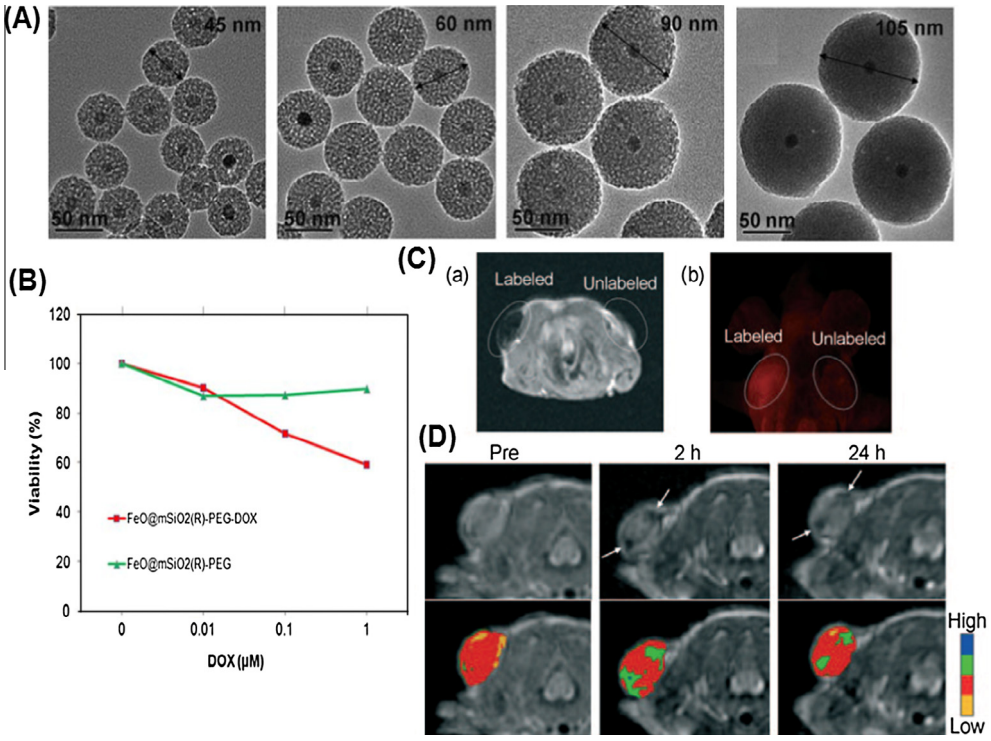

Fig. 5.6. (A) Magnetite-nanoparticle/mesoporous-silica core/shell NPs of various sizes (Fe_3O_4@$mSiO_2$). (B) *In vitro* cytotoxicity of Fe_3O_4@$mSiO_2$ and DOX-loaded Fe_3O_4@$mSiO_2$. (C) *In vivo* T_2-weighted MR and fluorescence images of subcutaneously injected cells labeled with Fe_3O_4@$mSiO_2$ and control cells without labeling into each dorsal shoulder of a nude mouse. (D) *In vivo* T_2-weighted MR images (upper row) and color maps (lower row) of the tumor before and after intravenous injection of Fe_3O_4@$mSiO_2$ to the tumor bearing nude mouse. A decrease of signal intensity on T_2-weighted MR images was detected at the tumor site (arrows) [547].

Along with magnetic-NPs, gold NPs have also been popularly researched in the hybrid materials with MSNs to provide multifunctionality for theranostics, because of their intrinsic optical properties to convert near infrared (NIR) light into heat and CT image [551,552]. Current clinical therapy investigations have shown that when combined with chemo-thermotherapy, additional enhancements result in anticancer efficacy, because hyperthermia can promote drug delivery into tumors, which increase drug toxicity [553,19]. However, gold NPS with nonporous structures exhibit low loading capacities and limited elasticity, restricting their application in effective drug delivery. Therefore, development of multifunctional NIR absorbing nanomaterials that can deliver both drugs and heat, are highly desired. Simple sol–gel methods have been reported for the synthesis of mesoporous silica-encapsulated gold nanorods [554]. The obtained materials have high biocompatibility and stability in biological environments. Most importantly, multifunctional hybrids have specific advantages for combinations of chemo-therapy and photothermal-therapy. Up to now, the use of both therapies applied to cancer cells has been rarely reported while their biomedical applications mainly remains in fluorescence imaging [555], drug release [3] or *in vitro* cancer research [556] rather than dual-model therapy (chemo-photothermal therapy *in vivo* and CT image) [555]. Thus, these *in vivo* studies allow research to elucidate the validity of drug-loaded gold nanorods encapsulated within silica, where safety is extremely significant.

Zhang et al. [556] reported that the development of mesoporous silica-coated gold nanorods as a novel cancer theranostic platform. The large specific surface area of mesoporous silica guarantees a high drug payload. To demonstrate the multiple functionality of new platforms, a well-known

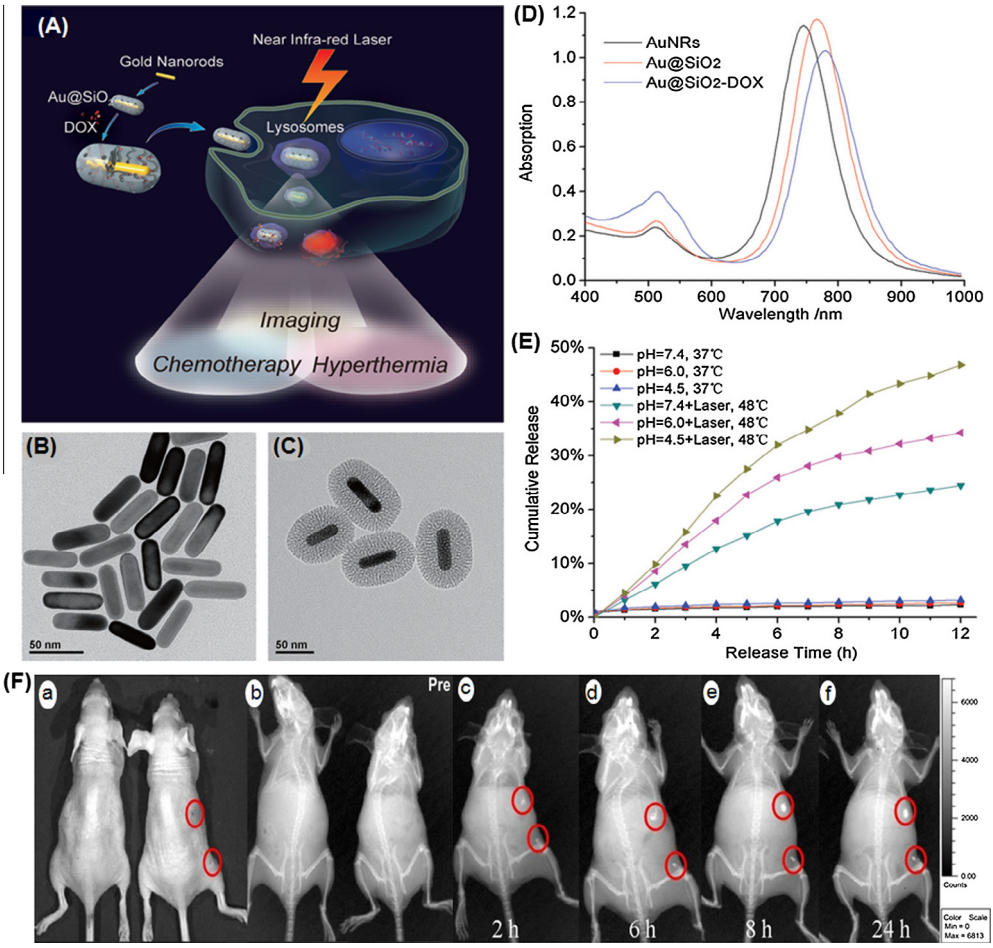

Fig. 5.7. (A) Schematic illustration of mesoporous silica-coated gold nanorods ($Au@SiO_2$) as a novel multifunctional theranostic platform for cancer treatment. TEM images of (B) AuNRs and (C) $Au@SiO_2$, (D) extinction spectra of AuNRs, $Au@SiO_2$, and $Au@SiO_2$–DOX, and (E) DOX release profiles from $Au@SiO_2$–DOX with and without NIR laser irradiation at different pHs [556]. (F) *In vivo* X-ray imaging of mice after subcutaneous injection (left) without and (right) with GNR-SiO_2-FA at different time points. (A) The photograph of mice; (B) the X-ray image at 0 h; (C) the X-ray image at 2 h; (D) the X-ray image at 6 h; (E) the X-ray image at 8 h; (F) the X-ray image at 24 h [430].

chemotherapy drug, DOX, was employed as a model drug. The theranostic principle based on the unique properties of $Au@SiO_2$ is illustrated in Fig. 5.7(a–e) [556]. One imaging modality of the silica-coated gold nanorods, two-photon imaging, was employed to visualize the intracellular colocalisation of material with DOX and some cellular compartments. NIR laser irradiation at a low intensity as used to enhance drug release from DOX-loaded silica-coated gold nanorods for chemotherapy, while at higher irradiation intensity it also gave rise to hyperthermia, which can kill the surrounding cells. Silica-coated gold nanorods can thus provide two therapeutic modes for cancer treatments.

As one of the most widely used diagnostic tools in hospitals today, X-ray CT is an imaging technique based on X-ray absorption difference (absorption contrast) of the body compositions. Due to their high atomic weight and X-ray absorption coefficient, small iodinated molecules are generally used as contrast agents to improve the visibility of internal body structures in X-ray CT procedures. However, these contrast agents only allow very short time imaging due to rapid renal excretion and may also cause renal toxicity. Recently, silica-coated gold nanorods have attracted much attention

for the development of new CT imaging agents, because gold has a higher atomic weight and X-ray absorption coefficient than iodine. Luo et al. [555] reported indocyanine green-loaded silica-coated gold nanorods for the dual capability of X-ray CT and fluorescence imaging. It was demonstrated that nanorod system could enhance CT contrast significantly and multiplexed images can be easily obtained by using this dual mode imaging agent. In another paper, the same group also showed that X-ray imaging could be employed to monitor the tumor targeting ability of folic acid-conjugated silica-coated gold nanorods during the whole blood circulation (Fig. 5.7F) [430]. The sol–gel chemistry offers a simple method to coat and build in chemical functionality to NP's.

5.4. Sol–gel based sensing devices

Biosensors rely on the interfacing of a biorecognition element to a physical transducer that converts the biological reaction into a measurable signal. Key attributes that can be optimized include response time, initial and long-term biological activity, analytical range, sensitivity, selectivity, detection limit, and reproducibility. To a certain extent, many of these parameters are determined by the biorecognition element on the basis of its binding constant to the analyte of interest but also by the specific detection method employed. Substantial changes in analytical performance can therefore be derived from changes in these parameters [557–559]. Typically, reduced accessibility or activity leads to poorer sensitivity and may alter the analytical range. Furthermore, analyte–matrix interactions can lead to an expanded analytical range, but lower sensitivity, although this can be controlled to some extent by the addition of charged polymers [560]. Other approaches include the ability to make the matrices either electrochemically active or optically transparent, the ability to achieve high protein loading, to tune the polarity and porosity of the matrix to selectively modulate enzyme activity, the potential to modulate the material composition to maximize the biocompatibility of the matrix, and the reduced leaching of biomolecules [561,562]. Some of the more recent articles that have aimed to review the development of these devise have focused on the application of hybrid sol–gel films and monoliths for optical and electrochemical sensing of inorganic species [563], MSNs for biosensing [299,427], zeolites and mesoporous silicates for electrochemical detection [564], and sol–gels and templated mesoporous materials for fluorescence-based sensing [565,566]. The versatility of mesoporous silicates has resulted in their application to sensors for a wide range of analytes in liquid and vapor phase environments. However concerns that often need to be addressed in the utility of these materials are ever present and include reversibility and reproducibility, selectivity, response and recovery time, and ease of application. These factors are especially important when considering the use of sol–gel based sensing devices for medical diagnostics or managing treatment.

Several properties of sol–gel-derived materials, most notably, those that are silica-based, render them particularly compatible with biosensor development. Firstly, they are transparent in the UV and visible spectral range, making them amenable to common detection techniques such as absorption, reflection, fluorescence, chemiluminescence, and bioluminescence [564,567–569]. Secondly, as a solid-phase support, the materials are mechanically robust, relatively chemically inert, resistant to thermal degradation, photochemical degradation, and biodegradation [564,569–571]. Thirdly, they can be doped with a wide variety of sensing elements because the silica framework grows around the guest biomolecules, stretching the upper limits on dopant size [569,572]. The interpenetrating networks of silica effectively serve to "cage" biomolecules, preventing them from leaching. While global biomolecule dynamics are restricted, the cage is still sufficiently loose to allow for local rotational and translational motions, including those required for substrate binding [196,573,574]. At the same time, this tight fitting precludes macromolecular exchange while allowing for unrestricted transport of small molecules including buffer ions, substrates, and products of reactions in and out of the porous structure as may be required in sensing applications [196,574].

Recent progress in the development of "protein friendly" sol–gel processing methods has allowed these materials to be utilized as components of numerous biosensors, using delicate biomolecules such as luciferase and kinases, or even membrane-bound receptors as biorecognition elements. Among the different nanoparticle biosensors, enzyme immobilised NPs have been reported in numerous publications [575]. While enzyme-based sensors show great specificity and low concentration detection limits, they suffer from denaturation and inactivation, plus they lack two important

characteristics held by mesoporous silicas: (I) high porosity and (II) optical transparency. The former property allows for the location of sensing molecules not only on the external surface of the material but also inside of the pores, which enables the loading of large amounts of sensing molecules giving fast responses and low detection limits. Silicate glass obtained by the sol–gel process has been used for biosensing purposes [576–578]. Microporous silica NPs have long been used for the creation of biosensors utilizing drugs, enzymes, antibodies [579–581] and DNA [582] as recognition elements. However, pores in sol–gel derived silica lack a high degree of order, which results in nonlinear paths, and consequently slow diffusion of the analytes to the sensing molecules. Some fraction of the sensing molecules might even be unreachable leading to less than optimal response. In contrast to microporous silica, mesoporous silica has much more available surface area due to its larger and more ordered pores. This allows for larger concentrations of accessible receptor molecules, the possibility to detect larger molecules, and a faster diffusion to the sites where the receptors are located, which altogether results in even faster and better response of the sensors.

Proteins have been used largely as active elements for the selectivity of mesoporous silica supported biosensors. For example, mesoporous silica was loaded with glucose oxidase and horseradish peroxidase and used as a sensor for glucose [583,584]. In another study myoglobin and hemoglobin were immobilised in mesoporous silica modified electrodes to be used as a sensor for H_2O_2 and NO_2^- [585,586]. The main reason for using enzymes and proteins as the recognition unit is their high specificity for substrates. However, these biomolecules are relatively expensive and lack long-term chemical stability. To avoid these disadvantages, while maintaining high analyte selectivity, research as a whole has pursued a new approach. Unlike the molecular imprinting approach, selectivity is attained not by synthesizing size or shape selective recognition receptors, but by controlling the diffusional penetration of analytes into the surface-functionalised mesopores. As described below, new mesoporous silica-based selective sensory systems have been reported by using this strategy.

To develop a biosensor suitable to distinguish between several structurally similar neurotransmitters, such as dopamine, tyrosine and glutamic acid, selective functionalisation of the exterior and interior surfaces can be exploited (Fig. 5.8) [514]. PLLA coated MCM-41-type mesoporous silica nanosphere (PLA-MSN) material can serve as a fluorescence sensor system for detection of amino-containing neurotransmitters in neutral aqueous buffer. Utilizing the PLLA layer as a gatekeeper, several structurally simple neurotransmitters can react with primary amine groups and form the corresponding fluorescent isoindole product. The observed large difference in the rates of diffusion is most likely due to the different electrostatic, hydrogen bonding, and dipolar interactions between these neurotransmitters and the PLLA layer. The isoelectric points of dopamine, tyrosine, and glutamic acid are 9.7, 5.7, and 3.2, respectively, whereas the isoelectric points of PLLA is typically below 2.0 which means the dopamine will be positively charged and the others will be negatively charged under physiological conditions. The PLLA layer of the PLA-MSN sensor shows a unique “sieving” effect that regulates the rates of diffusion of the amino acid-based neurotransmitters into the sensor mesopores of the material.

Another biosensor that was synthesized and studied by Descalzo et al. [587,588] involved aminomethylanthracene groups grafted onto MSNs and used for the recognition and detection of anions. The bulk of the grafted group combined with the steric restrictions provided by the pore size of the material led to the ability of the material to respond in different degrees to adenosine tri-, di-, and monophosphate. Adenosine triphosphate was able to quench the fluorescence of the material to a larger degree than the other two species, and small anions such as chloride, bromide and phosphate did not produce any response of the sensor. These authors compared the sensitivity toward Adenosine triphosphate of the aminomethylanthracene MSN with aminomethylanthracene grafted on fumed silica and observed a 100-fold improved sensitivity when the matrix was mesoporous [587,588].

A growing number of reports have demonstrated the versatility of mesoporous silicates as active components in pH sensing. These applications typically involve immobilising an indicating dye on a mesoporous surface or encapsulating it in silicate walls. In living organisms, intracellular pH plays key roles in enzyme, cell, and tissue activities, and microenvironments in endosomes (pH 5.5–6) and lysosomes (pH 4.5–5) are mildly acidic. Besides, some tumor cells possess lower extracellular pH (pH 6.4–6.9) compared to normal tissues (pH 7.2–7.4). Thus, monitoring pH changes and gradients are quite important to determine the efficiency of pharmaceutical therapies, diagnose certain cancer

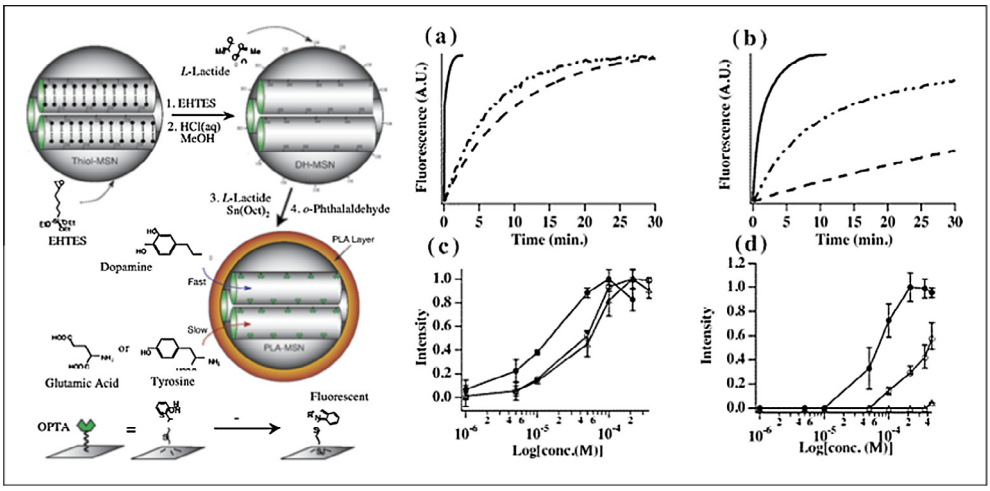

Fig. 5.8. Schematic representation of the synthesis of PLA-coated MSN-based fluorescence sensor system for detection of amine-containing neurotransmitters, i.e., dopamine, glutamic acid, and tyrosine (R–NH_2) (5,6-epoxyhexyltriethoxysilane = EHTES, cetyltrimethylammonium bromide (CTAB) surfactant = ·∼ ∼ ∼ ∼). Kinetic measurements of the fluorescence detection of dopamine (), tyrosine (– - - - - - - - -), and glutamic acid (- - -) with OPTA-SS (a) and PLA-MSN (b). Fluorescence increase of OPTA-SS (c) and PLA-MSN (d) as a function of dopamine (·), tyrosine (○), and glutamic acid (△) concentrations. The fluorescence intensities were measured 5 min after the introduction of every concentration of each neurotransmitter. Reprinted with permission from Ref. [514].

diseases, and investigate cellular internalisation pathways. If MSN-based drug nanocarriers are endowed with pH-sensing ability, they might be useful in practical applications for simultaneous chemotherapy and the monitoring of therapeutic efficiency. Moreover, this novel type of multifunctional MSN-based nanocarriers can be quite advantageous for investigating drug nanocarriers–cell interactions and understanding the underlying mechanism. The fabrication of fluorescent pH-sensing organic–inorganic hybrid MSN capable of tunable redox-responsive release of embedded guest molecules [589]. The reversible addition−fragmentation chain transfer copolymerization of N-(acryloxy)succinimide, oligo(ethylene glycol) monomethyl ether methacrylate, and 1,8-naphthalimide-based pH-sensing monomer at the surface of MSN led to fluorescent organic–inorganic hybrid MSN. The obtained hybrid MSN exhibits excellent water dispersibility and acts as sensitive fluorescent pH probes in the range pH 4–8 due to the presence of 1,8-naphthalimide moieties. After loading with rhodamine B as a model drug molecule, copolymer brushes at the surface of hybrid MSN were cross-linked with cystamine to block nanopore entrances for the effective retention of guest molecules. Taking advantage of disulfide-containing cross-linkers, the release rate of rhodamine B can be easily adjusted by adding varying concentrations of dithiothreitol, which can cleave the disulfide linkage to open blocked nanopores. The increase of dithiothreitol concentration from 0 to 20 mM led to 20–30 times enhancement of rhodamine B release.

FITC has also been modified with an amino-bearing siloxane to provide a precursor for direct mesoporous material synthesis [590]. The result is a material with fluorescein isothiocyanate on the pore walls, which is responsive to pH changes in the range from 3.1 to 11.2 that can be interrogated through laser excited photoluminescence. Grafting of silane-modified 5-methoxy-2-(pyridyl) thiazole) onto SBA-15 has been applied to sensing pH and cupric ion detection [21]. The material exhibited dual fluorescence emission bands. The first at 420 nm was quenched while the second at 448 nm increased in intensity as pH decreased in the range from 5.7 to 1. Addition of cupric ions at pH 6.0 quenched and blue-shifted fluorescence. An impressive detection limit of 3.2×10^{-6} M was obtained. This response was found to be somewhat selective for copper with smaller responses to ferric iron and mercuric mercury. Encapsulation of bromothymol blue provided a material that yielded visual color changes from orange–yellow to royal blue across pH values ranging from 2 to 12.

Evanescent wave absorbance spectroscopy (600 nm) was also used for interrogation [591]. Various sulfonephthalein indicators have also been encapsulated in hybrid xerogel films synthesized from mixtures of tetraethoxysilane and vinyltriethoxysilane for applications in pH sensing [592]. From a biomedical perspective, effective means of determining local changes in pH can be extremely useful. For example, microbial infections are often accompanied by a reduction in pH due to anaerobic respiration during sepsis. The ease with which trace element or drug concentrations within biological samples can be determined would also stand to provide great benefits to medical diagnostics and, ultimately, the care received by the patient.

6. Conclusions and future perspectives

In conclusion, the sol–gel synthesis method offers a molecular-level mixing and is capable of improving the chemical homogeneity of the resulting composite. This opens new doors not only to previously unattainable material compositions but also unique structures. Sol–gel derived bioceramics have a great potential for application as a coating on metallic substrates to provide a high degree of biocompatibility and promote a rapid healing response with minimal adverse biological events. Without a doubt, one of the main benefits of applying sol–gel approaches to the production of bioactive coatings is the relatively low temperatures under which synthesis can be achieved. However, compatibility is but one facet of sol–gel derived biomedical applications. Low temperature synthesis also allows for the inclusion of materials that would otherwise be destroyed by excessively high temperatures. Since sol–gel processes are carried out at such low temperatures, they can also allow the inclusion of biomolecules, therapeutic agents including drugs, growth factors, and proteins. These can be loaded during the sol–gel preparation process and released in a controlled manner. Further to this, the relatively low synthesis temperatures provide further benefits in that complications that can arise with the application of bioactive coatings can be avoided, such as mismatched thermal expansion coefficients found in conventional coatings, which can lead to the formation of cracks and poor interfacial bonding as a result of shear stresses induced upon cooling. The sol–gel method should be simple, stable, cost-effective, and scalable for facilitating future industrial production and clinical translocation.

As well as tunable chemistry, further advantages of the sol–gel synthesis process are the tunable structures that allow control over the morphology, porosity, size, and the ability to modify the surface for biomedical applications. The surface area and pore diameter are critical factors for drug adsorption and release in DDSs. MSNs have been the subject of significant research in drug-delivery applications with the possibility of embedding various protein molecules into these materials for biosensing purposes. The surface of MSNs can also be modified to promote their ability to deliver drugs or biomolecules to desired sites in a sustained manner that makes them interesting candidates for cancer therapy. Functionalisation can also be exploited in the development of sensing devices to allow not only therapy, but simultaneous diagnosis or so called theranostic purposes. Aside from direct loading of MSNs with biosensing molecules or methods of increasing the capacity thereof, the same steric properties responsible for the localization of elements of the sensing system can also be used to be filter substrates and thus add further specificity. It is the sol–gel process that underpins these new and advanced bioactives.

Concerns associated with non-viral gene delivery systems are also much lower than the viral vector counterpart. Whilst the relative merits of either approach are yet to be evaluated in full, non-viral DDSs are likely to experience less resistance in their journey from initial conception to mechanistic studies, clinical trials, and ultimate acceptance by the general public. This is not to say that alternative means should not be sought rather that non-biological delivery poses less of a potential hazard and thus the development of sol–gel based materials as DDSs may be a more attractive option.

The effect of shape is an area ripe for further research and from this, *in vitro* experiments will provide the basis for *in vivo* responses to be better predicted. However, it was also shown that many different structural features of MSNs could lead to different biological activities for these materials. Thus, probing and summarizing the overall biological responses induced by these materials, which possess a range of structural features and compositions, could be challenging. Nevertheless, in light of their

great potential applications in biomedical areas, many experts in the field seem to agree that the biological activities of these materials need to be fully assessed and evaluated in order to determine the proper physical or chemical traits that could make MSNs highly biocompatible.

A broad evaluation at the interface between the material's properties and its biological surroundings is crucial to fully determine whether a given material is biocompatible. This task, however, is very complicated and challenging in the case of engineered nanomaterials such as MSNs because they possess a variety of physical properties and chemical compositions, which could lead to a diverse range of biological responses and trigger a cascade of different biological events. While a large number of studies are being conducted by various researchers worldwide to fully understand these structure-related biological effects of MSNs, including their possible negative impacts on human health, some of the studies also revealed contradictory results about the biocompatibility (or cytotoxicity) of various MSNs, as we discussed in this review.

The chemical modification, along with the original synthetic condition, can tailor the particle size, shape, or surface properties of the MSNs. This, in turn, could influence the biological properties and activities of the nanomaterials. This aspect of functionalized MSNs was also considered in this review. In particular, examples illustrated that the favorable size, shape, or surface property of organic-functionalized and nonfunctionalized MSNs alike that leads to insignificant interference in a given biological system can generally be attributed to those that cost the least in terms of interfacial energy at the nano-bio boundary. Specifically, in contact with cell or intracellular organelles, MSNs of a particular size and shape with larger surface area can be thermodynamically favored in their cellular interactions, leading to more intracellular accumulation but reduced cell injury. Thus, proper surface modification of MSNs (e.g., making MSNs with positively charged surfaces) can enhance their endocytosis as well as exocytosis, while also mollifying their intracellular trafficking. However, size may play a more significant role compared to shape in causing toxicity *in vivo*, if any, as the body generally recognizes a certain dimension of foreign particles, allowing or disallowing their further penetration into different organs or sites in the body to enable it to take part in some biological processes. At the same time, different surface properties regulate particle circulation in the bloodstream, whereas different affinities to certain biological receptors due to functionalization can dictate the final fate or biocompatibility of the particles.

A new class of nanostructured materials, which has accelerated or improved bioactive behavior compared with conventional bioactive glasses are being developed. This improved bioactive behavior has been attributed to the highly ordered arrangement of uniform-sized mesopores. Moreover, the possibility of tailoring the structural and textural characteristics of bioactive glasses offers numerous advantages to modulate their bioactive responses. The structural and textural properties of mesoporous materials also permit the development of bioceramics with controlled delivery capability able to load and locally release drugs to treat different bone pathologies such as infection, osteoporosis and cancer. The appropriate functionalization of the inner surface of the mesopore channels allows for modulating drug loading and plays a key role in offering sustained drug release.

Improved bioactive behavior and controlled drug delivery capability, makes them excellent candidates to be used as starting materials for the manufacture of three-dimensional macroporous scaffolds for bone tissue engineering. Within this application, special attention should be given to the possibility of covalently grafting osteoinductive agents, such as peptides, proteins and growth factors) to the surface of the three-dimensional scaffolds, which would act as attractive signals for bone cells and promote the bone regeneration process.

For cancer therapy, MSNs show obvious advantages over other nanoparticulate DDSs because of their extraordinarily high drug loading, potential for controlled drug release behavior, and ability to delivery more than one component. However, great challenges still exist. To overcome the *in vivo* physiological barriers and achieve efficient delivery of nanoparticles to cancer cells, MSNs as nanocarriers should integrate the requirements of long circulation time, low reticuloendothelial system sequestration, ability to extravasate into tumor tissue, and cancer cell specific internalization. The properties of nanoparticulate DDSs and the physiological microenvironment in bodies are co-determinants for the final therapeutic benefits. Even if with efficient delivery to tumor sites, the physiological nature of cancer brings tremendous difficulties in efficient therapy. With the diversity and multifunctionality of MSN-based nanocomposites, it may be a promising way to develop

cooperative therapies such as utility of the synergistic effect of photothermal/magnetohyperthermal therapy and chemotherapy, or simultaneous utility of several nano-based formulations targeting different populations of cancer cells with different phenotypes. Certainly, a greater understanding about cancer biology and physiology is essential for more specific targeting options.

Acknowledgements

Authors acknowledge support from the National Research Foundation (Priority Research Centers Program No. 2009-0093829 and Global Research Laboratory Program No. 2015032163), the Commercialization Promotion Agency for R&D Outcomes, Republic of Korea.

This work was supported by the UCL EPSRC Industrial Doctoral Centre in Molecular Modelling & Materials Science.

References

[1] Brinker CJ. Better ceramics through chemistry – an overview of sol–gel technology. Abstr Pap Am Chem Soc 1990;200. 217-COLL.
[2] Rosenholm JM, Sahlgren C, Linden M. Towards multifunctional, targeted drug delivery systems using mesoporous silica nanoparticles – opportunities & challenges. Nanoscale 2010;2:1870–83.
[3] Yang P, Gai S, Lin J. Functionalized mesoporous silica materials for controlled drug delivery. Chem Soc Rev 2012;41:3679–98.
[4] Avnir D. Organic chemistry within ceramic matrixes: doped sol–gel materials. Acc Chem Res 1995;28:328–34.
[5] Ciriminna R, Fidalgo A, Pandarus V, Beland F, Ilharco LM, Pagliaro M. The sol–gel route to advanced silica-based materials and recent applications. Chem Rev 2013;113:6592–620.
[6] Hench LL. Sol–gel materials for bioceramic applications. Curr Opin Solid State Mater Sci 1997;2:604–10.
[7] Hughes OR. In: MacKenzie John D, Ulrich Donald R, editors. Ultrastructure processing of advanced ceramics. New York: Wiley-Interscience; 1988. 1013 pp. [$95.00. AIChE J 1989;35:876].
[8] Graham TJ. On the properties of silicic acid and other analogous substances. Chem Soc 1864;17:318.
[9] Helmont JBv. Joannis Baptistæ van Helmont, Toparchæ in Royenborch, Pellines, & c. Opuscula medica inaudita. I. De lithiasi. II. De febribus. III. De humoribus Galeni. IV. De peste. Editio secunda multò emendatior. ed. Amsterodami: Amsterodami: Apud Ludovicum Elzevirium; 1648.
[10] Wright JD, Sommersjik NAJM. Sol–gel materials: chemistry and application. CRC Press; 2000.
[11] Ebelmen M. Recherches sur les combinaisons des acides borique et silicique avec les éthers. Ann Chim Phys 1846;16:166.
[12] Patrick WA. Silica gel and process of making same. Google Patents; 1919.
[13] Kistler SS. Coherent expanded aerogels and jellies. Nature 1931;127:741.
[14] Balamurugan A, Kannan S, Rajeswari S. Structural and electrochemical behaviour of sol–gel zirconia films on 316L stainless-steel in simulated body fluid environment. Mater Lett 2003;57:4202–5.
[15] Haddow DB, James PF, Van Noort R. Sol–gel derived calcium phosphate coatings for biomedical applications. J Sol–Gel Sci Technol 1998;13:261–5.
[16] Haddow DB, James PF, VanNoort R. Characterization of sol–gel surfaces for biomedical applications. J Mater Sci – Mater Med 1996;7:255–60.
[17] Radin S, Ducheyne P. Controlled release of vancomycin from thin sol–gel films on titanium alloy fracture plate material. Biomaterials 2007;28:1721–9.
[18] Lee DE, Koo H, Sun IC, Ryu JH, Kim K, Kwon IC. Multifunctional nanoparticles for multimodal imaging and theragnosis. Chem Soc Rev 2012;41:2656–72.
[19] Lee JE, Lee N, Kim T, Kim J, Hyeon T. Multifunctional mesoporous silica nanocomposite nanoparticles for theranostic applications. Acc Chem Res 2011;44:893–902.
[20] Hervault A, Thanh NT. Magnetic nanoparticle-based therapeutic agents for thermo-chemotherapy treatment of cancer. Nanoscale 2014;6:11553–73.
[21] Lu AH, Salabas EL, Schuth F. Magnetic nanoparticles: synthesis, protection, functionalization, and application. Angew Chem 2007;46:1222–44.
[22] Blanch E, Garreta E, Gasset D, Genové E, Colominas C, Semino C, et al. Development of hydroxyapatite-based biomaterials scaffolds for hard tissue regeneration. Eur Cells Mater 2004;7:46.
[23] de Groot K. Bioceramics consisting of calcium phosphate salts. Biomaterials 1980;1:47–50.
[24] Liu DM, Yang Q, Troczynski T, Tseng WJ. Structural evolution of sol–gel-derived hydroxyapatite. Biomaterials 2002;23:1679–87.
[25] Ravikrishna R, Ren M, Valsaraj KT. Low-temperature synthesis of porous hydroxyapatite scaffolds using polyaphron templates. J Sol–Gel Sci Technol 2006;38:203–10.
[26] Foroutan F, de Leeuw NH, Martin RA, Palmer G, Owens GJ, Kim H-W, et al. Novel sol–gel preparation of $(P_2O_5)_{0.4}$–$(CaO)_{0.25}$–$(Na_2O)_X$–$(TiO_2)_{(0.35-X)}$ bioresorbable glasses ($X = 0.05$, 0.1, and 0.15). J Sol–Gel Sci Technol 2014;73:434–42.
[27] Ciriminna R, Sciortino M, Alonzo G, Schrijver A, Pagliaro M. From molecules to systems: sol–gel microencapsulation in silica-based materials. Chem Rev 2011;111:765–89.
[28] Vallet-Regi M. Ceramics for medical applications. J Chem Soc – Dalton Trans 2001:97–108.
[29] Stöber W, Fink A, Bohn E. Controlled growth of monodisperse silica spheres in the micron size range. J Colloid Interface Sci 1968;26:62–9.
[30] Kolbe G. Das Komplexchemische Verhalten der Kieselsäure. Jena: University of Jena; 1956.

[31] Iler RK. The chemistry of silica: solubility, polymerization, colloid and surface properties, and biochemistry. New York, Chichester: Wiley; 1979.
[32] Avnir D, Coradin T, Lev O, Livage J. Recent bio-applications of sol–gel materials. J Mater Chem 2006;16:1013–30.
[33] Liu DM, Chen IW. Encapsulation of protein molecules in transparent porous silica matrices via an aqueous colloidal sol–gel process. Acta Mater 1999;47:4535–44.
[34] Gash AE, Tillotson TM, Satcher JH, Poco JF, Hrubesh LW, Simpson RL. Use of epoxides in the sol–gel synthesis of porous iron(III) oxide monoliths from Fe(III) salts. Chem Mater 2001;13:999–1007.
[35] Livage J, Sanchez C. Sol–gel chemistry. J Non-Cryst Solids 1992;145:11–9.
[36] Kakihana M. Invited review "sol–gel" preparation of high temperature superconducting oxides. J Sol–Gel Sci Technol 1996;6:7–55.
[37] Lofgreen JE, Ozin GA. Controlling morphology and porosity to improve performance of molecularly imprinted sol–gel silica. Chem Soc Rev 2014;43:911–33.
[38] Choi DG, Yang SM. Effect of two-step sol–gel reaction on the mesoporous silica structure. J Colloid Interface Sci 2003;261:127–32.
[39] Brinker CJ. Hydrolysis and condensation of silicates – effects on structure. J Non-Cryst Solids 1988;100:31–50.
[40] Jones JR. Sol–gel derived glasses for medicine. In: Jones JR, Clare AG, editors. Bio-glasses: an introduction. West Sussex, UK: John Wiley and Sons Ltd.; 2012. p. 29–44.
[41] Pickup DM, Speight RJ, Knowles JC, Smith ME, Newport RJ. Sol–gel synthesis and structural characterisation of binary TiO_2–P_2O_5 glasses. Mater Res Bull 2008;43:333–42.
[42] Zera E, Campostrini R, Aravind PR, Blum Y, Soraru GD. Novel SiC/C aerogels through pyrolysis of polycarbosilane precursors. Adv Eng Mater 2014;16:814–9.
[43] Nandy S, Kundu D, Naskar MK. Synthesis of mesoporous Stober silica nanoparticles: the effect of secondary and tertiary alkanolamines. J Sol–Gel Sci Technol 2014;72:49–55.
[44] Nabavi M, Doeuff S, Sanchez C, Livage J. Chemical modification of metal alkoxides by solvents – a way to control sol–gel chemistry. J Non-Cryst Solids 1990;121:31–4.
[45] Talebian N, Kheiri M. Sol–gel derived nanostructured nickel oxide films: effect of solvent on crystallographic orientations. Solid State Sci 2014;27:79–83.
[46] Pickup DM, Guerry P, Moss RM, Knowles JC, Smith ME, Newport RJ. New sol–gel synthesis of a $(CaO)(0.3)(Na_2O)(0.2)(P_2O_5)(0.5)$ bioresorbable glass and its structural characterisation. J Mater Chem 2007;17:4777–84.
[47] Wang D, Bierwagen GR. Sol–gel coatings on metals for corrosion protection. Prog Org Coat 2009;64:327–38.
[48] Hench LL, West JK. The sol–gel process. Chem Rev 1990;90:33–72.
[49] Livage J, Henry M, Sanchez C. Sol–gel chemistry of transition-metal oxides. Prog Solid State Chem 1988;18:259–341.
[50] Colomban P. Gel technology in ceramics, glass–ceramics and ceramic composites. Ceram Int 1989;15:23–50.
[51] Livage J. Vanadium pentoxide gels. Chem Mater 1991;3:578–93.
[52] Abou Neel EA, Pickup DM, Valappil SP, Newport RJ, Knowles JC. Bioactive functional materials: a perspective on phosphate-based glasses. J Mater Chem 2009;19:690–701.
[53] Hoppe U. A structural model for phosphate glasses. J Non-Cryst Solids 1996;195:138–47.
[54] Han CS, Andersen J, Likodimos V, Falaras P, Linkugel J, Dionysiou DD. The effect of solvent in the sol–gel synthesis of visible light-activated, sulfur-doped TiO_2 nanostructured porous films for water treatment. Catal Today 2014;224:132–9.
[55] Romeo R, Arena G, Scolaro LM. Steric and electronic factors influencing the reactivity of tertiary phosphines toward platinum(II) complexes. Inorg Chem 1992;31:4879–84.
[56] Tolman CA. Steric effects of phosphorus ligands in organometallic chemistry and homogeneous catalysis. Chem Rev 1977;77:313–48.
[57] Gash AE, Tillotson TM, Satcher Jr JH, Hrubesh LW, Simpson RL. New sol–gel synthetic route to transition and main-group metal oxide aerogels using inorganic salt precursors; 2000.
[58] Perullini M, Amoura M, Roux C, Coradin T, Livage J, Japas ML, et al. Improving silica matrices for encapsulation of *Escherichia coli* using osmoprotectors. J Mater Chem 2011;21:4546.
[59] Smith DR, Nordberg M. General chemistry, sampling, analytical methods, and speciation. In: Nordberg GFNAF, editor. Handbook on the toxicology of metals. San Diego: Academic Press; 2015. p. 15–44 [chapter 2].
[60] Helm L, Merbach AE. Inorganic and bioinorganic solvent exchange mechanisms. Chem Rev 2005;105:1923–59.
[61] Talebian N, Doudi M, Kheiri M. The anti-adherence and bactericidal activity of sol–gel derived nickel oxide nanostructure films: solvent effect. J Sol–Gel Sci Technol 2013;69:172–82.
[62] Kessler VG, Spijksma GI, Seisenbaeva GA, Hakansson S, Blank DHA, Bouwmeester HJM. New insight in the role of modifying ligands in the sol–gel processing of metal alkoxide precursors: a possibility to approach new classes of materials. J Sol–Gel Sci Technol 2006;40:163–79.
[63] El Haskouri J, Moragues A, Beltrán A, Murcia-Mascarós S, Plazaola F, Legarra E, et al. Mesoporous iron phosphate/phosphonate hybrid materials. Microporous Mesoporous Mater 2014;187:14–22.
[64] Naiini AA, Young V, Verkade JG. New complexes of thriethanolamine (Tea): novel structural features of $[Y(TEA)_2](ClO_4)_3{\cdot}3C_5H_5N$ and $[Cd(TEA)_2](NO_3)_2$. Polyhedron 1995;14:393–400.
[65] Omori Y, Okada M, Takeda S, Matsumoto N. Fabrication of dispersible calcium phosphate nanocrystals via a modified Pechini method under non-stoichiometric conditions. Mater Sci Eng C: Mater Biol Appl 2014;42:562–8.
[66] Yang Z, Jiang Y, Xu HH, Huang YH. High-performance porous nanoscaled $LiMn_2O_4$ prepared by polymer-assisted sol–gel method. Electrochim Acta 2013;106:63–8.
[67] Valliant EM, Romer F, Wang D, McPhail DS, Smith ME, Hanna JV, et al. Bioactivity in silica/poly(gamma-glutamic acid) sol–gel hybrids through calcium chelation. Acta Biomater 2013;9:7662–71.
[68] Pechini MP. In: Co SE, editor. Method of preparing lead and alkaline earth titanates and niobates and coating method using the same to form a capacitor. USA; 1967.
[69] Larsen MJ. An investigation of the theoretical background for the stability of the calcium-phosphate salts and their mutual conversion in aqueous-solutions. Arch Oral Biol 1986;31:757–61.

[70] Kong YM, Bae CJ, Lee SH, Kim HW, Kim HE. Improvement in biocompatibility of ZrO_2–Al_2O_3 nano-composite by addition of HA. Biomaterials 2005;26:509–17.
[71] Vargas-Becerril N, Tellez-Jurado L, Reyes-Gasga J, Alvarez-Perez MA, Rodriguez-Lorenzo LM. Synthesis of nanosized carbonated apatite by a modified Pechini method: hydroxyapatite nucleation from a polymeric matrix. J Sol–Gel Sci Technol 2014;72:571–80.
[72] Geffcken W, Berger E. Deutsche Reichspatent 1939:411.
[73] Pereira MM, Jones JR, Hench LL. Bioactive glass and hybrid scaffolds prepared by sol–gel method for bone tissue engineering. Adv Appl Ceram 2005;104:35–42.
[74] Gupta R, Kumar A. Bioactive materials for biomedical applications using sol–gel technology. Biomed Mater 2008;3:034005.
[75] Wang C, He C, Tong Z, Liu X, Ren B, Zeng F. Combination of adsorption by porous $CaCO_3$ microparticles and encapsulation by polyelectrolyte multilayer films for sustained drug delivery. Int J Pharm 2006;308:160–7.
[76] Braun S, Rappoport S, Zusman R, Avnir D, Ottolenghi M. Biochemically active sol–gel glasses – the trapping of enzymes. Mater Lett 1990;10:1–5.
[77] Reetz MT, Zonta A, Simpelkamp J. Efficient heterogeneous biocatalysts by entrapment of lipases in hydrophobic sol–gel materials. Angew Chem Int Ed 1995;34:301–3.
[78] Liang RP, Qiu HD, Cai PX. A novel amperometric immunosensor based on three-dimensional sol–gel network and nanoparticle self-assemble technique. Anal Chim Acta 2005;534:223–9.
[79] Besanger T, Zhang Y, Brennan JD. Characterization of fluorescent phospholipid liposomes entrapped in sol–gel derived silica. J Phys Chem B 2002;106:10535–42.
[80] Hench LL. Challenges for bioceramics in the 21st century. Am Ceram Soc Bull 2005;84:18–21.
[81] Hench LL, Wilson J. Surface-active biomaterials. Science 1984;226:630–6.
[82] Li R, Clark AE, Hench LL. An investigation of bioactive glass powders by sol–gel processing. J Appl Biomater 1991;2:231–9.
[83] Pereira MM, Clark AE, Hench LL. Homogeneity and bioactivity of sol–gel derived glasses. J Dent Res 1994;73:276.
[84] Pereira MM, Clark AE, Hench LL. Calcium phosphate formation on sol–gel-derived bioactive glasses in vitro. J Biomed Mater Res 1994;28:693–8.
[85] Lenza RF, Vasconcelos WL, Jones JR, Hench LL. Surface-modified 3D scaffolds for tissue engineering. J Mater Sci – Mater Med 2002;13:837–42.
[86] Zhong J, Greenspan DC. Processing and properties of sol–gel bioactive glasses. J Biomed Mater Res 2000;53:694–701.
[87] Greenspan DC, Zhong JP, Chen XF, LaTorre GP. The evaluation of degradability of melt and sol–gel derived Bioglass (R) in-vitro. Bioceramics 1997;10:391–4.
[88] Sepulveda P, Jones JR, Hench Larry L. Bioactive sol–gel foams for tissue repair. J Biomed Mater Res 2001;59:340–8.
[89] Jones JR, Tsigkou O, Coates EE, Stevens MM, Polak JM, Hench LL. Extracellular matrix formation and mineralization on a phosphate-free porous bioactive glass scaffold using primary human osteoblast (HOB) cells. Biomaterials 2007;28:1653–63.
[90] Sepulveda P, Jones JR, Hench LL. Bioactive sol–gel foams for tissue repair. J Biomed Mater Res 2002;59:340–8.
[91] Jones JR, Poologasundarampillai G, Atwood RC, Bernard D, Lee PD. Non-destructive quantitative 3D analysis for the optimisation of tissue scaffolds. Biomaterials 2007;28:1404–13.
[92] Fu Q, Saiz E, Rahaman MN, Tomsia AP. Bioactive glass scaffolds for bone tissue engineering: state of the art and future perspectives. Mater Sci Eng C: Mater Biol Appl 2011;31:1245–56.
[93] Jones JR, Ehrenfried LM, Hench LL. Optimising bioactive glass scaffolds for bone tissue engineering. Biomaterials 2006;27:964–73.
[94] Kresge CT, Leonowicz ME, Roth WJ, Vartuli JC, Beck JS. Ordered mesoporous molecular-sieves synthesized by a liquid-crystal template mechanism. Nature 1992;359:710–2.
[95] Bottcher H, Slowik P, Suss W. Sol–gel carrier systems for controlled drug delivery. J Sol–Gel Sci Technol 1998;13:277–81.
[96] Lu F, Wu SH, Hung Y, Mou CY. Size effect on cell uptake in well-suspended, uniform mesoporous silica nanoparticles. Small 2009;5:1408–13.
[97] Qiao ZA, Zhang L, Guo MY, Liu YL, Huo QS. Synthesis of mesoporous silica nanoparticles via controlled hydrolysis and condensation of silicon alkoxide. Chem Mater 2009;21:3823–9.
[98] Chiang YD, Lian HY, Leo SY, Wang SG, Yamauchi Y, Wu KCW. Controlling particle size and structural properties of mesoporous silica nanoparticles using the Taguchi method. J Phys Chem C 2011;115:13158–65.
[99] Berggren A, Palmqvist AEC. Particle size control of colloidal suspensions of mesostructured silica. J Phys Chem C 2008;112:732–7.
[100] Gao F, Botella P, Corma A, Blesa J, Dong L. Monodispersed mesoporous silica nanoparticles with very large pores for enhanced adsorption and release of DNA. J Phys Chem B 2009;113:1796–804.
[101] Grun M, Lauer I, Unger KK. The synthesis of micrometer- and submicrometer-size spheres of ordered mesoporous oxide MCM-41. Adv Mater 1997;9:254–7.
[102] Brow RK. Review: the structure of simple phosphate glasses. J Non-Cryst Solids 2000;263:1–28.
[103] Livage J, Barboux P, Vandenborre MT, Schmutz C, Taulelle F. Sol–gel synthesis of phosphates. J Non-Cryst Solids 1992;147:18–23.
[104] Knowles JC. Phosphate based glasses for biomedical applications. J Mater Chem 2003;13:2395–401.
[105] Hench LL, Polak JM. Third-generation biomedical materials. Science 2002;295:1014–7.
[106] Pickup DM, Newport RJ, Knowles JC. Sol–gel phosphate-based glass for drug delivery applications. J Biomater Appl 2012;26:613–22.
[107] Navarro M, Ginebra MP, Planell JA. Cellular response to calcium phosphate glasses with controlled solubility. J Biomed Mater Res A 2003;67:1009–15.
[108] Carta D, Pickup DM, Knowles JC, Smith ME, Newport RJ. Sol–gel synthesis of the P_2O_5–CaO–Na_2O–SiO_2 system as a novel bioresorbable glass. J Mater Chem 2005;15:2134–40.
[109] Carta D, Knowles JC, Smith ME, Newport RJ. Synthesis and structural characterization of P_2O_5–CaO–Na_2O sol–gel materials. J Non-Cryst Solids 2007;353:1141–9.

[110] Kiani A, Lakhkar NJ, Salih V, Smith ME, Hanna JV, Newport RJ, et al. Titanium-containing bioactive phosphate glasses. Philos Trans A: Math Phys Eng Sci 2012;370:1352–75.
[111] Laurent S, Forge D, Port M, Roch A, Robic C, Vander Elst L, et al. Magnetic iron oxide nanoparticles: synthesis, stabilization, vectorization, physicochemical characterizations, and biological applications. Chem Rev 2008;108:2064–110.
[112] Sun C, Lee JS, Zhang M. Magnetic nanoparticles in MR imaging and drug delivery. Adv Drug Deliv Rev 2008;60:1252–65.
[113] Gupta AK, Gupta M. Synthesis and surface engineering of iron oxide nanoparticles for biomedical applications. Biomaterials 2005;26:3995–4021.
[114] Duran JD, Arias JL, Gallardo V, Delgado AV. Magnetic colloids as drug vehicles. J Pharm Sci 2008;97:2948–83.
[115] Singh RK, Kim TH, Patel KD, Knowles JC, Kim HW. Biocompatible magnetite nanoparticles with varying silica-coating layer for use in biomedicine: physicochemical and magnetic properties, and cellular compatibility. J Biomed Mater Res A 2012;100:1734–42.
[116] Kandori K, Kawashima Y, Ishikawa T. Effects of citrate ions on the formation of monodispersed cubic hematite particles. J Colloid Interface Sci 1992;152:284–8.
[117] Yin ZF, Wu L, Yang HG, Su YH. Recent progress in biomedical applications of titanium dioxide. Phys Chem Chem Phys 2013;15:4844–58.
[118] Zhang HZ, Banfield JF. Thermodynamic analysis of phase stability of nanocrystalline titania. J Mater Chem 1998;8:2073–6.
[119] Ääritalo V, Meretoja V, Tirri T, Areva S, Jämsä T, Tuukkanen J, et al. Development of a low temperature sol–gel-derived titania-silica implant coating. Mater Sci Appl 2010;01:118–26.
[120] Matijević E, Budnik M, Meites L. Preparation and mechanism of formation of titanium dioxide hydrosols of narrow size distribution. J Colloid Interface Sci 1977;61:302–11.
[121] Barringer EA, Bowen HK. Formation, packing, and sintering of monodisperse TiO_2 powders. J Am Ceram Soc 1982;65:C-199–201.
[122] Eiden-Assmann S, Widoniak J, Maret G. Synthesis and characterization of porous and nonporous monodisperse colloidal TiO_2 particles. Chem Mater 2004;16:6–11.
[123] Morales Bokhimi A, Novaro O, Lopez T, Sanchez E, Gomez R. Effect of hydrolysis catalyst on the Ti deficiency and crystallite size of sol–gel-TiO_2 crystalline phases. J Mater Res 1995;10:2788–96.
[124] Li GQ, Zhang S, Yu JH. Facile synthesis of single-phase TiO_2 nanocrystals with high photocatalytic performance. J Am Ceram Soc 2011;94:4112–5.
[125] Scolan E, Sanchez C. Synthesis and characterization of surface-protected nanocrystalline titania particles. Chem Mater 1998;10:3217–23.
[126] Khanna PK, Singh N, Charan S. Synthesis of nano-particles of anatase–TiO_2 and preparation of its optically transparent film in PVA. Mater Lett 2007;61:4725–30.
[127] Jiu JT, Wang FM, Sakamoto M, Takao J, Adachi M. Preparation of nanocrystalline TiO_2 with mixed template and its application for dye-sensitized solar cells. J Electrochem Soc 2004;151:A1653–8.
[128] Jiu J, Isoda S, Adachi M, Wang F. Preparation of TiO_2 nanocrystalline with 3–5nm and application for dye-sensitized solar cell. J Photochem Photobiol A 2007;189:314–21.
[129] Sugimoto T, Sakata K. Preparation of monodisperse pseudocubic α-Fe_2O_3 particles from condensed ferric hydroxide gel. J Colloid Interface Sci 1992;152:587–90.
[130] Miao L, Tanemura S, Toh S, Kaneko K, Tanemura M. Fabrication, characterization and Raman study of anatase TiO_2 nanorods by a heating-sol–gel template process. J Cryst Growth 2004;264:246–52.
[131] Lin Y, Wu GS, Yuan XY, Xie T, Zhang LD. Fabrication and optical properties of TiO_2 nanowire arrays made by sol–gel electrophoresis deposition into anodic alumina membranes. J Phys: Condens Matter 2003;15:2917.
[132] Bu SJ, Jin ZG, Liu XX, Yang LR, Cheng ZJ. Synthesis of TiO_2 porous thin films by polyethylene glycol templating and chemistry of the process. J Eur Ceram Soc 2005;25:673–9.
[133] Nagao M. Physisorption of water on zinc oxide surface. J Phys Chem – US 1971;75:3822–8.
[134] Grabarek Z, Gergely J. Zero-length crosslinking procedure with the use of active esters. Anal Biochem 1990;185:131–5.
[135] Horie M, Nishio K, Fujita K, Endoh S, Miyauchi A, Saito Y, et al. Protein adsorption of ultrafine metal oxide and its influence on cytotoxicity toward cultured cells. Chem Res Toxicol 2009;22:543–53.
[136] Spanhel L, Anderson MA. Semiconductor clusters in the sol–gel process: quantized aggregation, gelation, and crystal growth in concentrated zinc oxide colloids. J Am Chem Soc 1991;113:2826–33.
[137] Redmond G, Fitzmaurice D, Graetzel M. Visible-light sensitization by cis-bis(thiocyanato)bis(2,2′-bipyridyl-4,4′-dicarboxylato)ruthenium(II) of a transparent nanocrystalline ZnO film prepared by sol–gel techniques. Chem Mater 1994;6:686–91.
[138] Tokumoto MS, Pulcinelli SH, Santilli CV. In: Vincenzini P, editor. Advances in science and technology, ceramics: getting into the 2000's – part B. Techna Srl.; 1999. p. 73.
[139] Benhebal H, Chaib M, Salmon T, Geens J, Leonard A, Lambert SD, et al. Photocatalytic degradation of phenol and benzoic acid using zinc oxide powders prepared by the sol–gel process. Alexandria Eng J 2013;52:517–23.
[140] Yue S, Yan ZS, Shi YF, Ran GX. Synthesis of zinc oxide nanotubes within ultrathin anodic aluminum oxide membrane by sol–gel method. Mater Lett 2013;98:246–9.
[141] Spanhel L. Colloidal ZnO nanostructures and functional coatings: a survey. J Sol–Gel Sci Technol 2006;39:7–24.
[142] Guo L, Yang SH, Yang CL, Yu P, Wang JN, Ge WK, et al. Synthesis and characterization of poly(vinylpyrrolidone)-modified zinc oxide nanoparticles. Chem Mater 2000;12:2268–74.
[143] Fu YS, Du XW, Kulinich SA, Qiu JS, Qin WJ, Li R, et al. Stable aqueous dispersion of ZnO quantum dots with strong blue emission via simple solution route. J Am Chem Soc 2007;129:16029–33.
[144] Xiong HM, Wang ZD, Liu DP, Chen JS, Wang YG, Xia YY. Bonding polyether onto ZnO nanoparticles: an effective method for preparing polymer nanocomposites with tunable luminescence and stable conductivity. Adv Funct Mater 2005;15:1751–6.

[145] Xiong HM, Wang ZD, Xia YY. Polymerization initiated by inherent free radicals on nanoparticle surfaces: a simple method of obtaining ultrastable (ZnO)polymer core–shell nanoparticles with strong blue fluorescence. Adv Mater 2006;18:748–51.
[146] Yuan Q, Hein S, Misra RD. New generation of chitosan-encapsulated ZnO quantum dots loaded with drug: synthesis, characterization and in vitro drug delivery response. Acta Biomater 2010;6:2732–9.
[147] Low PS, Kularatne SA. Folate-targeted therapeutic and imaging agents for cancer. Curr Opin Chem Biol 2009;13:256–62.
[148] Leamon CP, Reddy JA. Folate-targeted chemotherapy. Adv Drug Deliv Rev 2004;56:1127–41.
[149] Ling DS, Hackett MJ, Hyeon T. Surface ligands in synthesis, modification, assembly and biomedical applications of nanoparticles. Nano Today 2014;9:457–77.
[150] Dorozhkin SV, Epple M. Biological and medical significance of calcium phosphates. Angew Chem 2002;41:3130–46.
[151] Bouler JM, LeGeros RZ, Daculsi G. Biphasic calcium phosphates: influence of three synthesis parameters on the HA/beta-TCP ratio. J Biomed Mater Res 2000;51:680–4.
[152] Gibson IR, Best SM, Bonfield W. Chemical characterization of silicon-substituted hydroxyapatite. J Biomed Mater Res 1999;44:422–8.
[153] Vallet-Regi M, Arcos D. Silicon substituted hydroxyapatites. A method to upgrade calcium phosphate based implants. J Mater Chem 2005;15:1509–16.
[154] Rg G. Hydroxyapatite-coated total hip prostheses. Two-year clinical and roentgenographic results of 100 cases. Clin Orthop Relat Res 1990;261:39–58.
[155] LeGeros RZ. Calcium phosphate materials in restorative dentistry: a review. Adv Dent Res 1988;2:164–80.
[156] Masuda YMK, Sakka S. Synthesis of hydroxyapatite from metal alkoxides through sol gel technique. J Ceram Soc Jpn 1990;98:1266–77.
[157] Deptuła A, Łada W, Olczak T, Borello A, Alvani C, di Bartolomeo A. Preparation of spherical powders of hydroxyapatite by sol–gel process. J Non-Cryst Solids 1992;147–148:537–41.
[158] Piveteau LD, Girona MI, Schlapbach L, Barboux P, Boilot JP, Gasser B. Thin films of calcium phosphate and titanium dioxide by a sol–gel route: a new method for coating medical implants. J Mater Sci – Mater Med 1999;10:161–7.
[159] Brendel T, Engel A, Russel C. Hydroxyapatite coatings by a polymeric route. J Mater Sci – Mater Med 1992;3:175–9.
[160] Gross KA, Chai CS, Kannangara GS, Ben-Nissan B, Hanley L. Thin hydroxyapatite coatings via sol–gel synthesis. J Mater Sci – Mater Med 1998;9:839–43.
[161] Layrolle P, Ito A, Tateishi T. Sol–gel synthesis of amorphous calcium phosphate and sintering into microporous hydroxyapatite bioceramics. J Am Ceram Soc 1998;81:1421–8.
[162] Russell SW, Luptak KA, Suchicital CTA, Alford TL, Pizziconi VB. Chemical and structural evolution of sol–gel-derived hydroxyapatite thin films under rapid thermal processing. J Am Ceram Soc 1996;79:837–42.
[163] Hwang K, Lim Y. Chemical and structural changes of hydroxyapatite films by using a sol–gel method. Surf Coat Technol 1999;115:172–5.
[164] Jillavenkatesa A, Condrate RA. Sol–gel processing of hydroxyapatite. J Mater Sci 1998;33:4111–9.
[165] Layrolle P, Lebugle A. Characterization and reactivity of nanosized calcium phosphates prepared in anhydrous ethanol. Chem Mater 1994;6:1996–2004.
[166] Takahashi HYM, Kakihana M, Yoshimura M. Synthesis of stoichiometric hydroxyapatite by a gel route from the aqueous solution of citric and phosphoneacetic acids. Eur J Solid State Inorg Chem 1995;32:829–35.
[167] Young RA, Holcomb DW. Variability of hydroxyapatite preparations. Calcif Tissue Int 1982;34(Suppl. 2):S17–32.
[168] Osaka A, Miura Y, Takeuchi K, Asada M, Takahashi K. Calcium apatite prepared from calcium hydroxide and orthophosphoric acid. J Mater Sci – Mater Med 1991;2:51–5.
[169] Slosarczyk A, Stobierska E, Paszkiewicz Z, Gawlicki M. Calcium phosphate materials prepared from precipitates with various calcium:phosphorus molar ratios. J Am Ceram Soc 1996;79:2539–44.
[170] Yoshimura M, Suda H, Okamoto K, Ioku K. Hydrothermal synthesis of biocompatible whiskers. J Mater Sci 1994;29:3399–402.
[171] Dunn B, Zink JI. Sol–gel chemistry and materials. Acc Chem Res 2007;40:729.
[172] Qiu QVP, Lowenberg B, Sayer M, Davies JE. Bone growth on sol–gel calcium phosphate thin films in vitro. Cells Mater 1993;3:351–60.
[173] Westheimer FH, Huang S, Covitz F. Rates and mechanisms of hydrolysis of esters of phosphorous acid. J Am Chem Soc 1988;110:181–5.
[174] Vijayalakshmi URS. Preparation and characterization of microcrystalline hydroxyapatite using sol gel method. Trends Biomater Artif Org 2006;19:57–62.
[175] Chai CS, Gross KA, Ben-Nissan B. Critical ageing of hydroxyapatite sol–gel solutions. Biomaterials 1998;19:2291–6.
[176] Bouyer E, Gitzhofer F, Boulos MI. Morphological study of hydroxyapatite nanocrystal suspension. J Mater Sci – Mater Med 2000;11:523–31.
[177] Han YC, Li SP, Wang XY, Chen XM. Synthesis and sintering of nanocrystalline hydroxyapatite powders by citric acid sol–gel combustion method. Mater Res Bull 2004;39:25–32.
[178] Liu DM, Troczynski T, Tseng WJ. Water-based sol–gel synthesis of hydroxyapatite: process development. Biomaterials 2001;22:1721–30.
[179] Kuriakose TA, Kalkura SN, Palanichamy M, Arivuoli D, Dierks K, Bocelli G, et al. Synthesis of stoichiometric nano crystalline hydroxyapatite by ethanol-based sol–gel technique at low temperature. J Cryst Growth 2004;263:517–23.
[180] Chai C, Ben-Nissan B, Pyke S, Evans L. Sol gel derived hydroxyapatite coatings for biomedical applications. Mater Manuf Process 1995;10:205–16.
[181] Ameen AP, Short RD, Johns R, Schwach G. The surface analysis of implant materials. 1. The surface composition of a titanium dental implant material. Clin Oral Implant Res 1993;4:144–50.
[182] Ting CC, Chen SY, Liu DM. Structural evolution and optical properties of TiO_2 thin films prepared by thermal oxidation of sputtered Ti films. J Appl Phys 2000;88:4628–33.
[183] Liu DM, Troczynski T, Tseng WJ. Aging effect on the phase evolution of water-based sol–gel hydroxyapatite. Biomaterials 2002;23:1227–36.

[184] Pierre AC. Introduction to sol–gel processing. Boston: Kluwer Academic Publishers; 1998.
[185] Judeinstein P, Sanchez C. Hybrid organic–inorganic materials: a land of multidisciplinarity. J Mater Chem 1996;6:511.
[186] Landry CJT, Coltrain BK, Wesson JA, Zumbulyadis N, Lippert JL. In situ polymerization of tetraethoxysilane in polymers: chemical nature of the interactions. Polymer 1992;33:1496–506.
[187] Barrera-Calva E, Méndez-Vivar J, Ortega-López M, Huerta-Arcos L, Morales-Corona J, Olayo-González R. Silica-copper oxide composite thin films as solar selective coatings prepared by dipping sol gel. Res Lett Mater Sci 2008;2008:1–5.
[188] Crouzet L, Leclercq D. Polyphosphazene–metal oxide hybrids by nonhydrolytic sol–gel processes. J Mater Chem 2000;10:1195–201.
[189] Tamaki R, Naka K, Chujo Y. Synthesis of poly(N,N-dimethylacrylamide) silica gel polymer hybrids by in situ polymerization method. Polym J 1998;30:60–5.
[190] Toki M, Chow TY, Ohnaka T, Samura H, Saegusa T. Structure of poly(vinylpyrrolidone)-silica hybrid. Polym Bull 1992;29:653–60.
[191] Landfester K. Miniemulsion polymerization and the structure of polymer and hybrid nanoparticles. Angew Chem 2009;48:4488–507.
[192] Mauritz KA, Jones CK. Novel poly(n-butyl methacrylate)/titanium oxide alloys produced by the sol–gel process for titanium alkoxides. J Appl Polym Sci 1990;40:1401–20.
[193] Yang F, Nelson GL. PMMA/silica nanocomposite studies: synthesis and properties. J Appl Polym Sci 2004;91:3844–50.
[194] Gill I, Ballesteros A. Bioencapsulation within synthetic polymers (part 1): sol–gel encapsulated biologicals. Trends Biotechnol 2000;18:282–96.
[195] Wojcik AB, Klein LC. Organic–inorganic gels based on silica and multifunctional acrylates. J Sol–Gel Sci Technol 1994;2:115–20.
[196] Gill I. Bio-doped nanocomposite polymers: sol–gel bioencapsulates. Chem Mater 2001;13:3404–21.
[197] Kamitakahara M, Kawashita M, Miyata N, Kokubo T, Nakamura T. Bioactivity and mechanical properties of polydimethylsiloxane (PDMS)–CaO–SiO_2 hybrids with different calcium contents. J Mater Sci – Mater Med 2002;13:1015–20.
[198] Pereira APV, Vasconcelos WL, Orefice RL. Novel multicomponent silicate-poly(vinyl alcohol) hybrids with controlled reactivity. J Non-Cryst Solids 2000;273:180–5.
[199] Martín AI, Salinas AJ, Vallet-Regí M. Bioactive and degradable organic–inorganic hybrids. J Eur Ceram Soc 2005;25:3533–8.
[200] Lee EJ, Teng SH, Jang TS, Wang P, Yook SW, Kim HE, et al. Nanostructured poly(epsilon-caprolactone)-silica xerogel fibrous membrane for guided bone regeneration. Acta Biomater 2010;6:3557–65.
[201] Shin KH, Koh YH, Kim HE. Synthesis and characterization of drug-loaded poly(epsilon-caprolactone)/silica hybrid nanofibrous scaffolds. J Nanomater 2013;2013:12.
[202] Song JH, Yoon BH, Kim HE, Kim HW. Bioactive and degradable hybridized nanofibers of gelatin–siloxane for bone regeneration. J Biomed Mater Res A 2008;84:875–84.
[203] Lee EJ, Shin DS, Kim HE, Kim HW, Koh YH, Jang JH. Membrane of hybrid chitosan–silica xerogel for guided bone regeneration. Biomaterials 2009;30:743–50.
[204] Lee EJ, Jun SH, Kim HE, Kim HW, Koh YH, Jang JH. Silica xerogel–chitosan nano-hybrids for use as drug eluting bone replacement. J Mater Sci – Mater Med 2010;21:207–14.
[205] Li X, Xie QR, Zhang J, Xia W, Gu H. The packaging of siRNA within the mesoporous structure of silica nanoparticles. Biomaterials 2011;32:9546–56.
[206] Catauro M, Bollino F, Papale F, Gallicchio M, Pacifico S. Influence of the polymer amount on bioactivity and biocompatibility of SiO_2/PEG hybrid materials synthesized by sol–gel technique. Mater Sci Eng C – Mater Biol Appl 2015;48:548–55.
[207] Catauro M, Bollino F, Papale F, Marciano S, Pacifico S. TiO_2/PCL hybrid materials synthesized via sol–gel technique for biomedical applications. Mater Sci Eng C – Mater Biol Appl 2015;47:135–41.
[208] Catauro M, Bollino F, Papale F, Mozetic P, Rainer A, Trombetta M. Biological response of human mesenchymal stromal cells to titanium grade 4 implants coated with PCL/ZrO_2 hybrid materials synthesized by sol–gel route: in vitro evaluation. Mater Sci Eng C – Mater Biol Appl 2014;45:395–401.
[209] Li X, Zhang J, Gu H. Adsorption and desorption behaviors of DNA with magnetic mesoporous silica nanoparticles. Langmuir: ACS J Surf Colloids 2011;27:6099–106.
[210] Yamamoto S, Miyamoto T, Kokubo T, Nakamura T. Preparation of polymer-silicate hybrid materials bearing silanol groups and the apatite formation on/in the hybrid materials. Polym Bull 1998;40:243–50.
[211] Takadama H, Kim HM, Kokubo T, Nakamura T. Mechanism of biomineralization of apatite on a sodium silicate glass: TEM-EDX study in vitro. Chem Mater 2001;13:1108–13.
[212] Rhee S-H, Choi J-Y, Kim H-M. Preparation of a bioactive and degradable poly(ε-caprolactone)/silica hybrid through a sol–gel method. Biomaterials 2002;23:4915–21.
[213] Ren L, Tsuru K, Hayakawa S, Osaka A. Sol–gel preparation and in vitro deposition of apatite on porous gelatin–siloxane hybrids. J Non-Cryst Solids 2001;285:116–22.
[214] Ren L, Tsuru K, Hayakawa S, Osaka A. Novel approach to fabricate porous gelatin–siloxane hybrids for bone tissue engineering. Biomaterials 2002;23:4765–73.
[215] Silva SS, Ferreira RAS, Fu LS, Carlos LD, Mano JF, Reis RL, et al. Functional nanostructured chitosan–siloxane hybrids. J Mater Chem 2005;15:3952–61.
[216] Katagiri K, Hashizume M, Ariga K, Terashima T, Kikuchi J. Preparation and characterization of a novel organic–inorganic nanohybrid "cerasome" formed with a liposomal membrane and silicate surface. Chemistry 2007;13:5272–81.
[217] Ruiz-Hitzky E, Letaief S, Prevot V. Novel organic–inorganic mesophases: self-templating synthesis and intratubular swelling. Adv Mater 2002;14:439–43.
[218] Liang X, Yue X, Dai Z, Kikuchi J. Photoresponsive liposomal nanohybrid cerasomes. Chem Commun (Camb) 2011;47:4751–3.

[219] Yue X, Dai Z. Recent advances in liposomal nanohybrid cerasomes as promising drug nanocarriers. Adv Colloid Interface Sci 2014;207:32–42.
[220] Zhao XS, Lu GQM, Millar GJ. Advances in mesoporous molecular sieve MCM-41. Ind Eng Chem Res 1996;35:2075–90.
[221] Sing KSW, Everett DH, Haul RAW, Moscou L, Pierotti RA, Rouquerol J, et al. Reporting physisorption data for gas/solid systems. Handbook of heterogeneous catalysis. Wiley-VCH Verlag GmbH & Co. KGaA; 2008.
[222] Broekhoff JCP. Mesopore determination from nitrogen sorption isotherms: fundamentals, scope, limitations. In: Delmon B, Grange P, Jacobs PA, Poncelet G, editors. Studies in surface science and catalysis. Elsevier; 1979. p. 663–84.
[223] Lowell S, Shields JE, Thomas MA, Thommes M. Characterization of porous solids and powders: surface area, pore size and density. Boston, MA, USA: Kluwer Academic Publisher; 2004. p. 43–5.
[224] Soler-Illia GJ, Azzaroni O. Multifunctional hybrids by combining ordered mesoporous materials and macromolecular building blocks. Chem Soc Rev 2011;40:1107–50.
[225] Soler-illia GJD, Sanchez C, Lebeau B, Patarin J. Chemical strategies to design textured materials: from microporous and mesoporous oxides to nanonetworks and hierarchical structures. Chem Rev 2002;102:4093–138.
[226] Huo QS, Margolese DI, Ciesla U, Demuth DG, Feng PY, Gier TE, et al. Organization of organic-molecules with inorganic molecular-species into nanocomposite biphase arrays. Chem Mater 1994;6:1176–91.
[227] Raman N, Sudharsan S, Pothiraj K. Synthesis and structural reactivity of inorganic–organic hybrid nanocomposites – a review. J Saudi Chem Soc 2012;16:339–52.
[228] Soler-Illia GJ, Innocenzi P. Mesoporous hybrid thin films: the physics and chemistry beneath. Chemistry 2006;12:4478–94.
[229] Di Renzo F, Testa F, Chen JD, Cambon H, Galarneau A, Plee D, et al. Textural control of micelle-templated mesoporous silicates: the effects of co-surfactants and alkalinity. Microporous Mesoporous Mater 1999;28:437–46.
[230] Khushalani D, Kuperman A, Ozin GA, Tanaka K, Garces J, Olken MM, et al. Metamorphic materials – restructuring siliceous mesoporous materials. Adv Mater 1995;7:842–6.
[231] Horcajada P, Ramila A, Perez-Pariente J, Vallet-Regi M. Influence of pore size of MCM-41 matrices on drug delivery rate. Microporous Mesoporous Mater 2004;68:105–9.
[232] Izquierdo-Barba I, Sousa E, Doadrio JC, Doadrio AL, Pariente JP, Martinez A, et al. Influence of mesoporous structure type on the controlled delivery of drugs: release of ibuprofen from MCM-48, SBA-15 and functionalized SBA-15. J Sol–Gel Sci Technol 2009;50:421–9.
[233] Manzano M, Aina V, Arean CO, Balas F, Cauda V, Colilla M, et al. Studies on MCM-41 mesoporous silica for drug delivery: effect of particle morphology and amine functionalization. Chem Eng J 2008;137:30–7.
[234] Niu D, Ma Z, Li Y, Shi J. Synthesis of core–shell structured dual-mesoporous silica spheres with tunable pore size and controllable shell thickness. J Am Chem Soc 2010;132:15144–7.
[235] Suteewong T, Sai H, Cohen R, Wang S, Bradbury M, Baird B, et al. Highly aminated mesoporous silica nanoparticles with cubic pore structure. J Am Chem Soc 2011;133:172–5.
[236] Fuertes AB, Valle-Vigon P, Sevilla M. Synthesis of colloidal silica nanoparticles of a tunable mesopore size and their application to the adsorption of biomolecules. J Colloid Interface Sci 2010;349:173–80.
[237] Kim MH, Na HK, Kim YK, Ryoo SR, Cho HS, Lee KE, et al. Facile synthesis of monodispersed mesoporous silica nanoparticles with ultralarge pores and their application in gene delivery. ACS Nano 2011;5:3568–76.
[238] Zhang J, Li X, Rosenholm JM, Gu HC. Synthesis and characterization of pore size-tunable magnetic mesoporous silica nanoparticles. J Colloid Interface Sci 2011;361:16–24.
[239] Yanagisawa TST, Kuroda K, Kato C. The preparation of alkyltriinethylaininonium–kaneinite complexes and their conversion to microporous materials. Bull Chem Soc Jpn 1990;63:988–92.
[240] Vartuli JC, Schmitt KD, Kresge CT, Roth WJ, Leonowicz ME, Mccullen SB, et al. Effect of surfactant silica molar ratios on the formation of mesoporous molecular-sieves – inorganic mimicry of surfactant liquid-crystal phases and mechanistic implications. Chem Mater 1994;6:2317–26.
[241] Zhao D, Feng J, Huo Q, Melosh N, Fredrickson GH, Chmelka BF, et al. Triblock copolymer syntheses of mesoporous silica with periodic 50 to 300 angstrom pores. Science 1998;279:548–52.
[242] Jones JR, Hench LL. Regeneration of trabecular bone using porous ceramics. Curr Opin Solid State Mater Sci 2003;7:301–7.
[243] Mahltig B, Fiedler D, Fischer A, Simon P. Antimicrobial coatings on textiles-modification of sol–gel layers with organic and inorganic biocides. J Sol–Gel Sci Technol 2010;55:269–77.
[244] Gao H, Shi W, Freund LB. Mechanics of receptor-mediated endocytosis. Proc Natl Acad Sci USA 2005;102:9469–74.
[245] Czuryszkiewicz T, Ahvenlammi J, Kortesuo P, Ahola M, Kleitz F, Jokinen M, et al. Drug release from biodegradable silica fibers. J Non-Cryst Solids 2002;306:1–10.
[246] Slowing II, Vivero-Escoto JL, Wu CW, Lin VS. Mesoporous silica nanoparticles as controlled release drug delivery and gene transfection carriers. Adv Drug Deliv Rev 2008;60:1278–88.
[247] Jones JR, Hench LL. Factors affecting the structure and properties of bioactive foam scaffolds for tissue engineering. J Biomed Mater Res B: Appl Biomater 2004;68:36–44.
[248] Jones JR, Lin S, Yue S, Lee PD, Hanna JV, Smith ME, et al. Bioactive glass scaffolds for bone regeneration and their hierarchical characterisation. Proc Inst Mech Eng H – J Eng Med 2010;224:1373–87.
[249] Park YS, Kim KN, Kim KM, Choi SH, Kim CK, Legeros RZ, et al. Feasibility of three-dimensional macroporous scaffold using calcium phosphate glass and polyurethane sponge. J Mater Sci 2006;41:4357–64.
[250] de Barros Coelho M, Magalhaes Pereira M. Sol–gel synthesis of bioactive glass scaffolds for tissue engineering: effect of surfactant type and concentration. J Biomed Mater Res B: Appl Biomater 2005;75:451–6.
[251] Padilla S, Sanchez-Salcedo S, Vallet-Regi M. Bioactive glass as precursor of designed-architecture scaffolds for tissue engineering. J Biomed Mater Res A 2007;81:224–32.
[252] Brovarone CV, Verne E, Appendino P. Macroporous bioactive glass–ceramic scaffolds for tissue engineering. J Mater Sci – Mater Med 2006;17:1069–78.
[253] Vitale-Brovarone C, Verne E, Robiglio L, Appendino P, Bassi F, Martinasso G, et al. Development of glass–ceramic scaffolds for bone tissue engineering: characterisation, proliferation of human osteoblasts and nodule formation. Acta Biomater 2007;3:199–208.

[254] Yuan HP, de Bruijn JD, Zhang XD, van Blitterswijk CA, de Groot K. Bone induction by porous glass ceramic made from Bioglass (R) (45S5). J Biomed Mater Res 2001;58:270–6.
[255] Yan HW, Zhang K, Blanford CF, Francis LF, Stein A. In vitro hydroxycarbonate apatite mineralization of $CaO–SiO_2$ sol–gel glasses with a three-dimensionally ordered macroporous structure. Chem Mater 2001;13:1374–82.
[256] Jie Q, Lin KL, Zhong JP, Shi YF, Li Q, Chang JA, et al. Preparation of macroporous sol–gel bioglass using PVA particles as pore former. J Sol–Gel Sci Technol 2004;30:49–61.
[257] Li N, Jie Q, Zhu SM, Wang RD. Preparation and characterization of macroporous sol–gel bioglass. Ceram Int 2005;31:641–6.
[258] Yun HS, Kim SE, Hyeon YT. Design and preparation of bioactive glasses with hierarchical pore networks. Chem Commun (Camb) 2007:2139–41.
[259] Li X, Wang XP, Chen HR, Jiang P, Dong XP, Shi JL. Hierarchically porous bioactive glass scaffolds synthesized with a PUF and P123 cotemplated approach. Chem Mater 2007;19:4322–6.
[260] Yun HS, Kim SE, Hyun YT. Preparation of bioactive glass ceramic beads with hierarchical pore structure using polymer self-assembly technique. Mater Chem Phys 2009;115:670–6.
[261] Lei B, Chen XF, Wang YJ, Zhao N. Synthesis and in vitro bioactivity of novel mesoporous hollow bioactive glass microspheres. Mater Lett 2009;63:1719–21.
[262] Yan X, Yu C, Zhou X, Tang J, Zhao D. Highly ordered mesoporous bioactive glasses with superior in vitro bone-forming bioactivities. Angew Chem 2004;43:5980–4.
[263] Li WJ, Laurencin CT, Caterson EJ, Tuan RS, Ko FK. Electrospun nanofibrous structure: a novel scaffold for tissue engineering. J Biomed Mater Res 2002;60:613–21.
[264] Shin M, Yoshimoto H, Vacanti JP. In vivo bone tissue engineering using mesenchymal stem cells on a novel electrospun nanofibrous scaffold. Tissue Eng 2004;10:33–41.
[265] Kim HW, Kim HE, Knowles JC. Production and potential of bioactive glass nanofibers as a next-generation biomaterial. Adv Funct Mater 2006;16:1529–35.
[266] Lu H, Zhang T, Wang XP, Fang QF. Electrospun submicron bioactive glass fibers for bone tissue scaffold. J Mater Sci – Mater Med 2009;20:793–8.
[267] Lai CY, Trewyn BG, Jeftinija DM, Jeftinija K, Xu S, Jeftinija S, et al. A mesoporous silica nanosphere-based carrier system with chemically removable CdS nanoparticle caps for stimuli-responsive controlled release of neurotransmitters and drug molecules. J Am Chem Soc 2003;125:4451–9.
[268] Mura S, Nicolas J, Couvreur P. Stimuli-responsive nanocarriers for drug delivery. Nat Mater 2013;12:991–1003.
[269] Wachtman JB, Cannon WR, Matthewson MJ. Frontmatter. Mechanical properties of ceramics. John Wiley & Sons, Inc.; 2009. p. i–xvi.
[270] Pelleg J. Mechanical properties of ceramics. Springer; 2014.
[271] Venkateswara Rao A, Haranath D. Effect of methyltrimethoxysilane as a synthesis component on the hydrophobicity and some physical properties of silica aerogels. Microporous Mesoporous Mater 1999;30:267–73.
[272] Woignier T, Phalippou J. Mechanical strength of silica aerogels. J Non-Cryst Solids 1988;100:404–8.
[273] Calas S, Despetis F, Woignier T, Phalippou J. Mechanical strength evolution from aerogels to silica glass. J Porous Mater 1997;4:211–7.
[274] Murtagh MJ, Graham EK, Pantano CG. Elastic-moduli of silica-gels prepared with tetraethoxysilane. J Am Ceram Soc 1986;69:775–9.
[275] Woignier T, Scherer GW, Alaoui A. Stress in aerogel during depressurization of autoclave: II. Silica gels. J Sol–Gel Sci Technol 1994;3:141–50.
[276] Woignier T, Duffours L, Colombel P, Durin C. Aerogels materials as space debris collectors. Adv Mater Sci Eng 2013;2013:1–6.
[277] Klein LC. Sol–gel optics: processing and applications. US: Springer; 1994.
[278] Rao AV, Bhagat SD, Hirashima H, Pajonk GM. Synthesis of flexible silica aerogels using methyltrimethoxysilane (MTMS) precursor. J Colloid Interface Sci 2006;300:279–85.
[279] Nadargi DY, Latthe SS, Hirashima H, Rao AV. Studies on rheological properties of methyltriethoxysilane (MTES) based flexible superhydrophobic silica aerogels. Microporous Mesoporous Mater 2009;117:617–26.
[280] Yu S, Guo Z, Liu W. Biomimetic transparent and superhydrophobic coatings: from nature and beyond nature. Chem Commun 2015;51:1775–94.
[281] Li HC, Wang DG, Hu JH, Chen CZ. Effect of various additives on microstructure, mechanical properties, and in vitro bioactivity of sodium oxide-calcium oxide-silica-phosphorus pentoxide glass-ceramics. J Colloid Interface Sci 2013;405:296–304.
[282] Watts SJ, Hill RG, O'Donnell MD, Law RV. Influence of magnesia on the structure and properties of bioactive glasses. J Non-Cryst Solids 2010;356:517–24.
[283] Martin RA, Moss RM, Lakhkar NJ, Knowles JC, Cuello GJ, Smith ME, et al. Structural characterization of titanium-doped Bioglass using isotopic substitution neutron diffraction. Phys Chem Chem Phys 2012;14:15807–15.
[284] Kortesuo P, Ahola M, Karlsson S, Kangasniemi I, Yli-Urpo A, Kiesvaara J. Silica xerogel as an implantable carrier for controlled drug delivery – evaluation of drug distribution and tissue effects after implantation. Biomaterials 2000;21:193–8.
[285] Ono Y, Nakashima K, Sano M, Hojo J, Shinkai S. Template effect of cholesterol-based organogels on sol–gel polymerization creates novel silica with a helical structure. Chem Lett 1999;28:1119–20.
[286] Brasack I, Bottcher H, Hempel U. Biocompatibility of modified silica–protein composite layers. J Sol–Gel Sci Technol 2000;19:479–82.
[287] Rhee SH. Effect of molecular weight of poly(epsilon-caprolactone) on interpenetrating network structure, apatite-forming ability, and degradability of poly(epsilon-caprolactone)/silica nano-hybrid materials. Biomaterials 2003;24:1721–7.
[288] Maeda H, Kasuga T, Hench LL. Preparation of poly(L-lactic acid)–polysiloxane–calcium carbonate hybrid membranes for guided bone regeneration. Biomaterials 2006;27:1216–22.

[289] Liang C, Joseph MM, James CML, Hao L. The role of surface charge on the uptake and biocompatibility of hydroxyapatite nanoparticles with osteoblast cells. Nanotechnology 2011;22:105708.
[290] Hoffmann F, Cornelius M, Morell J, Froba M. Silica-based mesoporous organic–inorganic hybrid materials. Angew Chem 2006;45:3216–51.
[291] Bruhwiler D. Postsynthetic functionalization of mesoporous silica. Nanoscale 2010;2:887–92.
[292] Hoffmann F, Froba M. Vitalising porous inorganic silica networks with organic functions – PMOs and related hybrid materials. Chem Soc Rev 2011;40:608–20.
[293] Tarn D, Ashley CE, Xue M, Carnes EC, Zink JI, Brinker CJ. Mesoporous silica nanoparticle nanocarriers: biofunctionality and biocompatibility. Acc Chem Res 2013;46:792–801.
[294] Doadrio JC, Sousa EMB, Izquierdo-Barba I, Doadrio AL, Perez-Pariente J, Vallet-Regi M. Functionalization of mesoporous materials with long alkyl chains as a strategy for controlling drug delivery pattern. J Mater Chem 2006;16:462–6.
[295] Nieto A, Balas F, Colilla M, Manzano M, Vallet-Regi M. Functionalization degree of SBA-15 as key factor to modulate sodium alendronate dosage. Microporous Mesoporous Mater 2008;116:4–13.
[296] Boussif O, Lezoualch F, Zanta MA, Mergny MD, Scherman D, Demeneix B, et al. A versatile vector for gene and oligonucleotide transfer into cells in culture and in-vivo – polyethylenimine. Proc Natl Acad Sci USA 1995;92:7297–301.
[297] Manzano M, Colilla M, Vallet-Regi M. Drug delivery from ordered mesoporous matrices. Expert Opin Drug Deliv 2009;6:1383–400.
[298] Serda RE, Mack A, van de Ven AL, Ferrati S, Dunner Jr K, Godin B, et al. Logic-embedded vectors for intracellular partitioning, endosomal escape, and exocytosis of nanoparticles. Small 2010;6:2691–700.
[299] Slowing I, Trewyn BG, Lin VS. Effect of surface functionalization of MCM-41-type mesoporous silica nanoparticles on the endocytosis by human cancer cells. J Am Chem Soc 2006;128:14792–3.
[300] Hudson SP, Padera RF, Langer R, Kohane DS. The biocompatibility of mesoporous silicates. Biomaterials 2008;29:4045–55.
[301] Balas F, Manzano M, Horcajada P, Vallet-Regi M. Confinement and controlled release of bisphosphonates on ordered mesoporous silica-based materials. J Am Chem Soc 2006;128:8116–7.
[302] Song SW, Hidajat K, Kawi S. Functionalized SBA-15 materials as carriers for controlled drug delivery: influence of surface properties on matrix–drug interactions. Langmuir: ACS J Surf Colloids 2005;21:9568–75.
[303] Orcel G, Hench LL, Artaki I, Jonas J, Zerda TW. Effect of formamide additive on the chemistry of silica sol–gels II. Gel structure. J Non-Cryst Solids 1988;105:223–31.
[304] West JK, Zhu BF, Cheng YC, Hench LL. Quantum-chemistry of sol–gel silica clusters. J Non-Cryst Solids 1990;121:51–5.
[305] Kalampounias AG. IR and Raman spectroscopic studies of sol–gel derived alkaline-earth silicate glasses. Bull Mater Sci 2011;34:299–303.
[306] Gnado J, Dhamelincourt P, Pelegris C, Traisnel M, Mayot AL. Raman spectra of oligomeric species obtained by tetraethoxysilane hydrolysis–polycondensation process. J Non-Cryst Solids 1996;208:247–58.
[307] Innocenzi P. Infrared spectroscopy of sol–gel derived silica-based films: a spectra-microstructure overview. J Non-Cryst Solids 2003;316:309–19.
[308] Fischer D, Pospiech D, Scheler U, Navarro R, Messori M, Fabbri P. Monitoring of the sol–gel synthesis of organic–inorganic hybrids by FTIR transmission, FTIR/ATR, NIR and Raman spectroscopy. Macromol Symp 2008;265:134–43.
[309] Hook RJ. A ^{29}Si NMR study of the sol–gel polymerisation rates of substituted ethoxysilanes. J Non-Cryst Solids 1996;195:1–15.
[310] Delattre L, Babonneau F. ^{17}O solution NMR characterization of the preparation of sol–gel derived SiO_2/TiO_2 and SiO_2/ZrO_2 glasses. Chem Mater 1997;9:2385–94.
[311] Belton DJ, Deschaume O, Perry CC. An overview of the fundamentals of the chemistry of silica with relevance to biosilicification and technological advances. FEBS J 2012;279:1710–20.
[312] Merzbacher CI, White WB. Structure of Na in aluminosilicate glasses – a far-infrared reflectance spectroscopic study. Am Mineral 1988;73:1089–94.
[313] Kamitsos EI, Patsis AP, Kordas G. Infrared-reflectance spectra of heat-treated sol–gel-derived silica. Phys Rev B: Condens Matter 1993;48:12499–505.
[314] Rao AV, Kalesh RR, Amalnerkar DP, Seth T. Synthesis and characterization of hydrophobic TMES/TEOS based silica aerogels. J Porous Mater 2003;10:23–9.
[315] Hegde ND, Rao AV. Physical properties of methyltrimethoxysilane based elastic silica aerogels prepared by the two-stage sol–gel process. J Mater Sci 2007;42:6965–71.
[316] Yu YX, Wu XY, Guo DQ, Fang JY. Preparation of flexible, hydrophobic, and oleophilic silica aerogels based on a methyltriethoxysilane precursor. J Mater Sci 2014;49:7715–22.
[317] Chen Q, Miyata N, Kokubo T, Nakamura T. Bioactivity and mechanical properties of PDMS-modified $CaO–SiO_2–TiO_2$ hybrids prepared by sol–gel process. J Biomed Mater Res 2000;51:605–11.
[318] Miyata N, Fuke K, Chen Q, Kawashita M, Kokubo T, Nakamura T. Apatite-forming ability and mechanical properties of PTMO-modified $CaO–SiO_2$ hybrids prepared by sol–gel processing: effect of CaO and PTMO contents. Biomaterials 2002;23:3033–40.
[319] Farooq I, Tylkowski M, Muller S, Janicki T, Brauer DS, Hill RG. Influence of sodium content on the properties of bioactive glasses for use in air abrasion. Biomed Mater 2013;8:065008.
[320] Ni SR, Du RL, Ni SY. The influence of Na and Ti on the in vitro degradation and bioactivity in 58S sol–gel bioactive glass. Adv Mater Sci Eng 2012;2012.
[321] Grussaute H, Montagne L, Palavit G, Bernard JL. Phosphate speciation in $Na_2O–CaO–P_2O_5–SiO_2$ and $Na_2O–TiO_2–P_2O_5–SiO_2$ glasses. J Non-Cryst Solids 2000;263:312–7.
[322] Brauer DS, Karpukhina N, Law RV, Hill RG. Effect of TiO_2 addition on structure, solubility and crystallisation of phosphate invert glasses for biomedical applications. J Non-Cryst Solids 2010;356:2626–33.
[323] Hill R. An alternative view of the degradation of bioglass. J Mater Sci Lett 1996;15:1122–5.
[324] Hill RG, Brauer DS. Predicting the bioactivity of glasses using the network connectivity or split network models. J Non-Cryst Solids 2011;357:3884–7.
[325] Thorpe MF. Continuous deformations in random networks. J Non-Cryst Solids 1983;57:355–70.

[326] Phillips JC, Thorpe MF. Constraint theory, vector percolation and glass-formation. Solid State Commun 1985;53:699–702.
[327] Delannoy P, Bazot D, Marie PJ. Long-term treatment with strontium ranelate increases vertebral bone mass without deleterious effect in mice. Metabol – Clin Exp 2002;51:906–11.
[328] Grynpas MD, Marie PJ. Effects of low doses of strontium on bone quality and quantity in rats. Bone 1990;11:313–9.
[329] Staiger MP, Pietak AM, Huadmai J, Dias G. Magnesium and its alloys as orthopedic biomaterials: a review. Biomaterials 2006;27:1728–34.
[330] Rude RK, Gruber HE, Norton HJ, Wei LY, Frausto A, Mills BG. Bone loss induced by dietary magnesium reduction to 10% of the nutrient requirement in rats is associated with increased release of substance P and tumor necrosis factor-α. J Nutr 2004;134:79–85.
[331] Brandão-Neto J, Stefan V, Mendonça BB, Bloise W, Castro AVB. The essential role of zinc in growth. Nutr Res 1995;15:335–58.
[332] Yamaguchi M. Role of zinc in bone formation and bone resorption. J Trace Elem Exp Med 1998;11:119–35.
[333] Zhu YF, Shang FJ, Li B, Dong Y, Liu YF, Lohe MR, et al. Magnetic mesoporous bioactive glass scaffolds: preparation, physicochemistry and biological properties. J Mater Chem B 2013;1:1279–88.
[334] Wu C, Fan W, Zhu Y, Gelinsky M, Chang J, Cuniberti G, et al. Multifunctional magnetic mesoporous bioactive glass scaffolds with a hierarchical pore structure. Acta Biomater 2011;7:3563–72.
[335] Choi MKKM, Kang MH. The effect of boron supplementation on bone strength in ovariectomized rats fed with diets containing different calcium levels. Food Sci Biotechnol 2005;14:242e8.
[336] Uysal T, Ustdal A, Sonmez MF, Ozturk F. Stimulation of bone formation by dietary boron in an orthopedically expanded suture in rabbits. Angle Orthod 2009;79:984–90.
[337] Patntirapong S, Habibovic P, Hauschka PV. Effects of soluble cobalt and cobalt incorporated into calcium phosphate layers on osteoclast differentiation and activation. Biomaterials 2009;30:548–55.
[338] Peters K, Schmidt H, Unger RE, Otto M, Kamp G, Kirkpatrick CJ. Software-supported image quantification of angiogenesis in an in vitro culture system: application to studies of biocompatibility. Biomaterials 2002;23:3413–9.
[339] Saltman PD, Strause LG. The role of trace minerals in osteoporosis. J Am Coll Nutr 1993;12:384–9.
[340] Beattie JH, Avenell A. Trace element nutrition and bone metabolism. Nutr Res Rev 1992;5:167–88.
[341] Maeno S, Niki Y, Matsumoto H, Morioka H, Yatabe T, Funayama A, et al. The effect of calcium ion concentration on osteoblast viability, proliferation and differentiation in monolayer and 3D culture. Biomaterials 2005;26:4847–55.
[342] Valerio P, Pereira MM, Goes AM, Leite MF. Effects of extracellular calcium concentration on the glutamate release by bioactive glass (BG60S) preincubated osteoblasts. Biomed Mater 2009;4:045011.
[343] Julien M, Khoshniat S, Lacreusette A, Gatius M, Bozec A, Wagner EF, et al. Phosphate-dependent regulation of MGP in osteoblasts: role of ERK1/2 and Fra-1. J Bone Miner Res 2009;24:1856–68.
[344] Carlisle EM. Silicon: a possible factor in bone calcification. Science 1970;167:279–80.
[345] Reffitt DM, Ogston N, Jugdaohsingh R, Cheung HF, Evans BA, Thompson RP, et al. Orthosilicic acid stimulates collagen type 1 synthesis and osteoblastic differentiation in human osteoblast-like cells in vitro. Bone 2003;32:127–35.
[346] Amini AR, Wallace JS, Nukavarapu SP. Short-term and long-term effects of orthopedic biodegradable implants. J Long Term Eff Med Implants 2011;21:93–122.
[347] Finnie KS, Waller DJ, Perret FL, Krause-Heuer AM, Lin HQ, Hanna JV, et al. Biodegradability of sol–gel silica microparticles for drug delivery. J Sol–Gel Sci Technol 2008;49:12–8.
[348] Jones JR. Review of bioactive glass: from Hench to hybrids. Acta Biomater 2013;9:4457–86.
[349] Sepulveda P, Jones JR, Hench LL. In vitro dissolution of melt-derived 45S5 and sol–gel derived 58S bioactive glasses. J Biomed Mater Res 2002;61:301–11.
[350] Varila L, Fagerlund S, Lehtonen T, Tuominen J, Hupa L. Surface reactions of bioactive glasses in buffered solutions. J Eur Ceram Soc 2012;32:2757–63.
[351] Pantano CG, Clark AE, Hench LL. Multilayer corrosion films on bioglass surfaces. J Am Ceram Soc 1974;57:412–3.
[352] Ramila A, Vallet-Regi M. Static and dynamic in vitro study of a sol–gel glass bioactivity. Biomaterials 2001;22:2301–6.
[353] Yue S, Lee PD, Poologasundarampillai G, Jones JR. Evaluation of 3-D bioactive glass scaffolds dissolution in a perfusion flow system with X-ray microtomography. Acta Biomater 2011;7:2637–43.
[354] Bunker BC. Molecular mechanisms for corrosion of silica and silicate-glasses. J Non-Cryst Solids 1994;179:300–8.
[355] Criscenti LJ, Kubicki JD, Brantley SL. Silicate glass and mineral dissolution: calculated reaction paths and activation energies for hydrolysis of a q3 si by H3O+ using ab initio methods. J Phys Chem A 2006;110:198–206.
[356] Edén M. The split network analysis for exploring composition–structure correlations in multi-component glasses: I. Rationalizing bioactivity-composition trends of bioglasses. J Non-Cryst Solids 2011;357:1595–602.
[357] Douglas RW, Elshamy TMM. Reactions of glasses with aqueous solutions. J Am Ceram Soc 1967;50:1–8.
[358] Pereira MM, Hench LL. Mechanisms of hydroxyapatite formation on porous gel–silica substrates. J Sol–Gel Sci Technol 1996;7:59–68.
[359] Nandiyanto ABD, Kim SG, Iskandar F, Okuyama K. Synthesis of spherical mesoporous silica nanoparticles with nanometer-size controllable pores and outer diameters. Microporous Mesoporous Mater 2009;120:447–53.
[360] Saravanapavan P, Jones JR, Pryce RS, Hench LL. Bioactivity of gel–glass powders in the $CaO–SiO_2$ system: a comparison with ternary ($CaO–P_2O_5–SiO_2$) and quaternary glasses ($SiO_2–CaO–P_2O_5–Na_2O$). J Biomed Mater Res A 2003;66:110–9.
[361] Li PJ, Ohtsuki C, Kokubo T, Nakanishi K, Soga N, Nakamura T, et al. Apatite formation induced by silica-gel in a simulated body-fluid. J Am Ceram Soc 1992;75:2094–7.
[362] Cacciotti I, Lombardi M, Bianco A, Ravaglioli A, Montanaro L. Sol–gel derived 45S5 bioglass: synthesis, microstructural evolution and thermal behaviour. J Mater Sci – Mater Med 2012;23:1849–66.
[363] Bunker BC, Arnold GW, Wilder JA. Phosphate-glass dissolution in aqueous-solutions. J Non-Cryst Solids 1984;64:291–316.
[364] Alexander GB, Heston WM, Iler RK. The solubility of amorphous silica in water. J Phys Chem 1954;58:453–5.
[365] Etou M, Tsuji Y, Somiya K, Okaue Y, Yokoyama T. The dissolution of amorphous silica in the presence of tropolone under acidic conditions. Clays Clay Miner 2014;62:235–42.
[366] Hench LL. Bioceramics – from concept to clinic. J Am Ceram Soc 1991;74:1487–510.

[367] Wilson J, Pigott GH, Schoen FJ, Hench LL. Toxicology and biocompatibility of bioglasses. J Biomed Mater Res 1981;15:805–17.
[368] Murphy S, Wren AW, Towler MR, Boyd D. The effect of ionic dissolution products of Ca–Sr–Na–Zn–Si bioactive glass on in vitro cytocompatibility. J Mater Sci – Mater Med 2010;21:2827–34.
[369] Xynos ID, Edgar AJ, Buttery LD, Hench LL, Polak JM. Ionic products of bioactive glass dissolution increase proliferation of human osteoblasts and induce insulin-like growth factor II mRNA expression and protein synthesis. Biochem Biophys Res Commun 2000;276:461–5.
[370] Xynos ID, Edgar AJ, Buttery LDK, Hench LL, Polak JM. Gene-expression profiling of human osteoblasts following treatment with the ionic products of Bioglass (R) 45S5 dissolution. J Biomed Mater Res 2001;55:151–7.
[371] Lai W, Garino J, Ducheyne P. Silicon excretion from bioactive glass implanted in rabbit bone. Biomaterials 2002;23:213–7.
[372] Yao AH, Wang DP, Huang WH, Fu Q, Rahaman MN, Day DE. In vitro bioactive characteristics of borate-based glasses with controllable degradation behavior. J Am Ceram Soc 2007;90:303–6.
[373] Fu H, Rahaman MN, Day DE, Huang W. Effect of pyrophosphate ions on the conversion of calcium–lithium–borate glass to hydroxyapatite in aqueous phosphate solution. J Mater Sci – Mater Med 2010;21:2733–41.
[374] Vallet-Regi M, Rámila A, del Real RP, Pérez-Pariente J. A new property of MCM-41: drug delivery system. Chem Mater 2001;13:308–11.
[375] Chen AM, Zhang M, Wei D, Stueber D, Taratula O, Minko T, et al. Co-delivery of doxorubicin and Bcl-2 siRNA by mesoporous silica nanoparticles enhances the efficacy of chemotherapy in multidrug-resistant cancer cells. Small 2009;5:2673–7.
[376] Lu J, Liong M, Zink JI, Tamanoi F. Mesoporous silica nanoparticles as a delivery system for hydrophobic anticancer drugs. Small 2007;3:1341–6.
[377] Gu JL, Su SS, Li YS, He QJ, Zhong FY, Shi JL. Surface modification–complexation strategy for cisplatin loading in mesoporous nanoparticles. J Phys Chem Lett 2010;1:3446–50.
[378] Sood A, Panchagnula R. Peroral route: an opportunity for protein and peptide drug delivery. Chem Rev 2001;101:3275–303.
[379] Maham A, Tang Z, Wu H, Wang J, Lin Y. Protein-based nanomedicine platforms for drug delivery. Small 2009;5:1706–21.
[380] Yoshida M, Lahann J. Smart nanomaterials. ACS Nano 2008;2:1101–7.
[381] Vallet-Regi M, Balas F, Arcos D. Mesoporous materials for drug delivery. Angew Chem 2007;46:7548–58.
[382] Ariga K, Vinu A, Hill J, Mori T. Coordination chemistry and supramolecular chemistry in mesoporous nanospace. Coord Chem Rev 2007;251:2562–91.
[383] Beck JS, Vartuli JC, Roth WJ, Leonowicz ME, Kresge CT, Schmitt KD, et al. A new family of mesoporous molecular-sieves prepared with liquid-crystal templates. J Am Chem Soc 1992;114:10834–43.
[384] Fan J, Yu C, Gao F, Lei J, Tian B, Wang L, et al. Cubic mesoporous silica with large controllable entrance sizes and advanced adsorption properties. Angew Chem 2003;42:3146–50.
[385] Vallet-Regí M, Balas F, Colilla M, Manzano M. Bone-regenerative bioceramic implants with drug and protein controlled delivery capability. Prog Solid State Chem 2008;36:163–91.
[386] Cavallaro G, Pierro P, Palumbo FS, Testa F, Pasqua L, Aiello R. Drug delivery devices based on mesoporous silicate. Drug Deliv 2004;11:41–6.
[387] Qu FY, Zhu GS, Huang SY, Li SG, Sun JY, Zhang DL, et al. Controlled release of Captopril by regulating the pore size and morphology of ordered mesoporous silica. Microporous Mesoporous Mater 2006;92:1–9.
[388] Muñoz B, Rámila A, Pérez-Pariente J, Díaz I, Vallet-Regí M. MCM-41 organic modification as drug delivery rate regulator. Chem Mater 2003;15:500–3.
[389] Azaïs T, Tourné-Péteilh C, Aussenac F, Baccile N, Coelho C, Devoisselle J-M, et al. Solid-state NMR study of ibuprofen confined in MCM-41 material. Chem Mater 2006;18:6382–90.
[390] Verstappen CC, Heimans JJ, Hoekman K, Postma TJ. Neurotoxic complications of chemotherapy in patients with cancer: clinical signs and optimal management. Drugs 2003;63:1549–63.
[391] Gupta PK. Drug targeting in cancer chemotherapy: a clinical perspective. J Pharm Sci 1990;79:949–62.
[392] Ferrari M. Cancer nanotechnology: opportunities and challenges. Nat Rev Cancer 2005;5:161–71.
[393] Jotterand F. Nanomedicine: how it could reshape clinical practice. Nanomedicine (Lond) 2007;2:401–5.
[394] Moghimi SM, Hunter AC, Murray JC. Nanomedicine: current status and future prospects. FASEB J 2005;19:311–30.
[395] Farokhzad OC, Langer R. Nanomedicine: developing smarter therapeutic and diagnostic modalities. Adv Drug Deliv Rev 2006;58:1456–9.
[396] Chung TH, Wu SH, Yao M, Lu CW, Lin YS, Hung Y, et al. The effect of surface charge on the uptake and biological function of mesoporous silica nanoparticles in 3T3-L1 cells and human mesenchymal stem cells. Biomaterials 2007;28:2959–66.
[397] Zhang XQ, Xu X, Bertrand N, Pridgen E, Swami A, Farokhzad OC. Interactions of nanomaterials and biological systems: implications to personalized nanomedicine. Adv Drug Deliv Rev 2012;64:1363–84.
[398] Chou LY, Ming K, Chan WC. Strategies for the intracellular delivery of nanoparticles. Chem Soc Rev 2011;40:233–45.
[399] Conner SD, Schmid SL. Regulated portals of entry into the cell. Nature 2003;422:37–44.
[400] Mayor S, Pagano RE. Pathways of clathrin-independent endocytosis. Nat Rev Mol Cell Biol 2007;8:603–12.
[401] Kumari S, Mg S, Mayor S. Endocytosis unplugged: multiple ways to enter the cell. Cell Res 2010;20:256–75.
[402] Scita G, Di Fiore PP. The endocytic matrix. Nature 2010;463:464–73.
[403] Jiang W, Kim BYS, Rutka JT, Chan WCW. Nanoparticle-mediated cellular response is size-dependent. Nat Nanotechnol 2008;3:145–50.
[404] Soenen SJ, Nuytten N, De Meyer SF, De Smedt SC, De Cuyper M. High intracellular iron oxide nanoparticle concentrations affect cellular cytoskeleton and focal adhesion kinase-mediated signaling. Small 2010;6:832–42.
[405] Thomas TP, Shukla R, Kotlyar A, Liang B, Ye JY, Norris TB, et al. Dendrimer-epidermal growth factor conjugate displays superagonist activity. Biomacromolecules 2008;9:603–9.
[406] Rejman J, Oberle V, Zuhorn IS, Hoekstra D. Size-dependent internalization of particles via the pathways of clathrin- and caveolae-mediated endocytosis. Biochem J 2004;377:159–69.

[407] Xing XL, He XX, Peng JF, Wang KM, Tan WH. Uptake of silica-coated nanoparticles by HeLa cells. J Nanosci Nanotechnol 2005;5:1688–93.
[408] Mornet S, Lambert O, Duguet E, Brisson A. The formation of supported lipid bilayers on silica nanoparticles revealed by cryoelectron microscopy. Nano Lett 2005;5:281–5.
[409] Sauer AM, Schlossbauer A, Ruthardt N, Cauda V, Bein T, Brauchle C. Role of endosomal escape for disulfide-based drug delivery from colloidal mesoporous silica evaluated by live-cell imaging. Nano Lett 2010;10:3684–91.
[410] Kunzmann A, Andersson B, Thurnherr T, Krug H, Scheynius A, Fadeel B. Toxicology of engineered nanomaterials: focus on biocompatibility, biodistribution and biodegradation. Biochim Biophys Acta 2011;1810:361–73.
[411] Zahr AS, Davis CA, Pishko MV. Macrophage uptake of core–shell nanoparticles surface modified with poly(ethylene glycol). Langmuir: ACS J Surf Colloids 2006;22:8178–85.
[412] Lin YS, Abadeer N, Haynes CL. Stability of small mesoporous silica nanoparticles in biological media. Chem Commun (Camb) 2011;47:532–4.
[413] He Q, Zhang J, Shi J, Zhu Z, Zhang L, Bu W, et al. The effect of PEGylation of mesoporous silica nanoparticles on nonspecific binding of serum proteins and cellular responses. Biomaterials 2010;31:1085–92.
[414] Zhao Y, Sun X, Zhang G, Trewyn BG, Slowing II, Lin VS. Interaction of mesoporous silica nanoparticles with human red blood cell membranes: size and surface effects. ACS Nano 2011;5:1366–75.
[415] He Q, Zhang Z, Gao F, Li Y, Shi J. In vivo biodistribution and urinary excretion of mesoporous silica nanoparticles: effects of particle size and PEGylation. Small 2011;7:271–80.
[416] Huang X, Li L, Liu T, Hao N, Liu H, Chen D, et al. The shape effect of mesoporous silica nanoparticles on biodistribution, clearance, and biocompatibility in vivo. ACS Nano 2011;5:5390–9.
[417] Acosta-Torres LS, Lopez-Marin LM, Barcelo FH, Castano VM. Bioengineering of ceramics: evolution, challenges and opportunities. Nanotechnol Sci Tech 2010:1–22.
[418] Kim J, Piao Y, Hyeon T. Multifunctional nanostructured materials for multimodal imaging, and simultaneous imaging and therapy. Chem Soc Rev 2009;38:372–90.
[419] Foroutan F, Jokerst JV, Gambhir SS, Vermesh O, Kim HW, Knowles JC. Sol–gel synthesis and electrospraying of biodegradable $(P_2O_5)55$–$(CaO)30$–$(Na_2O)15$ glass nanospheres as a transient contrast agent for ultrasound stem cell imaging. ACS Nano 2015;9:1868–77.
[420] Feliu N, Fadeel B. Nanotoxicology: no small matter. Nanoscale 2010;2:2514–20.
[421] Lee JE, Lee N, Kim H, Kim J, Choi SH, Kim JH, et al. Uniform mesoporous dye-doped silica nanoparticles decorated with multiple magnetite nanocrystals for simultaneous enhanced magnetic resonance imaging, fluorescence imaging, and drug delivery. J Am Chem Soc 2010;132:552–7.
[422] Chithrani BD, Ghazani AA, Chan WC. Determining the size and shape dependence of gold nanoparticle uptake into mammalian cells. Nano Lett 2006;6:662–8.
[423] Osaki F, Kanamori T, Sando S, Sera T, Aoyama Y. A quantum dot conjugated sugar ball and its cellular uptake. On the size effects of endocytosis in the subviral region. J Am Chem Soc 2004;126:6520–1.
[424] He Q, Zhang Z, Gao Y, Shi J, Li Y. Intracellular localization and cytotoxicity of spherical mesoporous silica nano- and microparticles. Small 2009;5:2722–9.
[425] Petros RA, DeSimone JM. Strategies in the design of nanoparticles for therapeutic applications. Nat Rev Drug Discov 2010;9:615–27.
[426] Geng Y, Dalhaimer P, Cai S, Tsai R, Tewari M, Minko T, et al. Shape effects of filaments versus spherical particles in flow and drug delivery. Nat Nanotechnol 2007;2:249–55.
[427] Trewyn BG, Nieweg JA, Zhao Y, Lin VSY. Biocompatible mesoporous silica nanoparticles with different morphologies for animal cell membrane, penetration. Chem Eng J 2008;137:23–9.
[428] Yu T, Malugin A, Ghandehari H. Impact of silica nanoparticle design on cellular toxicity and hemolytic activity. ACS Nano 2011;5:5717–28.
[429] Huang X, Teng X, Chen D, Tang F, He J. The effect of the shape of mesoporous silica nanoparticles on cellular uptake and cell function. Biomaterials 2010;31:438–48.
[430] Huang P, Bao L, Zhang C, Lin J, Luo T, Yang D, et al. Folic acid-conjugated silica-modified gold nanorods for X-ray/CT imaging-guided dual-mode radiation and photo-thermal therapy. Biomaterials 2011;32:9796–809.
[431] Yang H, Zeng HJ, Hao LJ, Zhao NR, Du C, Liao H, et al. Effects of hydroxyapatite microparticle morphology on bone mesenchymal stem cell behavior. J Mater Chem B 2014;2:4703–10.
[432] Chauhan VP, Popovic Z, Chen O, Cui J, Fukumura D, Bawendi MG, et al. Fluorescent nanorods and nanospheres for real-time in vivo probing of nanoparticle shape-dependent tumor penetration. Angew Chem 2011;50:11417–20.
[433] Decuzzi P, Pasqualini R, Arap W, Ferrari M. Intravascular delivery of particulate systems: does geometry really matter? Pharm Res 2009;26:235–43.
[434] Mitragotri S. In drug delivery, shape does matter. Pharm Res 2009;26:232–4.
[435] Nel A, Xia T, Madler L, Li N. Toxic potential of materials at the nanolevel. Science 2006;311:622–7.
[436] Tao Z, Morrow MP, Asefa T, Sharma KK, Duncan C, Anan A, et al. Mesoporous silica nanoparticles inhibit cellular respiration. Nano Lett 2008;8:1517–26.
[437] Eom HJ, Choi J. SiO_2 nanoparticles induced cytotoxicity by oxidative stress in human bronchial epithelial cell, beas-2B. Environ Health Toxicol 2011;26:e2011013.
[438] Maurer-Jones MA, Lin YS, Haynes CL. Functional assessment of metal oxide nanoparticle toxicity in immune cells. ACS Nano 2010;4:3363–73.
[439] Lin YS, Haynes CL. Impacts of mesoporous silica nanoparticle size, pore ordering, and pore integrity on hemolytic activity. J Am Chem Soc 2010;132:4834–42.
[440] Slowing II, Wu CW, Vivero-Escoto JL, Lin VS. Mesoporous silica nanoparticles for reducing hemolytic activity towards mammalian red blood cells. Small 2009;5:57–62.
[441] Tao Z, Wang G, Goodisman J, Asefa T. Accelerated oxidation of epinephrine by silica nanoparticles. Langmuir: ACS J Surf Colloids 2009;25:10183–8.

[442] Tao Z, Toms BB, Goodisman J, Asefa T. Mesoporosity and functional group dependent endocytosis and cytotoxicity of silica nanomaterials. Chem Res Toxicol 2009;22:1869–80.
[443] Radin S, Chen T, Ducheyne P. The controlled release of drugs from emulsified, sol gel processed silica microspheres. Biomaterials 2009;30:850–8.
[444] Lutolf MP, Hubbell JA. Synthetic biomaterials as instructive extracellular microenvironments for morphogenesis in tissue engineering. Nat Biotechnol 2005;23:47–55.
[445] Langer R, Tirrell DA. Designing materials for biology and medicine. Nature 2004;428:487–92.
[446] Albrektsson T, Johansson C. Osteoinduction, osteoconduction and osseointegration. Eur Spine J: Off Publ Eur Spine Soc, Eur Spinal Deformity Soc, Eur Sect Cerv Spine Res Soc 2001;10(Suppl. 2):S96–S101.
[447] Langer R, Vacanti JP. Tissue engineering. Science 1993;260:920–6.
[448] Elisseeff J, McIntosh W, Fu K, Blunk BT, Langer R. Controlled-release of IGF-I and TGF-beta1 in a photopolymerizing hydrogel for cartilage tissue engineering. J Orthop Res 2001;19:1098–104.
[449] Shea LD, Smiley E, Bonadio J, Mooney DJ. DNA delivery from polymer matrices for tissue engineering. Nat Biotechnol 1999;17:551–4.
[450] Griffith LG. Polymeric biomaterials. Acta Mater 2000;48:263–77.
[451] Lee KY, Mooney DJ. Hydrogels for tissue engineering. Chem Rev 2001;101:1869–80.
[452] Thomson RC, Yaszemski MJ, Powers JM, Mikos AG. Hydroxyapatite fiber reinforced poly(alpha-hydroxy ester) foams for bone regeneration. Biomaterials 1998;19:1935–43.
[453] Kim SS, Ahn KM, Park MS, Lee JH, Choi CY, Kim BS. A poly(lactide-co-glycolide)/hydroxyapatite composite scaffold with enhanced osteoconductivity. J Biomed Mater Res A 2007;80:206–15.
[454] Witte F, Kaese V, Haferkamp H, Switzer E, Meyer-Lindenberg A, Wirth CJ, et al. In vivo corrosion of four magnesium alloys and the associated bone response. Biomaterials 2005;26:3557–63.
[455] Hench LL. The story of Bioglass. J Mater Sci – Mater Med 2006;17:967–78.
[456] Hench LL. Bioactive ceramics. Ann N Y Acad Sci 1988;523:54–71.
[457] Cao WP, Hench LL. Bioactive materials. Ceram Int 1996;22:493–507.
[458] Hench LL, Splinter RJ, Allen WC, Greenlee TK. Bonding mechanism at the interface of ceramic prosthetic materials. J Biomed Mater Res Biomed Mater Symp 1972;2:117–41.
[459] Hoppe A, Guldal NS, Boccaccini AR. A review of the biological response to ionic dissolution products from bioactive glasses and glass–ceramics. Biomaterials 2011;32:2757–74.
[460] Ali S, Farooq I, Iqbal K. A review of the effect of various ions on the properties and the clinical applications of novel bioactive glasses in medicine and dentistry. Saudi Dent J 2014;26:1–5.
[461] Zhou H, Wei J, Wu X, Shi J, Liu C, Jia J, et al. The bio-functional role of calcium in mesoporous silica xerogels on the responses of osteoblasts in vitro. J Mater Sci – Mater Med 2010;21:2175–85.
[462] Rahaman MN, Day DE, Bal BS, Fu Q, Jung SB, Bonewald LF, et al. Bioactive glass in tissue engineering. Acta Biomater 2011;7:2355–73.
[463] Kaur G, Pickrell G, Kimsawatde G, Homa D, Allbee HA, Sriranganathan N. Synthesis, cytotoxicity, and hydroxyapatite formation in 27-Tris-SBF for sol–gel based $CaO–P_2O_5–SiO_2–B_2O_3–ZnO$ bioactive glasses. Sci Rep 2014;4:4392.
[464] Olmo N, Martin AI, Salinas AJ, Turnay J, Vallet-Regi M, Lizarbe MA. Bioactive sol–gel glasses with and without a hydroxycarbonate apatite layer as substrates for osteoblast cell adhesion and proliferation. Biomaterials 2003;24:3383–93.
[465] Vallet-Regi M, Salinas AJ, Roman J, Gil M. Effect of magnesium content on the in vitro bioactivity of $CaO–MgO–SiO_2–P_2O_5$ sol–gel glasses. J Mater Chem 1999;9:515–8.
[466] Pérez-Pariente J, Balas F, Vallet-Regí M. Surface and chemical study of SiO_2 P_2O_5 CaO (MgO) bioactive glasses. Chem Mater 2000;12:750–5.
[467] Saboori A, Rabiee M, Mutarzadeh F, Sheikhi M, Tahriri M, Karimi M. Synthesis, characterization and in vitro bioactivity of sol–gel-derived $SiO_2–CaO–P_2O_5–MgO$ bioglass. Mater Sci Eng C – Biomim Supramol Syst 2009;29:335–40.
[468] Lao J, Jallot E, Nedelec J-M. Strontium-delivering glasses with enhanced bioactivity: a new biomaterial for antiosteoporotic applications? Chem Mater 2008;20:4969–73.
[469] Isaac J, Nohra J, Lao J, Jallot E, Nedelec JM, Berdal A, et al. Effects of strontium-doped bioactive glass on the differentiation of cultured osteogenic cells. Eur Cells Mater 2011;21:130–43.
[470] Oh SA, Kim SH, Won JE, Kim JJ, Shin US, Kim HW. Effects on growth and osteogenic differentiation of mesenchymal stem cells by the zinc-added sol–gel bioactive glass granules. J Tissue Eng 2011;2010:475260.
[471] Uchino T, Ohtsuki C, Kamitakahara M, Miyazaki T, Hayakawa S, Osaka A. Synthesis of bioactive HEMA-MPS-$CaCl_2$ hybrid gels: effects of catalysts in the sol–gel processing on mechanical properties and in vitro hydroxyapatite formation in a simulated body fluid. J Biomater Appl 2009;23:519–32.
[472] Nandini VV, Venkatesh KV, Nair KC. Alginate impressions: a practical perspective. J Conserv Dent 2008;11:37–41.
[473] Oryan AMA, Sharifi P. Advances in injured tendon engineering with emphasis on the role of collagen implants. Hard Tissue 2012;1:12.
[474] Janicki P, Schmidmaier G. What should be the characteristics of the ideal bone graft substitute? Combining scaffolds with growth factors and/or stem cells. Injury 2011;42(Suppl. 2):S77–81.
[475] Greenwald AS, Boden SD, Goldberg VM, Khan Y, Laurencin CT, Rosier RN, et al. Bone-graft substitutes: facts, fictions, and applications. J Bone Joint Surg Am 2001;83-A(Suppl. 2 Pt 2):98–103.
[476] Dhandayuthapani B, Yoshida Y, Maekawa T, Kumar DS. Polymeric scaffolds in tissue engineering application: a review. Int J Polym Sci 2011;2011:1–19.
[477] Moshiri AOA. Role of tissue engineering in tendon reconstructive surgery and regenerative medicine: current concepts, approaches and concerns. Hard Tissue 2012;29:2.
[478] Chen GUT, Tateishi T. Scaffold design for tissue engineering. Macromol Biosci 2002;2:67–77.
[479] Patel HBM, Srinivasan G. Biodegradable polymer scaffold for tissue engineering. Artif Organs 2011;25:20–9.

[480] El-Fiqi A, Lee JH, Lee EJ, Kim HW. Collagen hydrogels incorporated with surface-aminated mesoporous nanobioactive glass: improvement of physicochemical stability and mechanical properties is effective for hard tissue engineering. Acta Biomater 2013;9:9508–21.
[481] Silva AR, Paula AC, Martins TM, Goes AM, Pereria MM. Synergistic effect between bioactive glass foam and a perfusion bioreactor on osteogenic differentiation of human adipose stem cells. J Biomed Mater Res A 2014;102:818–27.
[482] Finkemeier CG. Bone-grafting and bone-graft substitutes 2002.
[483] Hench LL. Bioceramics. J Am Ceram Soc 2005;81:1705–28.
[484] Kokubo T. Apatite formation on surfaces of ceramics, metals and polymers in body environment. Acta Mater 1998;46:2519–27.
[485] Day RM. Bioactive glass stimulates the secretion of angiogenic growth factors and angiogenesis in vitro. Tissue Eng 2005;11:768–77.
[486] Gorustovich AA, Roether JA, Boccaccini AR. Effect of bioactive glasses on angiogenesis: a review of in vitro and in vivo evidences. Tissue Eng B: Rev 2010;16:199–207.
[487] Zhang D, Lepparanta O, Munukka E, Ylanen H, Viljanen MK, Eerola E, et al. Antibacterial effects and dissolution behavior of six bioactive glasses. J Biomed Mater Res A 2010;93:475–83.
[488] Allan I, Newman H, Wilson M. Antibacterial activity of particulate bioglass against supra- and subgingival bacteria. Biomaterials 2001;22:1683–7.
[489] Day RM, Boccaccini AR. Effect of particulate bioactive glasses on human macrophages and monocytes in vitro. J Biomed Mater Res A 2005;73:73–9.
[490] Anderson JM. Biological responses to materials. Annu Rev Mater Res 2001;31:81–110.
[491] Amini AR, Laurencin CT, Nukavarapu SP. Bone tissue engineering: recent advances and challenges. Crit Rev Biomed Eng 2012;40:363–408.
[492] Sundelacruz S, Kaplan DL. Stem cell- and scaffold-based tissue engineering approaches to osteochondral regenerative medicine. Semin Cell Dev Biol 2009;20:646–55.
[493] Williams DF. On the mechanisms of biocompatibility. Biomaterials 2008;29:2941–53.
[494] Hulbert SF, Young FA, Mathews RS, Klawitter JJ, Talbert CD, Stelling FH. Potential of ceramic materials as permanently implantable skeletal prostheses. J Biomed Mater Res 1970;4:433–56.
[495] Rivera-Chacon DM, Alvarado-Velez M, Acevedo-Morantes CY, Singh SP, Gultepe E, Nagesha D, et al. Fibronectin and vitronectin promote human fetal osteoblast cell attachment and proliferation on nanoporous titanium surfaces. J Biomed Nanotechnol 2013;9:1092–7.
[496] Garcia AJ. Get a grip: integrins in cell–biomaterial interactions. Biomaterials 2005;26:7525–9.
[497] Freed LE, Vunjak-Novakovic G, Biron RJ, Eagles DB, Lesnoy DC, Barlow SK, et al. Biodegradable polymer scaffolds for tissue engineering. Bio/Technology 1994;12:689–93.
[498] Hughes FJ, Turner W, Belibasakis G, Martuscelli G. Effects of growth factors and cytokines on osteoblast differentiation. Periodontol 2000;2006(41):48–72.
[499] Lee CH, Singla A, Lee Y. Biomedical applications of collagen. Int J Pharm 2001;221:1–22.
[500] Canal C, Ginebra MP. Fibre-reinforced calcium phosphate cements: a review. J Mech Behav Biomed Mater 2011;4:1658–71.
[501] Ariani MD, Matsuura A, Hirata I, Kubo T, Kato K, Akagawa Y. New development of carbonate apatite–chitosan scaffold based on lyophilization technique for bone tissue engineering. Dent Mater J 2013;32:317–25.
[502] Vozzi G, Corallo C, Carta S, Fortina M, Gattazzo F, Galletti M, et al. Collagen–gelatin–genipin–hydroxyapatite composite scaffolds colonized by human primary osteoblasts are suitable for bone tissue engineering applications: in vitro evidences. J Biomed Mater Res A 2014;102:1415–21.
[503] Akkouch A, Zhang Z, Rouabhia M. Engineering bone tissue using human dental pulp stem cells and an osteogenic collagen–hydroxyapatite–poly(L-lactide-co-epsilon-caprolactone) scaffold. J Biomater Appl 2014;28:922–36.
[504] Jung UW, Lee JS, Lee G, Lee IK, Hwang JW, Kim MS, et al. Role of collagen membrane in lateral onlay grafting with bovine hydroxyapatite incorporated with collagen matrix in dogs. J Periodontal Implant Sci 2013;43:64–71.
[505] Patlolla A, Arinzeh TL. Evaluating apatite formation and osteogenic activity of electrospun composites for bone tissue engineering. Biotechnol Bioeng 2014;111:1000–17.
[506] Benita S, Lambert G. Ocular drug delivery by cationic emulsions. Isopt: Proceedings of the 5th international symposium on ocular pharmacology and therapeutics 2004:7–13.
[507] Manzano M, Vallet-Regi M. New developments in ordered mesoporous materials for drug delivery. J Mater Chem 2010;20:5593–604.
[508] Torchilin VP. Recent advances with liposomes as pharmaceutical carriers. Nat Rev Drug Discov 2005;4:145–60.
[509] Shivanand P, Sprockel OL. A controlled porosity drug delivery system. Int J Pharm 1998;167:83–96.
[510] Vivero-Escoto JL, Slowing II, Trewyn BG, Lin VS. Mesoporous silica nanoparticles for intracellular controlled drug delivery. Small 2010;6:1952–67.
[511] Unger KK, Kumar D, Grun M, Buchel G, Ludtke S, Adam T, et al. Synthesis of spherical porous silicas in the micron and submicron size range: challenges and opportunities for miniaturized high-resolution chromatographic and electrokinetic separations. J Chromatogr A 2000;892:47–55.
[512] Kosuge K, Singh PS. Mesoporous silica spheres via l-alkylamine templating route. Microporous Mesoporous Mater 2001;44:139–45.
[513] Torney F, Trewyn BG, Lin VSY, Wang K. Mesoporous silica nanoparticles deliver DNA and chemicals into plants. Nat Nanotechnol 2007;2:295–300.
[514] Radu DR, Lai CY, Jeftinija K, Rowe EW, Jeftinija S, Lin VS. A polyamidoamine dendrimer-capped mesoporous silica nanosphere-based gene transfection reagent. J Am Chem Soc 2004;126:13216–7.
[515] Hom C, Lu J, Liong M, Luo H, Li Z, Zink JI, et al. Mesoporous silica nanoparticles facilitate delivery of siRNA to shutdown signaling pathways in mammalian cells. Small 2010;6:1185–90.
[516] Park IY, Kim IY, Yoo MK, Choi YJ, Cho MH, Cho CS. Mannosylated polyethylenimine coupled mesoporous silica nanoparticles for receptor-mediated gene delivery. Int J Pharm 2008;359:280–7.

[517] Xia T, Kovochich M, Liong M, Meng H, Kabehie S, George S, et al. Polyethyleneimine coating enhances the cellular uptake of mesoporous silica nanoparticles and allows safe delivery of siRNA and DNA constructs. ACS Nano 2009;3:3273–86.
[518] Meng H, Liong M, Xia T, Li Z, Ji Z, Zink JI, et al. Engineered design of mesoporous silica nanoparticles to deliver doxorubicin and P-glycoprotein siRNA to overcome drug resistance in a cancer cell line. ACS Nano 2010;4:4539–50.
[519] Kumar MNVR, Sameti M, Mohapatra SS, Kong X, Lockey RF, Bakowsky U, et al. Cationic silica nanoparticles as gene carriers: synthesis, characterization and transfection efficiency *in vitro* and *in vivo*. J Nanosci Nanotechnol 2004;4:876–81.
[520] Bharali DJ, Klejbor I, Stachowiak EK, Dutta P, Roy I, Kaur N, et al. Organically modified silica nanoparticles: a nonviral vector for in vivo gene delivery and expression in the brain. Proc Natl Acad Sci USA 2005;102:11539–44.
[521] Solberg SM, Landry CC. Adsorption of DNA into mesoporous silica. J Phys Chem B 2006;110:15261–8.
[522] Rosenholm JM, Sahlgren C, Linden M. Multifunctional mesoporous silica nanoparticles for combined therapeutic, diagnostic and targeted action in cancer treatment. Curr Drug Targets 2011;12:1166–86.
[523] Merisko-Liversidge EM, Liversidge GG. Drug nanoparticles: formulating poorly water-soluble compounds. Toxicol Pathol 2008;36:43–8.
[524] Hillegass JM, Blumen SR, Cheng K, MacPherson MB, Alexeeva V, Lathrop SA, et al. Increased efficacy of doxorubicin delivered in multifunctional microparticles for mesothelioma therapy. Int J Cancer 2011;129:233–44.
[525] Wang TT, Chai F, Fu Q, Zhang LY, Liu HY, Li L, et al. Uniform hollow mesoporous silica nanocages for drug delivery in vitro and in vivo for liver cancer therapy. J Mater Chem 2011;21:5299–306.
[526] Meng H, Xue M, Xia T, Ji Z, Tarn DY, Zink JI, et al. Use of size and a copolymer design feature to improve the biodistribution and the enhanced permeability and retention effect of doxorubicin-loaded mesoporous silica nanoparticles in a murine xenograft tumor model. ACS Nano 2011;5:4131–44.
[527] Bhattarai SR, Muthuswamy E, Wani A, Brichacek M, Castaneda AL, Brock SL, et al. Enhanced gene and siRNA delivery by polycation-modified mesoporous silica nanoparticles loaded with chloroquine. Pharm Res 2010;27:2556–68.
[528] Zhu Y, Ikoma T, Hanagata N, Kaskel S. Rattle-type Fe_3O_4@SiO_2 hollow mesoporous spheres as carriers for drug delivery. Small 2010;6:471–8.
[529] Zhao Y, Trewyn BG, Slowing II, Lin VS. Mesoporous silica nanoparticle-based double drug delivery system for glucose-responsive controlled release of insulin and cyclic AMP. J Am Chem Soc 2009;131:8398–400.
[530] Zhu YF, Meng WJ, Gao H, Hanagata N. Hollow mesoporous silica/poly(L-lysine) particles for codelivery of drug and gene with enzyme-triggered release property. J Phys Chem C 2011;115:13630–6.
[531] Ashley CE, Carnes EC, Phillips GK, Padilla D, Durfee PN, Brown PA, et al. The targeted delivery of multicomponent cargos to cancer cells by nanoporous particle-supported lipid bilayers. Nat Mater 2011;10:389–97.
[532] Ranganathan P, Weaver KL, Capobianco AJ. Notch signalling in solid tumours: a little bit of everything but not all the time. Nat Rev Cancer 2011;11:338–51.
[533] Mamaeva V, Rosenholm JM, Bate-Eya LT, Bergman L, Peuhu E, Duchanoy A, et al. Mesoporous silica nanoparticles as drug delivery systems for targeted inhibition of notch signaling in cancer. Mol Ther 2011;19:1538–46.
[534] Rim HP, Min KH, Lee HJ, Jeong SY, Lee SC. PH-tunable calcium phosphate covered mesoporous silica nanocontainers for intracellular controlled release of guest drugs. Angew Chem 2011;50:8853–7.
[535] Muhammad F, Guo M, Qi W, Sun F, Wang A, Guo Y, et al. PH-triggered controlled drug release from mesoporous silica nanoparticles via intracellular dissolution of ZnO nanolids. J Am Chem Soc 2011;133:8778–81.
[536] He Q, Gao Y, Zhang L, Zhang Z, Gao F, Ji X, et al. A pH-responsive mesoporous silica nanoparticles-based multi-drug delivery system for overcoming multi-drug resistance. Biomaterials 2011;32:7711–20.
[537] Weissleder R, Pittet MJ. Imaging in the era of molecular oncology. Nature 2008;452:580–9.
[538] Guerrero-Martinez A, Perez-Juste J, Liz-Marzan LM. Recent progress on silica coating of nanoparticles and related nanomaterials. Adv Mater 2010;22:1182–95.
[539] Lim EK, Kim T, Paik S, Haam S, Huh YM, Lee K. Nanomaterials for theranostics: recent advances and future challenges. Chem Rev 2015;115:327–94.
[540] Xie J, Liu G, Eden HS, Ai H, Chen X. Surface-engineered magnetic nanoparticle platforms for cancer imaging and therapy. Acc Chem Res 2011;44:883–92.
[541] Xie J, Lee S, Chen X. Nanoparticle-based theranostic agents. Adv Drug Deliv Rev 2010;62:1064–79.
[542] Mahajan KD, Fan Q, Dorcena J, Ruan G, Winter JO. Magnetic quantum dots in biotechnology – synthesis and applications. Biotechnol J 2013;8:1424–34.
[543] Sathe TR, Agrawal A, Nie S. Mesoporous silica beads embedded with semiconductor quantum dots and iron oxide nanocrystals: dual-function microcarriers for optical encoding and magnetic separation. Anal Chem 2006;78:5627–32.
[544] Koole R, van Schooneveld MM, Hilhorst J, Castermans K, Cormode DP, Strijkers GJ, et al. Paramagnetic lipid-coated silica nanoparticles with a fluorescent quantum dot core: a new contrast agent platform for multimodality imaging. Bioconjug Chem 2008;19:2471–9.
[545] Yu MK, Park J, Jon S. Targeting strategies for multifunctional nanoparticles in cancer imaging and therapy. Theranostics 2012;2:3–44.
[546] Kim J, Lee JE, Lee J, Yu JH, Kim BC, An K, et al. Magnetic fluorescent delivery vehicle using uniform mesoporous silica spheres embedded with monodisperse magnetic and semiconductor nanocrystals. J Am Chem Soc 2006;128:688–9.
[547] Kim J, Kim HS, Lee N, Kim T, Kim H, Yu T, et al. Multifunctional uniform nanoparticles composed of a magnetite nanocrystal core and a mesoporous silica shell for magnetic resonance and fluorescence imaging and for drug delivery. Angew Chem 2008;47:8438–41.
[548] Popovic Z, Liu W, Chauhan VP, Lee J, Wong C, Greytak AB, et al. A nanoparticle size series for in vivo fluorescence imaging. Angew Chem 2010;49:8649–52.
[549] Perrault SD, Walkey C, Jennings T, Fischer HC, Chan WC. Mediating tumor targeting efficiency of nanoparticles through design. Nano Lett 2009;9:1909–15.
[550] Kim S, Lim YT, Soltesz EG, De Grand AM, Lee J, Nakayama A, et al. Near-infrared fluorescent type II quantum dots for sentinel lymph node mapping. Nat Biotechnol 2004;22:93–7.

[551] Agarwal A, Mackey MA, El-Sayed MA, Bellamkonda RV. Remote triggered release of doxorubicin in tumors by synergistic application of thermosensitive liposomes and gold nanorods. ACS Nano 2011;5:4919–26.
[552] Kuo WS, Chang CN, Chang YT, Yang MH, Chien YH, Chen SJ, et al. Gold nanorods in photodynamic therapy, as hyperthermia agents, and in near-infrared optical imaging. Angew Chem 2010;49:2711–5.
[553] Park H, Yang J, Lee J, Haam S, Choi IH, Yoo KH. Multifunctional nanoparticles for combined doxorubicin and photothermal treatments. ACS Nano 2009;3:2919–26.
[554] Gorelikov I, Matsuura N. Single-step coating of mesoporous silica on cetyltrimethyl ammonium bromide-capped nanoparticles. Nano Lett 2008;8:369–73.
[555] Luo T, Huang P, Gao G, Shen G, Fu S, Cui D, et al. Mesoporous silica-coated gold nanorods with embedded indocyanine green for dual mode X-ray CT and NIR fluorescence imaging. Opt Express 2011;19:17030–9.
[556] Zhang Z, Wang L, Wang J, Jiang X, Li X, Hu Z, et al. Mesoporous silica-coated gold nanorods as a light-mediated multifunctional theranostic platform for cancer treatment. Adv Mater 2012;24:1418–23.
[557] Gupta R, Chaudhury NK. Entrapment of biomolecules in sol–gel matrix for applications in biosensors: problems and future prospects. Biosens Bioelectron 2007;22:2387–99.
[558] Badjić JD, Kostić NM. Effects of encapsulation in sol–gel silica glass on esterase activity, conformational stability, and unfolding of bovine carbonic anhydrase II. Chem Mater 1999;11:3671–9.
[559] Fang B, Gu A, Wang G, Wang W, Feng Y, Zhang C, et al. Silver oxide nanowalls grown on Cu substrate as an enzymeless glucose sensor. ACS – Appl Mater Interfaces 2009;1:2829–34.
[560] Xiuyun W, Shunichi U. Polymers for biosensors construction 2013.
[561] Datta S, Christena LR, Rajaram YRS. Enzyme immobilization: an overview on techniques and support materials. 3 Biotech 2013;3:1–9.
[562] Hasanzadeh M, Shadjou N, de la Guardia M, Eskandani M, Sheikhzadeh P. Mesoporous silica-based materials for use in biosensors. TRAC – Trends Anal Chem 2012;33:117–29.
[563] Carrington NA, Xue ZL. Inorganic sensing using organofunctional sol–gel materials. Acc Chem Res 2007;40:343–50.
[564] Walcarius A, Collinson MM. Analytical chemistry with silica sol–gels: traditional routes to new materials for chemical analysis. Annu Rev Anal Chem 2009;2:121–43.
[565] Basabe-Desmonts L, Reinhoudt DN, Crego-Calama M. Design of fluorescent materials for chemical sensing. Chem Soc Rev 2007;36:993–1017.
[566] Ariga K, Hill JP, Endo H. Developments in molecular recognition and sensing at interfaces. Int J Mol Sci 2007;8:864–83.
[567] Jeronimo PC, Araujo AN, Conceicao BSMMM. Optical sensors and biosensors based on sol–gel films. Talanta 2007;72:13–27.
[568] Kandimalla VB, Tripathi VS, Ju H. A conductive ormosil encapsulated with ferrocene conjugate and multiwall carbon nanotubes for biosensing application. Biomaterials 2006;27:1167–74.
[569] Rickus JL, Tobin AJ, Zink JI, Dunn B. Photochemical enzyme co-factor regeneration: towards continuous glutamate monitoring with a sol–gel optical biosensor. In: Shea KJ, Yan M, Roberts MJ, Cremer PS, Crooks RM, Sailor MJ, editors. Molecularly imprinted materials – sensors and other devices; 2002. p. 155–60.
[570] Avnir D, Braun S, Lev O, Ottolenghi M. Enzymes and other proteins entrapped in sol–gel materials. Chem Mater 1994;6:1605–14.
[571] Collinson MM. Recent trends in analytical applications of organically modified silicate materials. TRAC – Trends Anal Chem 2002;21:30–8.
[572] Dunn B, Zink JI. Probes of pore environment and molecule–matrix interactions in sol–gel materials. Chem Mater 1997;9:2280–91.
[573] Zhao F, Yin Y, Lu WW, Leong JC, Zhang W, Zhang J, et al. Preparation and histological evaluation of biomimetic three-dimensional hydroxyapatite/chitosan–gelatin network composite scaffolds. Biomaterials 2002;23:3227–34.
[574] Avnir D, Levy D, Reisfeld R. The nature of the silica cage as reflected by spectral changes and enhanced photostability of trapped rhodamine-6g. J Phys Chem – US 1984;88:5956–9.
[575] Zong S, Cao Y, Zhou Y, Ju H. Zirconia nanoparticles enhanced grafted collagen tri-helix scaffold for unmediated biosensing of hydrogen peroxide. Langmuir: ACS J Surf Colloids 2006;22:8915–9.
[576] Dave BC, Dunn B, Valentine JS, Zink JI. Sol–gel encapsulation methods for biosensors. Anal Chem 1994;66:A1120–7.
[577] Zink JI, Valentine JS, Dunn B. Biomolecular materials based on sol–gel encapsulated proteins. New J Chem 1994;18:1109–15.
[578] Zusman R, Rottman C, Ottolenghi M, Avnir D. Doped sol–gel glasses as chemical sensors. J Non-Cryst Solids 1990;122:107–9.
[579] Coradin T, Allouche J, Boissiere M, Livage J. Sol–gel biopolymer/silica nanocomposites in biotechnology. Curr Nanosci 2006;2:219–30.
[580] Moon JH, McDaniel W, Hancock LF. Facile fabrication of poly(p-phenylene ethynylene)/colloidal silica composite for nucleic acid detection. J Colloid Interface Sci 2006;300:117–22.
[581] Besombes JL, Cosnier S, Labbe P, Reverdy G. Improvement of the analytical characteristics of an enzyme electrode for free and total cholesterol via laponite clay additives. Anal Chim Acta 1995;317:275–80.
[582] Corrie S, Lawrie G, Battersby B, Trau M. Organosilica particles for DNA screening applications 2006 [Ieee].
[583] Wei Y, Dong H, Xu J, Feng Q. Simultaneous immobilization of horseradish peroxidase and glucose oxidase in mesoporous sol–gel host materials. ChemPhysChem 2002;3:802–8.
[584] Blin JL, Gerardin C, Carteret C, Rodehuser L, Selve C, Stebe MJ. Direct one-step immobilization of glucose oxidase in well-ordered mesostructured silica using a nonionic fluorinated surfactant. Chem Mater 2005;17:1479–86.
[585] Dai Z, Liu S, Ju H, Chen H. Direct electron transfer and enzymatic activity of hemoglobin in a hexagonal mesoporous silica matrix. Biosens Bioelectron 2004;19:861–7.
[586] Dai Z, Xu X, Ju H. Direct electrochemistry and electrocatalysis of myoglobin immobilized on a hexagonal mesoporous silica matrix. Anal Biochem 2004;332:23–31.

[587] Descalzo AB, Rurack K, Weisshoff H, Martinez-Manez R, Marcos MD, Amoros P, et al. Rational design of a chromo- and fluorogenic hybrid chemosensor material for the detection of long-chain carboxylates. J Am Chem Soc 2005;127:184–200.
[588] Descalzo AB, Jimenez D, Marcos MD, Martinez-Manez R, Soto J, El Haskouri J, et al. A new approach to chemosensors for anions using MCM-41 grafted with amino groups. Adv Mater 2002;14:966–9.
[589] Wan X, Wang D, Liu S. Fluorescent pH-sensing organic/inorganic hybrid mesoporous silica nanoparticles with tunable redox-responsive release capability. Langmuir: ACS J Surf Colloids 2010;26:15574–9.
[590] Wirnsberger G, Scott BJ, Stucky GD. PH sensing with mesoporous thin films. Chem Commun 2001:119–20.
[591] Miled OB, Grosso D, Sanchez C, Livage J. An optical fibre pH sensor based on dye doped mesostructured silica. J Phys Chem Solids 2004;65:1751–5.
[592] Safavi A, Maleki N, Bagheri M. Modification of chemical performance of dopants in xerogel films with entrapped ionic liquid. J Mater Chem 2007;17:1674–81.